12-12-2014

Biofilm Microenvironment Analysis Systems for Medicine and Agriculture

Jinzi Deng
University of Connecticut - Storrs, jinzi.deng@uconn.edu

Biofilm Microenvironment Analysis Systems for Medicine and Agriculture

Jinzi Deng, PhD

University of Connecticut, 2014

Biofilms are aggregated bacteria embedded in extracellular polymeric substances (EPS). Biofilms are the dominant growth form of bacteria in most natural environments, and are also important in many industrial and *in vivo* settings. The function of a biofilm system is inherently different from the function of the same cells dispersed in liquid culture. Existing methods to study biofilm either do not maintain the essential biofilm architecture or do not capture the dynamic nature of their responses. This research describes the development of a set of biofilm microenvironment analysis systems that maintain the essential micro-scale structure of biofilms. These systems are relevant to both medical and environmental applications. Many critical enabling technologies were developed as part of this work, include contact printing for patterning arrays of identical bacterial biofilms; wide field and confocal microscopy and white light interferometry for characterization of biofilm geometry; development of a spatially continuous non-destructive optical oxygen sensor; soft lithography and photolithography to create synthetic biofilm microenvironments with controlled nonlinear gradients and realistic soil microstructures; optical analysis and high-throughput digital image processing methods; thermogravimetric analysis and dynamic vapor sorption to measure water retention in biofilms; and three-dimensional dynamic mass transport and reaction modeling to infer bulk oxygen respiration rates in intact biofilms. In the medical context, this research offers practical methods for high-throughput screening of antimicrobials and antimicrobial dosing rates, and a tool for better understanding the relationships among

antimicrobial concentration, antimicrobial flux, and exposure time in inhibiting bacterial biofilms, and thereby a strategy to minimize induced resistance. In the agricultural context, emulated soil micromodels were developed to directly observe the effects of biofilm EPS on pore-scale water retention. Experiments with a synthetic microenvironment confirmed that EPS and micromodel geometry act together to limit evaporation at pore throats. Conservation of the biofilm microenvironment enables emergent properties of the biofilm to be studied systematically in a laboratory setting. By conserving the complex and micro-structured features of the biofilm system, microbial systems engineering approaches offer new approaches to finding more effective treatments to disease, and for more sustainable and resilient food production.

Biofilm Microenvironment Analysis Systems for Medicine and Agriculture

Jinzi Deng

B.S., East China University of Science and Technology, China, 2008

Diploma, Fachhochschule Luebeck, Germany, 2008

M.S., University of Connecticut, US, 2012

A Dissertation

Submitted in Partial Fulfillment of the

Requirements for the Degree of

Doctor of Philosophy

at the

University of Connecticut

2014

APPROVAL PAGE

Doctor of Philosophy Dissertation

Biofilm Microenvironment Analysis Systems for Medicine and Agriculture

Presented by

Jinzi Deng, B.S., M.S.

Major Advisor

_____

Dr. Leslie M. Shor

Associate Advisor

_____

Dr. Daniel Gage

Associate Advisor

_____

Dr. Jeffrey McCutcheon

Associate Advisor

_____

Dr. Ranjan Srivastava

Associate Advisor

_____

Dr. Yong Wang

University of Connecticut

2014

ACKNOWLEDGEMENTS

I would like to acknowledge financial support from University of Connecticut and a Large Faculty Grant, the Department of Chemical & Biomolecular Engineering , NSF EFRI award 1137249, the USDA through AFRI 2011-0373 and a research grant from BASF.

I would like to express my sincere grateful attitude to all the members on my committee for their time and invaluable contributions: Dr. Daniel Gage, Dr. Ranjan Srivastava, Dr. Jefferey McCutcheon and Dr. Yong Wang, especially my major advisor, Dr. Leslie Shor for her guidance and support for the past five years. Her brilliant research ideas opened my mind and had given me precious motivation when working on the projects. I appreciated her patience, understanding during my difficult times in research. Without her guidance, I would never have been able to finish this work. In completing this work, Dr. Gage has offered me great amount of help, by providing expert suggestions for working with microbes. His classes also enlightened me and have given me a deeper understanding of metabolic activities of microorganisms. Dr. McCutcheon has been a great teacher to me too. I was his TA for during my second semester at UConn. He gave me a lot of advise on class preparation and teaching. I appreciate the great opportunity to be able to actually stand in front of students and lead the discuss session of his class. I also want to thank Dr. Srivastava, for his great comments in my general exam. After I discussed the proposal of this work with him, I obtained a deeper understanding of how I should approach the research. I am also so appreciate of Dr. Wang's drug delivery class. The comprehensive information on drug delivery and the importance of time-dependent effects really opened my eyes. The course was very helpful for my research on dynamic antibiotic delivery. I

appreciate the long talk with him when I first come to the States five years ago, about how I should proceed to become a qualified graduate researcher.

I would like to thank my lab mates, Dr. Jessica Chau, Grant Bouchillon, Andrea Kadilak, Rebecca Rubinstein, Erika Orner and Brian Cruz who as good friends were always willing to help me and give me their suggestions. They are like my family here in the States. I really appreciate their effort s to create the comfortable environment we enjoy in the lab. It would have been a lonely lab without them. Many thanks to Reed Goodwin for all his expert suggestions and hands on help at the bench. He helped me to get started with microscopy when I first started in the lab. I also want to thank Dr. Carrol Noris for her kind help and precious time with confocal microscopy imaging of biofilms as well as all her help in setting up controlled temperature and humidity for biofilms on microscope. I appreciate the ultimate support and training from Dr. Laura Pinatti and Mr. Mark Dudley in IMS on Thermal analysis equipments and white light scanning interferometry. I also want to thank Dr. Michael Pikal for letting me to use Dynamic Vapor Sorption in his lab and Dr. Ekneet Sahni and Dr. Lokesh Kumar for their assistance in equipment operation. I am grateful for all the support from the Vanderbilt Institute for Integrative Biosystems Research and Education (VIIBRE) and its undergraduate research program funded by Gideon Searle, the Systems Biology and Bioengineering Undergraduate Research Experience (SyBBURE). I am thankful for all undergraduates who had been working together with me for this work, especially Leonela Villegas, for her endeavor and precious time. This work is impossible without all these help and support.

And thanks to Susan Soucy, Leah Winterberge and Marita Decozio-Wiley, for their help in ordering, reimbursement and all their kind support and precious information.

I would also like to thank my parents for their love and care. They were always supporting me and encouraging me with their best wishes.

Finally, I would like to thank my fiancé Xu. He is always there through the good times and bad. Together we will paint a beautiful life.

TABLE OF CONTENTS

LIST OF FIGURES

LIST OF TABLES

Chapter 1 Overview

1.1 Introduction

Bacterial biofilms are a heterogeneous community of bacteria distributed in a matrix comprised primarily of hydrated polysaccharides. For decades, biofilms have drawn great attention in various fields, including medical, industrial and environmental settings. In clinics, biofilm associated bacteria tend to form biofilms in implanted medical devices (Donlan 2001), e.g. heart assist devices, or develop into biofilm associated diseases, for instance, Cystic Fibrosis and chronic wounds. In industrial settings, especially waste water treatment plants, biofilms foul membranes (Donlan and Costerton 2002) and drastically decrease water flux, heat exchange, and separation efficiency. Bacterial biofilm is also commonly seen in soil. Extracellular polymeric substance (EPS) produced by soil biofilms can affect soil water retention by modifying soil structure, e.g. aggregating soil particles together and shifting water retention curves.

Mortality from biofilm associated infections are often associated with poor clinical outcomes, with mortality rates similar to cardiovascular diseases and higher than cancer (Lasa et al. 2005). The extracellular matrix in biofilm protects the embedded cells from extracellular stress, increases lateral transfer of resistance genes, and promotes antimicrobial tolerance by maintaining cells in respiration-limited phenotype. Biofilms can tolerate antimicrobial concentrations orders of magnitude higher than that of the same species dispersed in liquid phase (Nishimura et al. 2006; Surdeau et al. 2006). Even at high antibiotic concentrations, investigators

report failure to eradicate biofilm-associated bacteria in clinical settings (Hayden et al. 2005; Jones et al. 2008).

Although antibiotics have saved countless lives, and new drugs are under development, increasing prevalence of antibiotic resistance is an ever-present and growing threat. Back in the 1940s when Penicillin was first discovered, resistance to Penicillin in *Staphylococcus aureus* was very uncommon. However, within 10 years, 40% of *S. aureus* exhibited Penicillin resistance, and the proportion increased to 80% by1960 (Chambers 2001). Improper use of antibiotic (i.e. dose and dosing regimen) may enhance the incidence of antibiotic resistance genes in bacterial populations (Bassetti et al. 2001; Gaynes 1997). The emergence of widespread, and multi-drug resistance among individual bacteria, and in particular in biofilms, is a driving force behind development of new medicines and treatment regimes.

In determining effectiveness of a new antibiotic, and establishing treatment regimes that minimizes resistance, the drug, drug combination, dose, and dosing rate are all important. Unfortunately, there have been few studies that have considered dynamic or time-dependent responses of biofilm exposed to antimicrobial agents. Most methods to study biofilm antimicrobial susceptibility focus on the end point of treatment, and employ constant antibiotic concentrations. However, in the clinic, antimicrobial concentrations will naturally fluctuate depending on the dosing regime and pharmacokinetics. The failure to mimic realistic biofilm morphology and clinically-relevant time courses of antimicricrobial concentrations may be one reason why drug screening in the lab so infrequently identifies effective therapies in the clinic.

1.2 Research Objectives

The purpose of this work was to develop biofilm microenvironment analysis systems to maintain the essential micro-scale structure of bacterial biofilms and reproduce the essential emergent functionality of biofilm systems in a laboratory setting. The major research objectives and the associated specific aims were as follows:

(1) Determine the dependence of biofilm antimicrobial susceptibility to the dosing rate of the antimicrobial (Chapter 3), with the specific aims:

- Develop a spatially continuous, reversible, non-disruptive optical sensor for quantifying oxygen concentration at the base of individual biofilms.
- Create microfluidic diffusion device for producing quaternary overlapping gradients of dissolved constituents suitable for delivering antimicrobial at varied dosing rates.
- Create a three-dimensional time-dependent mass transport model to determine antimicrobial concentration and dosing rate in space and time.
- Verify the high-throughput dosing system by accurately determining antimicriboal susceptibility with position in the array, and comparing results with conventional, low-throughput methods.

(2) Measure the respiratory state of intact biofilms with exposure to Daptomycin, and estimate the proportion of slowly-respiring or persister cells in a biofilm during antimicrobial treatment. (Chapter 4), with the specific aims:

- Measure changing oxygen availability at the base of individual biofilms during exposure in antibiotics using fluorescence intensity as a proxy for oxygen concentration.

- Calibrate the output of the optical sensor to establish a relationship between fluorescence intensity and local oxygen concentration.

- Measure the three dimensional morphology of contact-printed biofilms using a scanning white light interferometric three dimensional surface structure analyzer.

- Create a three-dimensional, time-dependent model of oxygen diffusion and respiration to relate the dynamically-changing oxygen concentrations at the base of biofilms with changes in the respiration state of the biofilm during antibiotic exposure.

- Characterize the heterogeneity of antibiotic susceptibility of bacteria in the biofilm and provide recommendations to improve treatment effectiveness and reduce development of resistance.

(3) Develop and validate an assay to measure the extent of EPS-mediated drying resistance in bacteria-amended emulated soil miromodels (Chapter 5), with the specific aims:

- Develop an emulated soil micromodel: a novel microfluidic device that mimics the natural soil structure and particle size distribution of real soils, and enables direct and real-time observation of microbe-habitat structure interactions.

- Characterize the rate of water loss from microfluidic devices loaded with different soil bacteria strains: mucoid and non-mucoid versions of *Sinorhizobium meloliti*.

- Develop high-throughput optical methods to characterize the changes in water content during drying.
- Characterize the rate of water loss from mucoid and non-mucoid *Sinorhizobium meloliti* using Thermal Gravimetric Analysis (TGA).
- Characterize the rate of water loss from mucoid and non-mucoid *Sinorhizobium meloliti* biofilms without soil structure using Dynamic Vapor Sorption (DVS).

1.3 References

Bassetti M, Di Biagio A, Rebesco B, Amalfitano ME, Topal J, Bassetti D. 2001. The effect of formulary restriction in the use of antibiotics in an Italian hospital. European Journal of Clinical Pharmacology 57(6-7):529-534.

Chambers HF. 2001. The changing epidemiology of staphylococcus aureus? Emerging Infectious Diseases 7(2):178-182.

Donlan RM. 2001. Biofilm formation: A clinically relevant microbiological process. Clinical Infectious Diseases 33(8):1387-1392.

Donlan RM, Costerton JW. 2002. Biofilms: Survival mechanisms of clinically relevant microorganisms. Clinical Microbiology Reviews 15(2):167-+.

Gaynes R. 1997. The impact of antimicrobial use on the emergence of antimicrobial-resistant bacteria in hospitals. Infectious Disease Clinics of North America 11(4):757-&.

Hayden MK, Rezai K, Hayes RA, Lolans K, Quinn JP, Weinstein RA. 2005. Development of daptomycin resistance in vivo in methicillin-resistant Staphylococcus aureus. Journal of Clinical Microbiology 43(10):5285-5287.

Jones T, Yeaman MR, Sakoulas G, Yang SJ, Proctor RA, Sahl HG, Schrenzel J, Xiong YQ, Bayer AS. 2008. Failures in clinical treatment of Staphylococcus aureus infection with daptomycin are associated with alterations in surface charge, membrane phospholipid asymmetry, and drug binding. Antimicrobial Agents and Chemotherapy 52(1):269-278.

Lasa I, Del Pozo JL, Penadés JR, Leiva J. 2005. Bacterial biofilms and infection. Anales del Sistema Sanitario de Navarra 28(2):163-175.

Nishimura S, Tsurumoto T, Yonekura A, Adachi K, Shindo H. 2006. Antimicrobial susceptibility of Staphylococcus aureus and Staphylococcus epidermidis biofilms isolated from infected total hip arthroplasty cases. Journal of Orthopaedic Science 11(1):46-50.

Surdeau N, Laurent-Maquin D, Bouthors S, Gelle MP. 2006. Sensitivity of bacterial biofilms and planktonic cells to a new antimicrobial agent, Oxsil (R) 320N. Journal of Hospital Infection 62(4):487-493.

Chapter 2 Background

2.1 Biofilm Intrinsic and Induced Antimicrobial Resistance

Bacterial biofilms are a heterogeneous community of bacteria distributed in a matrix comprised primarily of hydrated polysaccharides. Compared to bacteria dispersed in liquid cultures, biofilm-associated bacteria can tolerate antimicrobial concentrations orders of magnitude higher (Nishimura et al. 2006; Surdeau et al. 2006). Three main mechanisms are cited for increased antimicrobial resistance of biofilms: (1) dampened fluctuations in extracellular environment through moderating effect of extracellular polymeric substance (EPS); (2) maintenance of metabolic heterogeneity of bacteria inside biofilms; (3) enhanced coordination through secretion of autoinducer or improved transfer of resistance genes through the community via lateral gene transfer (Anderl et al. 2000; Davies 2003; Mah et al. 2003; Stewart 2002; Stewart and Costerton 2001). These mechanisms occur simultaneously and their importance is influenced by the method employed to study biofilm resistance.

As described in Chapter 1, emergence of biofilm antimicrobial resistance represents a serious threat to public health. However, most existing studies on biofilm antimicrobial resistance measure biofilm response to discrete antimicrobial concentrations delivered uniformly in a liquid solution or dispersed in agar plates. In either case, the biofilm is challenged with a single, fixed antimicrobial concentration in a bulk solution and test results limited to CFU counting of viable bacteria at the end of treatment.

However, biofilms in medical, industrial or nature settings usually experience changing micro-chemical environment. Existing techniques fail to mimic the dynamic environment that

biofilms usually experience. Ignoring the important dynamic variables in these experiments and failing to mimic the dynamic environment in nature lead to inaccurate susceptibility testing results. For example, MIC (minimum inhibitory concentration) varies widely (Brazier et al. 2008) due to differences between strains (Salmon and Watts 2000) and experimental methods involved (Schuurmans et al. 2009). Schuurmans et al. reported MIC values of the same strain of bacteria varying by up to a factor of 16 due to the varied timing of the measurement. The same authors documented variations of up to a factor 100 when antibiotic pre-exposure is considered (Schuurmans et al. 2009).

2.2 Conventional Methods to Study Biofilm

Biofilms have been studied using flow cells (Lee 2008; Park et al. 2011; Rusconi et al. 2010; Shumi et al. 2010), diffusion cells (Walters et al. 2003), or multiwell plates (Houari and Di Martino 2007; Presterl et al. 2009) as well as with microfluidic devices (Lee 2008). Based on the operating conditions and capabilities, these techniques are classified into two categories: high content and high throughput techniques.

2.2.1 High Content Methods

High content methods usually refer to experiments that produce high-resolution data. In biofilm studies, real-time visualization of biofilm responses is commonly utilized. These techniques often feature real time, direct observation of the whole experimental process, owing to fluorescent labels (Waharte et al. 2010) or variation in optical density (Lee 2008) in order to study the cumulative effect of one environmental factor over a longer period of time.

Most biofilm studies carried out in flow cells support real time observation, making it feasible to investigate, e.g. initial attachment under different shear stresses (Park et al. 2011;

Rusconi et al. 2010) or environmental conditions (Shumi et al. 2010), or biofilm growth (Lee 2008) or diffusion limitation though the biofilm (Waharte et al. 2010). In a typical flow cell apparatus (Olson et al. 2010), a confluent bacterial lawn is grown in a transparent chamber, either in batch mode or continuous flow mode. These systems tend to be relatively large with the surface area of biofilm in a typical flow cell extending over several square millimeters, e.g. 2.4 mm^2 (Kim et al. 2010) up to 960 mm^2 (Olson et al. 2010). Biofilm in the chamber is typically exposed to an antimicrobial (Macia et al. 2011) and responses of the biofilm is observed using an inverted microscope (Merritt et al. 2005). This technique has been used to measure diffusion of fluorescent tracers to quantify antimicrobial penetration velocity (Stewart et al. 2009; Takenaka et al. 2008) and to characterize the porous microstructure of biofilms (Anderl et al. 2000; Davies 2003).

Antimicrobial responses of biofilms on agar also can be studied with a diffusion cell. In a diffusion cell, a biofilm is positioned between two filter disks, one on an agar substrate and the other embedded with antimicrobial. Walters et al. used a diffusion cell to measure the tolerance of *P. aeruginosa* biofilms to steady-state exposure of ciprofloxacin and Tobramycin, and found metabolic heterogeneity due to uneven nutrient and oxygen availability accounted for the enhanced biofilm resistance (Walters et al. 2003).

High content methods, especially microscopy, are widely used for high-resolutions investigation of biofilm responses to antimicrobials. However, typically biofilms are screened one-by-one against a single constant antimicrobial formulation. And direct observation is usually limited on biofilm optical density change over time as well as fluorescent labeled antimicrobial diffusion into biofilm. Not a lot of study can provide high content observation on biofilm

responses to antimicrobial exposure in respiratory level. Also, these methods do not facilitate high-throughput investigations. Variability in culture phenotype and biofilm morphology, can lead to high physiological variability, and biofilm responses are also strong functions of antibiotic dose, delivery rate, and other aspects of the micro-environment. Studies with low-throughput will have difficulty reporting the full variability and range of biofilm responses.

2.2.2 High Throughput Methods

High throughput techniques often feature automated experiments that provide large scale repetition. In high throughput techniques, analyses with many different experimental conditions become feasible. High throughput screening of biofilm antimicrobial susceptibility has been most often performed using well plates (Benoit et al. 2010; Houari and Di Martino 2007; Presterl et al. 2009). Here biofilms are cultured on surfaces of the plates (Muesken et al. 2010), on coupons (Curtin et al. 2003), on lid pegs (Ceri et al. 1999), or in microfluidic channels between wells (Benoit et al. 2010; Zhang et al. 2011). Biomass and cell viability in response to antimicrobial exposure can be measured optically. These methods are widely used to measure the minimum inhibitory concentration (MIC) and minimum biofilm eradication concentration (MBEC). However, test of viable bacteria in biofilm in well plates usually take place at the end of antibiotic exposure and sometimes requires staining, which can be toxic to the bacteria and thus ends the experiment. As a result, the output of high-throughput experiments can be low-throughput in the time resolution of measurements provided.

2.3 Microfluidic Techniques

An emerging technology that can combine advantage of high-throughput with high content for dynamic studies is microfluidic devices. Microfluidics allow user-defined geometric

control in flow cells and growth chambers with micron-scale resolution. By exactly controlling the geometry of the device and the operating conditions, simple deterministic physics governs concentration, flux and shear stress in space and time. Also, the scale of features in microfluidic devices match the scale of physical and chemical heterogeneity of real microbial habitats (Weibel et al. 2007a). Importantly, the microfluidic platform allows direct observation of microbial responses for high-content investigations. Microfluidics have been used to study motility and chemotaxis of bacteria (Ahmed et al. 2010; Binz et al. 2010; Cheng et al. 2007; Kim and Kim 2010; Kovarik et al. 2010; Seymour et al. 2010) and protozoa (Nam et al. 2009; Wang et al. 2008a; Wang et al. 2005a); to monitor communication among bacteria (Choi et al. 2011; Choi et al. 2012) and to understand intracellular signaling pathways and the dynamics of gene regulation in cells (Bennett and Hasty 2009).

Microfluidics allow investigations take place in micro-structure habitats, including in artificial porous media (Markov et al. 2010b; Willingham et al. 2008), to measure spatial organization of microorganisms in a physically (Cho et al. 2007a) or chemically micro-structured habitat (Stocker et al. 2008), and to detect and quantify microorganisms from environmental samples (Dharmasiri et al. 2010; Yamaguchi et al. 2011) or in clinical settings (Mach and Di Carlo 2010). Recently, investigators have employed microfluidics to study biofilms including the effects of shear stress (Park et al. 2011), divalent metal ions (Shumi et al. 2010) and oxygen concentration (Skolimowski et al. 2010) on the attachment of bacteria to a substrate. Recent microfluidic devices combing both aspects (Benoit et al. 2010; Kim et al. 2012; Kim et al. 2010) have begun to play significant role in biofilm investigation. For example, Kim et al used a microfluidic device to study susceptibility of a continuous biofilm to an antibiotic gradient (Kim et al. 2010). They grew a uniform *P. aeruginosa* PAO1 biofilm in a microfluidic flow cell then

challenged the continuous biofilm with a linear, steady state antimicrobial gradient flowing on top of it. Although most of the novel methods using microfluidic devices can combine high-throughput and high content measurement, the designs may not be able to provide varied antimicrobial dosing rates in a large range and measurements of biofilm responses continuously throughout the time course of the experiment.

2.4 Time-dependent Studies of Biofilm Antimicrobial Susceptibility

In most studies on biofilm antimicrobial susceptibility, biofilms are exposed to constant antimicrobial concentrations for a few days, and the antimicrobial susceptibility is tested at the end of antimicrobial exposure by plating or CFU counting. However, some attempts have been made to investigate dynamic responses of biofilm to antimicrobial exposure. For example, Reyes-Romero et al. developed an AC heat transfer sensor to monitor biofilm growth and inhibition with antibiotic exposure. The amplitude and phase shifts of the temperature signal indicate the thickness and consistent change of biofilm (Reyes-Romero et al. 2014). Takenaka et al. used a green fluorophore to stain bacteria in biofilm (Takenaka et al. 2008). Loss of green fluorescence upon antimicrobial exposure was monitored dynamically with confocal microscopy. However, these techniques rely on indirect parameters, e.g. heat production, electrical impedance, to describe biofilm growth.

Despite these few examples to the contrary, there have been relatively few studies investigating biofilm response during antibiotic treatment, regardless of variations in the antimicrobial concentration. The structure and function of lab systems used to measure responses of biofilms is a poor representation of the structure and function of real biofilm systems. As a result, results from most existing lab investigations have limited applicability to real biofilm

systems. For example, lab tests may inaccurately represent the prevalence of lateral transfer of resistance genes within or between biofilms, and poorly-controlled or replicated lab tests lead to the huge variation in antimicrobial susceptibility reported by different labs (Schuurmans et al. 2009; Terwee et al. 2010).

To the author's best knowledge, there is no established method to investigate effect of antimicrobial dosing rate coupled with dynamic observation of biofilm respiratory response to different antimicrobial treatment in one experiment.

2.5 Biofilm Antimicrobial Susceptibility and Daptomycin

Emergence of biofilm antibiotic resistance is continually driving the development of new antibiotics. The compound commercially known as Daptomycin (also known as LY146032) was discovered in late 1980s (Carpenter and Chambers 2004), and was first approved by FDA for treating Gram-positive infectious disease in human in 2003 (Raja et al. 2003). Daptomycin has been widely used in the treatment of Gram-positive bacteria, especially *Staphylococcus aureu* (Steenbergen et al. 2005) and can be effective in treatment of *S. aureus* biofilms (LaPlante and Woodmansee 2009). In the presence of Ca^{2+}, Daptomycin can disrupt multiple cell membrane functions (Raja et al. 2003) and with exposure, disrupted bacterial cell membrane potential is observed (Alborn Jr et al. 1991). As the compound accumulates in the bacteria cell membrane it can cause leakage. Release of intracellular ions including K^+ lead to rapid cell death (Silverman et al. 2003). This distinct and respiration-independent mode of action made Daptomycin very effective in treating bacterial biofilms.

Although a reduced respiration phenotype is no protection against Daptomycin, sub-lethal exposure to Daptomycin can still promote resistance. Given the ability of microbial

systems to adapt to their environment, development of resistance should perhaps be considered inevitable. Literature reports already report variable and diminishing effectiveness of Daptomycin against *S. aureus* (Hayden et al. 2005; Silverman et al. 2001). Jones et al. reports decreased susceptibility in *S. aureus* blood MSSA strains are associated with increased membrane fluidity, Daptomycin-induced depolarization, increased net positive membrane charges and increased translocation of charged molecules (Jones et al. 2008). Hayden et al. have shown development of Daptomycin resistance in clinically-isolated strains, with 160-fold increase of MIC within 50 days (Hayden et al. 2005). Silverman et al. reported up to 32 fold increase of MIC using both serial-passage and chemical mutagenesis methods (Silverman et al. 2001). Udekwu and Levin reported that with daily dosing of 100× MIC, densities of *S. aureus* in continuous culture never fall below 10^5 CFU per ml (Udekwu and Levin 2012).

As with any antibiotic, development of Daptomycin resistance is exacerbated by improper use. However, the Daptomycin concentrations and dosing regimes associated with the greatest effectiveness and lowest incidence of resistance in *S. aureus* biofilms are not well studied or understood.

2.6 Effect of Soil Biofilm on Soil Water Retention

Although biofilm bacterial infections are extremely serious from a public health standpoint, biofilms may also provide important benefits in an environmental context. In soils, bacteria form biofilms to avoid water stress and predation by protozoa (Or et al. 2007b; Or et al. 2007c). EPS secreted by bacteria has been shown to change into a highly cross-linked structure and to tightly bind water in dry conditions, or to expand to hold more water in wet conditions (Or et al. 2007b). EPS and biofilms do not just benefit themselves: as little as 1% EPS has been

shown to dramatically shift the water retention curve for whole soils (Robertson and Firestone 1992). Therefore, soil rich in biofilms may be more tolerant to dry conditions, leading to greater terrestrial productivity of all organisms dependent on moisture in soils.

Water content in the unsaturated zone of soil is affected by atmospheric conditions, vegetation, soil physical properties, and microbial activity. Capillary forces in the spaces between soil particles allow soils to hold moisture that would otherwise drain or evaporate. The strength of capillarity in soil is a function of the soil texture (particle size distribution) and soil structure (aggregation of particles). The theory of water retention behavior of uniform or structureless soils is well-developed, but real soils are highly non-uniform at a variety of spatial scales. From an agricultural standpoint, formation of non-uniform soil structure through physical, chemical, and biological aggregation processes can lead to a beneficial mix of macropores that promote efficient exchange of soil gases, and micropores that retain moisture for plants and microbes (Smucker et al. 2007).

Microbial secretions are known to increase soil aggregation (Gajic et al. 2010; Kaci et al. 2005; Karki and Goodman 2011). In unsaturated soils, microbial activities can also help to establish and sustain preferential flow paths that increase drainage rates (Morales et al. 2010). On the negative side, microbial secretions can clog pores, thus reducing hydraulic conductivity and drainage rates, and promoting water-logging with it associated poor gaseous transport.

Global climate change is associated with increased soil dryness in many important agricultural locations. In addition to increased evaporation rates, intensification of the hydrological cycle will result in more intense precipitation events and longer rain return intervals. Globally, more than 2 billion people are already experiencing severe water stress, with >40% of

local freshwater supplies already allocated to agriculture, industry, and domestic purposes (Oki and Kanae 2006). Sustainably producing food, feed, and fiber, while maintaining environmental quality alongside economic viability and quality of life, will hinge on water supply in many locations.

As described above, two important factors influencing water retention in soil are the physical structure of soil and activities of soil microbes. However, little is known about how EPS acts within a structured porous media to alter moisture content or the rate of water loss with drying (Or et al. 2007c). One additional aspect of this dissertation research is to develop soil biofilm systems for agriculture research, as well, to better understand the combined effects of soil structure and microbial EPS production on pore-scale water evaporation rate.

2.7 References

Ahmed T, Shimizu TS, Stocker R. 2010. Bacterial Chemotaxis in Linear and Nonlinear Steady Microfluidic Gradients. Nano Letters 10(9):3379-3385.

Alborn Jr WE, Allen NE, Preston DA. 1991. Daptomycin disrupts membrane potential in growing Staphylococcus aureus. Antimicrobial Agents and Chemotherapy 35(11):2282-2287.

Anderl JN, Franklin MJ, Stewart PS. 2000. Role of antibiotic penetration limitation in Klebsiella pneumoniae biofilm resistance to ampicillin and ciprofloxacin. Antimicrobial Agents and Chemotherapy 44(7):1818-1824.

Bennett MR, Hasty J. 2009. Microfluidic devices for measuring gene network dynamics in single cells. Nature Reviews Genetics 10(9):628-638.

Benoit MR, Conant CG, Ionescu-Zanetti C, Schwartz M, Matin A. 2010. New Device for High-Throughput Viability Screening of Flow Biofilms. Applied and Environmental Microbiology 76(13):4136-4142.

Binz M, Lee AP, Edwards C, Nicolau DV. 2010. Motility of bacteria in microfluidic structures. Microelectronic Engineering 87(5-8):810-813.

Brazier JS, Raybould R, Patel B, Duckworth G, Pearson A, Charlett A, Duerden BI, Network HPARM. 2008. Distribution and antimicrobial susceptibility patterns of Clostridium difficile PCR ribotypes in English hospitals, 2007-08. Euro Surveill. 13(41):541-544.

Ceri H, Olson ME, Stremick C, Read RR, Morck D, Buret A. 1999. The Calgary Biofilm Device: New technology for rapid determination of antibiotic susceptibilities of bacterial biofilms. Journal of Clinical Microbiology 37(6):1771-1776.

Cheng S-Y, Heilman S, Wasserman M, Archer S, Shuler ML, Wu M. 2007. A hydrogel-based microfluidic device for the studies of directed cell migration. Lab on a Chip 7(6):763-769.

Cho H, Jonsson H, Campbell K, Melke P, Williams JW, Jedynak B, Stevens AM, Groisman A, Levchenko A. 2007. Self-organization in high-density bacterial colonies: Efficient crowd control. PLoS Biology 5(11):2614-2623.

Choi WS, Ha D, Park S, Kim T. 2011. Synthetic multicellular cell-to-cell communication in inkjet printed bacterial cell systems. Biomaterials 32(10):2500-2507.

Choi WS, Kim M, Park S, Lee SK, Kim T. 2012. Patterning and transferring hydrogel-encapsulated bacterial cells for quantitative analysis of synthetically engineered genetic circuits. Biomaterials 33(2):624-33.

Curtin J, Cormican M, Fleming G, Keelehan J, Colleran E. 2003. Linezolid compared with eperezolid, vancomycin, and gentamicin in an in vitro model of antimicrobial lock therapy for Staphylococcus epidermidis central venous catheter-related biofilm infections. Antimicrobial Agents and Chemotherary 47(10):3145-3148.

Davies D. 2003. Understanding biofilm resistance to antibacterial agents. Nature Reviews Drug Discovery 2(2):114-122.

Dharmasiri U, Witek MA, Adams AA, Osiri JK, Hupert ML, Bianchi TS, Roelke DL, Soper SA. 2010. Enrichment and Detection of Escherichia coli O157:H7 from Water Samples Using an Antibody Modified Microfluidic Chip. Analytical Chemistry 82(7):2844-2849.

Gajic B, Durovic N, Dugalic G. 2010. Composition and stability of soil aggregates in Fluvisols under forest, meadows, and 100 years of conventional tillage. Journal of Plant Nutrition and Soil Science 173:502-509.

Hayden MK, Rezai K, Hayes RA, Lolans K, Quinn JP, Weinstein RA. 2005. Development of daptomycin resistance in vivo in methicillin-resistant Staphylococcus aureus. Journal of Clinical Microbiology 43(10):5285-5287.

Houari A, Di Martino P. 2007. Effect of chlorhexidine and benzalkonium chloride on bacterial biofilm formation. Letters in Applied Microbiology 45(6):652-656.

Jones T, Yeaman MR, Sakoulas G, Yang SJ, Proctor RA, Sahl HG, Schrenzel J, Xiong YQ, Bayer AS. 2008. Failures in clinical treatment of Staphylococcus aureus infection with daptomycin are associated with alterations in surface charge, membrane phospholipid asymmetry, and drug binding. Antimicrobial Agents and Chemotherapy 52(1):269-278.

Kaci Y, Heyraud A, Barakat M, Heulin T. 2005. Isolation and identification of an EPS-producing Rhizobium strain from arid soil (Algeria): characterization of its EPS and the effect of inoculation on wheat rhizosphere soil structure. Research in Microbiology 156:522-531.

Karki U, Goodman M. 2011. Short-term soil quality response to forage species and pH. Grass and Forage Science 66:290-299.

Kim J, Hegde M, Kim SH, Wood TK, Jayaraman A. 2012. A microfluidic device for high throughput bacterial biofilm studies. Lab on a Chip 12(6):1157-1163.

Kim KP, Kim Y-G, Choi C-H, Kim H-E, Lee S-H, Chang W-S, Lee C-S. 2010. In situ monitoring of antibiotic susceptibility of bacterial biofilms in a microfluidic device. Lab on a Chip 10(23):3296-3299.

Kim M, Kim T. 2010. Diffusion-Based and Long-Range Concentration Gradients of Multiple Chemicals for Bacterial Chemotaxis Assays. Analytical Chemistry 82(22):9401-9409.

Kovarik ML, Brown PJB, Kysela DT, Berne C, Kinsella AC, Brun YV, Jacobson SC. 2010. Microchannel-Nanopore Device for Bacterial Chemotaxis Assays. Analytical Chemistry 82(22):9357-9364.

LaPlante KL, Woodmansee S. 2009. Activities of daptomycin and vancomycin alone and in combination with rifampin and gentamicin against biofilm-forming methicillin-resistant Staphylococcus aureus isolates in an experimental model of endocarditis. Antimicrobial Agents and Chemotherapy 53(9):3880-3886.

Lee J-HLJBKWY. 2008. Microfluidic devices for studying growth and detachment of Staphylococcus epidermidis biofilms. Biomedical Microdevices 10:489-498.

Mach AJ, Di Carlo D. 2010. Continuous Scalable Blood Filtration Device Using Inertial Microfluidics. Biotechnology and Bioengineering 107(2):302-311.

Macia MD, Perez JL, Molin S, Oliver A. 2011. Dynamics of Mutator and Antibiotic-Resistant Populations in a Pharmacokinetic/Pharmacodynamic Model of Pseudomonas aeruginosa Biofilm Treatment. Antimicrobial Agents and Chemotherapy 55(11):5230-5237.

Mah TF, Pitts B, Pellock B, Walker GC, Stewart PS, O'Toole GA. 2003. A genetic basis for Pseudomonas aeruginosa biofilm antibiotic resistance. Nature 426(6964):306-310.

Markov DA, Samson PC, Schaffer DK, Dhummakupt A, Wikswo JP, Shor LM. 2010. Window on a microworld: simple microfluidic systems for studying microbial transport in porous media. Journal of Visualized Experiments (39).

Merritt JH, Kadouri DE, O'Toole GA. 2005. Growing and analyzing static biofilms. Current Protocols in Microbioloy Chapter 1.

Morales VL, Parlange JY, Steenhuis TS. 2010. Are preferential flow paths perpetuated by microbial activity in the soil matrix? A review. Journal of Hydrology 393(1-2):29-36.

Muesken M, Di Fiore S, Romling U, Haeussler S. 2010. A 96-well-plate-based optical method for the quantitative and qualitative evaluation of Pseudomonas aeruginosa biofilm formation and its application to susceptibility testing. Nature Protocols 5(8):1460-1469.

Nam S-W, Kim S-T, Lee K-M, Kim SH, Kou S, Lim J, Hwang H, Joo MK, Jeong B, Yoo SH and others. 2009. N-Methyl-D-Aspartate Receptor-Mediated Chemotaxis and Ca(2+) Signaling in Tetrahymena pyriformis. Protist 160(2):331-342.

Nishimura S, Tsurumoto T, Yonekura A, Adachi K, Shindo H. 2006. Antimicrobial susceptibility of Staphylococcus aureus and Staphylococcus epidermidis biofilms isolated from infected total hip arthroplasty cases. Journal of Orthopaedic Science 11(1):46-50.

Oki T, Kanae S. 2006. Global Hydrological Cycles and World Water Resources. Science 313(5790):1068 - 1072.

Olson ME, Slater SR, Rupp ME, Fey PD. 2010. Rifampicin enhances activity of daptomycin and vancomycin against both a polysaccharide intercellular adhesin (PIA)-dependent and -independent Staphylococcus epidermidis biofilm. Journal of Antimicrobial Chemotherary 65(10):2164-2171.

Or D, Phutane S, Dechesne A. 2007a. Extracellular polymeric substances affecting pore-scale hydrologic conditions for bacterial activity in unsaturated soils. Vadose Zone Journal 6(2):298-305.

Or D, Smets BF, Wraith JM, Dechesne A, Friedman SP. 2007b. Physical constraints affecting bacterial habitats and activity in unsaturated porous media - a review. Advances in Water Resources 30(6-7):1505-1527.

Or D, Smets BF, Wraith JM, Dechesne A, Friedman SP. 2007c. Physical constraints affecting bacterial habitats and activity in unsaturated porous media - a review. Advances in Water Resources 30(6-7):1505-1527.

Park A, Jeong H-H, Lee J, Kim KP, Lee C-S. 2011. Effect of shear stress on the formation of bacterial biofilm in a microfluidic channel. BioChip Journal 5(3):236-241.

Presterl E, Hajdu S, Lassnigg AM, Hirschl AM, Holinka J, Graninger W. 2009. Effects of Azithromycin in Combination with Vancomycin, Daptomycin, Fosfomycin, Tigecycline, and Ceftriaxone on Staphylococcus epidermidis Biofilms. Antimicrobial Agents and Chemotherapy 53(8):3205-3210.

Reyes-Romero DF, Behrmann O, Dame G, Urban GA. 2014. Dynamic thermal sensor for biofilm monitoring. Sensors and Actuators, A: Physical 213:43-51.

Robertson EB, Firestone MK. 1992. Relationship between desiccation and exopolysaccharide production in a soil Pseudomonas sp. . Applied and Environmental Microbiology 58:1284-1291.

Rusconi R, Lecuyer S, Guglielmini L, Stone HA. 2010. Laminar flow around corners triggers the formation of biofilm streamers. Journal of the Royal Society, Interface 7(50):1293-1299.

Salmon SA, Watts JL. 2000. Minimum inhibitory concentration determinations for various antimicrobial agents against 1570 bacterial isolates from turkey poults. Avian Diseases 44(1):85-98.

Schuurmans JM, Hayali ASN, Koenders BB, ter Kuile BH. 2009. Variations in MIC value caused by differences in experimental protocol. Journal of Microbiological Methods 79(1):44-47.

Seymour JR, Ahmed T, Durham WM, Stocker R. 2010. Chemotactic response of marine bacteria to the extracellular products of Synechococcus and Prochlorococcus. Aquatic Microbial Ecology 59(2):161-168.

Shumi W, Lim J, Nam S-W, Lee K, Kim SH, Kim M-H, Cho K-S, Park S. 2010. Environmental factors that affect Streptococcus mutans biofilm formation in a microfluidic device mimicking teeth. BioChip Journal 4(4):257-263.

Silverman JA, Oliver N, Andrew T, Tongchuan LI. 2001. Resistance studies with daptomycin. Antimicrobial Agents and Chemotherapy 45(6):1799-1802.

Skolimowski M, Nielsen MW, Emneus J, Molin S, Taboryski R, Sternberg C, Dufva M, Geschke O. 2010. Microfluidic dissolved oxygen gradient generator biochip as a useful tool in bacterial biofilm studies. Lab on a Chip 10(16):2162-2169.

Smucker AJM, Park E, Dorner J, Horn R. 2007. Soil micropore development and contributions to soluble carbon transport within macroaggregates. Vadose Zone Journal 6(2):282-290.

Steenbergen JN, Alder J, Thorne GM, Tally FP. 2005. Daptomycin: A lipopeptide antibiotic for the treatment of serious Gram-positive infections. Journal of Antimicrobial Chemotherapy 55(3):283-288.

Stewart PS. 2002. Mechanisms of antibiotic resistance in bacterial biofilms. International Journal of Medical Microbiology 292(2):107-113.

Stewart PS, Costerton JW. 2001. Antibiotic resistance of bacteria in biofilms. Lancet 358(9276):135-138.

Stewart PS, Davison WM, Steenbergen JN. 2009. Daptomycin Rapidly Penetrates a Staphylococcus epidermidis Biofilm. Antimicrobial Agents and Chemotherapy 53(8):3505-3507.

Stocker R, Seymour JR, Samadani A, Hunt DE, Polz MF. 2008. Rapid chemotactic response enables marine bacteria to exploit ephemeral microscale nutrient patches. Proceeding of the National Academy of Sciences of the United States of America 105(11):4209-4214.

Surdeau N, Laurent-Maquin D, Bouthors S, Gelle MP. 2006. Sensitivity of bacterial biofilms and planktonic cells to a new antimicrobial agent, Oxsil (R) 320N. Journal of Hospital Infections 62(4):487-493.

Takenaka S, Trivedi HM, Corbin A, Pitts B, Stewart PS. 2008. Direct visualization of spatial and temporal patterns of antimicrobial action within model oral biofilms. Applied and Environmental Microbiology 74(6):1869-1875.

Terwee CB, Roorda LD, Dekker J, Bierma-Zeinstra SM, Peat G, Jordan KP, Croft P, de Vet HCW. 2010. Mind the MIC: large variation among populations and methods. Journal of Clinical Epidemiology 63(5):524-534.

Udekwu KI, Levin BR. 2012. Staphylococcus aureus in continuous culture: A tool for the rational design of antibiotic treatment protocols. PLoS ONE 7(7).

Waharte F, Steenkeste K, Briandet R, Fontaine-Aupart M-P. 2010. Diffusion Measurements inside Biofilms by Image-Based Fluorescence Recovery after Photobleaching (FRAP) Analysis with a Commercial Confocal Laser Scanning Microscope. Applied and Environmental Microbiology 76(17):5860-5869.

Walters MC, Roe F, Bugnicourt A, Franklin MJ, Stewart PS. 2003. Contributions of antibiotic penetration, oxygen limitation, and low metabolic activity to tolerance of Pseudomonas aeruginosa biofilms to ciprofloxacin and tobramycin. Antimicrobial Agents and Chemotherapy 47(1):317-323.

Wang W, Shor LA, LeBoeuf EJ, Wikswo JP, Taghon GL, Kosson DS. 2008. Protozoan migration in bent microfluidic channels. Applied and Environmental Microbiology 74(6):1945-1949.

Wang W, Shor LM, LeBoeuf EJ, Wikswo JP, Kosson DS. 2005. Mobility of protozoa through narrow channels. Applied and Environmental Microbiology 71(8):4628-4637.

Weibel DB, DiLuzio WR, Whitesides GM. 2007. Microfabrication meets microbiology. Nature Reviews Microbiology 5(3):209-218.

Willingham TW, Werth CJ, Valocchi AJ. 2008. Evaluation of the effects of porous media structure on mixing-controlled reactions using pore-scale modeling and micromodel experiments. Environmental Science & Technology 42(9):3185-3193.

Yamaguchi N, Torii M, Uebayashi Y, Nasu M. 2011. Rapid, Semiautomated Quantification of Bacterial Cells in Freshwater by Using a Microfluidic Device for On-Chip Staining and Counting. Applied and Environmental Microbiology 77(4):1536-1539.

Zhang W, Sileika TS, Chen C, Liu Y, Lee J, Packman AI. 2011. A novel planar flow cell for studies of biofilm heterogeneity and flow-biofilm interactions. Biotechnology and Bioengineering 108(11):2571-82.

Chapter 3 Dynamic Dosing Assay Relating Real-time Respiration Responses of *Staphylococcus aureus* Biofilms to Changing Micro-chemical Conditions[1]

3.1 Abstract

Bacterial biofilms are a metabolically heterogeneous community of bacteria distributed in an extracellular matrix comprised primarily of hydrated polysaccharides. Effective inhibitory concentrations measured under planktonic conditions are not applicable to biofilms, and inhibition concentrations measured for biofilms vary widely. Here we introduce a novel microfluidic approach for screening respiration inhibition of bacteria in a biofilm array morphology. The device geometry and operating conditions allow antimicrobial concentration and flux to vary systematically and predictably with space and time. One experiment can screen biofilm respiratory responses to many different antimicrobial concentrations and dosing rates in parallel. To validate the assay, onset of respiration inhibition following NaN_3 exposure is determined optically using an O_2-sensing thin film. Onset of respiration inhibition obeys a clear and reproducible pattern based on time for diffusive transport of the respiration inhibitor to each biofilm in the array. This approach can be used for high-throughput screening of antimicrobial effectiveness as a function of microbial characteristics, antimicrobial properties, or antimicrobial dosing rates. The approach may also be useful in better understanding acquired antimicrobial resistance or for screening antimicrobial combinations.

[1] Published as Deng J, Dhummakupt A, Samson PC, Wikswo JP, Shor LM. 2013. Dynamic Dosing Assay Relating Real-Time Respiration Responses of Staphylococcus aureus Biofilms to Changing microchemical Conditions. *Anal. Chem*. 85(11):5411-5419.

3.2 Introduction

Bacterial biofilms are comprised of pure or mixed cultures distributed in a self-secreted hydrogel matrix. Respiration of living cells within the biofilm and the absence of bulk mixing cause micro-scale gradients to persist in biofilms, as typified by decreasing O_2 concentrations with depth for aerobic biofilms (Stewart and Franklin 2008). Persistent gradients promote phenotypic differentiation, while proximity of cells facilitates lateral transfer of antimicrobial resistance genes (Anderson and O'Toole 2008). In addition to their importance in clinical settings, biofilms in industry reduce the efficiency of water desalination(Herzberg and Elimelech 2007) and heat exchangers (Rao et al. 2009). In environmental systems, biofilms can protect bacteria from predation (Matz et al. 2005). they protect plant roots from pathogens (Weller 1988), and they help retain moisture in soils (Or et al. 2007a).

Biofilm-associated bacteria exist in a distinct physiological state from planktonic cells, so inhibitory concentrations measured for planktonic cultures do not apply to biofilms. Generally speaking, biofilm-associated bacteria can tolerate much higher antimicrobial concentrations than can planktonic cultures (Nishimura et al. 2006; Surdeau et al. 2006). For example, Anderl et al. show that bacteria growing as a “biofilm” on an agar plate exhibit a markedly different antimicrobial susceptibility than bacteria grown in liquid suspension. In their work, antimicrobial exposures that reduced the number of live planktonic cells by four orders of magnitude caused virtually no change in the biofilm-associated cultures (Nishimura et al. 2006; Surdeau et al. 2006).

Further complicating matters, antimicrobial susceptibility of biofilms varies widely (Brazier et al. 2008; Perez et al. 2008) due to differences between parent and mutant strains (Pereira et al. 2011) or among phenotypes (Nelson et al. 2010) or due to adaptation to

experimental conditions (Pagedar et al. 2012). For example, Nelson et al. reported that minimum biofilm eradication concentrations ($MBEC_{99.9}$) for *P. aeruginosa* PA14 biofilms differ by a factor of 24 (Nelson et al. 2010).

The methods used to study biofilm inhibition by antimicrobials include flow cells, diffusion cells, multiwell plates, and microfluidic devices. These techniques can usually be classified as high-throughput or high-content. High-throughput screening of biofilm antimicrobial susceptibility is most often done using well plates (Houari and Di Martino 2007; Muesken et al. 2010; Presterl et al. 2009) or their variations where biofilms are cultured on coupons (Curtin et al. 2003), on lid pegs (Ceri et al. 1999), or in microfluidic channels between wells (Benoit et al. 2010). Well plate methods are widely used to measure the minimum inhibitory concentration (MIC) and other aspects of antimicrobial environments (Houari and Di Martino 2007). However, the inferior optical properties of many high-throughput platforms lead to a reliance on disruptive staining assays and measurement of aggregate responses at a single time point.

In contrast to one-time observations in most high-throughput assays, high-content techniques frequently feature real-time observation of cellular responses by tracking a fluorescent tag (Takenaka et al. 2008) or variation in optical density (Meyer et al. 2011). Some biofilm studies are carried out in flow cells that allow visualization of attachment and biofilm development as a function of shear stress (Park et al. 2011; Rusconi et al. 2010; Zhang et al. 2011) or changing chemical conditions (Shumi et al. 2010). Other flow cell studies have monitored biofilm growth dynamics (Lee 2008) or quantified diffusion limitations through the biofilm (Waharte et al. 2010). In a typical flow cell study, a confluent bacteria lawn is grown in a transparent chamber. These systems tend to be relatively large, with the surface area of biofilm

in a typical flow cell extending over several mm^2, e.g., ranging from 2.4 mm^2 (Kim et al. 2010) to 960 mm^2 (Olson et al. 2010). Biofilm in the chamber is typically exposed to a constant antimicrobial concentration at the biofilm-antimicrobial solution interface (Macia et al. 2011) and the response of the biofilm is observed at steady state using an inverted microscope (Merritt et al. 2005). This technique has also been used to measure diffusion of fluorescent tracers (Stewart et al. 2009). to quantify antimicrobial penetration velocity (Takenaka et al. 2008), and to characterize the microstructure of biofilms (Anderl et al. 2000; Davies 2003; MORTEN HENTZER and SØREN MOLIN 2001; Sauer et al. 2002b).

Microfluidic approaches are used increasingly in microbiology, for example, to study cellular responses to chemical signals (Park et al. 2010) and to O_2 availability (Lam et al. 2009). Microfluidic approaches have employed a variety of cell culture geometries including co-culture (Hammoudi et al. 2010) and individual cell trap (Chung et al. 2011) designs. Microfluidic devices offer the advantages of controlled geometry and operating conditions with direct optical analysis at micron-scale resolution (Crane et al. 2010). Physical features and chemical gradients in microfluidic devices can match the spatial and temporal scale of real microbial habitats (Weibel et al. 2007a). Recently, investigators have also employed microfluidics to study biofilms, including measuring the effects of shear stress (Park et al. 2011) and divalent metal ion (Shumi et al. 2010) and O_2 concentrations (Skolimowski et al. 2010) on the attachment of bacteria to substrates. Benoit et al. used a pneumatic multiwell microfluidic design to measure single-end point responses of 24 biofilms grown in micro-scale flow cells (Benoit et al. 2010). Kim et al. used a microfluidic device to study susceptibility of a continuous biofilm to a steady-state antibiotic gradient (Kim et al. 2010) They grew a single confluent 300 μm (width) × 50 μm (height) × 8 mm (length) *P. aeruginosa* PAO1 biofilm in a microfluidic flow cell, and then

challenged different positions across the biofilm with different steady-state antimicrobial concentrations. The authors conclude that this device can be useful for screening minimal biofilm eradication concentration (MBEC) by associating responses at various positions in the biofilm with the corresponding overlying antimicrobial concentrations. A more intricate design by Kim et al. challenged eight biofilms in separate flow cells with the graduated effluent of a microfluidic mixer (Kim et al. 2012). However, there is no existing assay to study biofilm responses to different antimicrobial dosing rates.

Dose and dosing rate information is essential in the safe and effective administration of any pharmaceutical agent. However, in the case of antibiotics, where bacterial pathogens may acquire, inherit, and spread resistance traits, optimal dosage is especially important for maximal reduction in bacterial load and for minimizing the emergence of resistant strains (Ball et al. 2002).

In this study, a novel dynamic dosing assay is described to relate real-time respiration responses of *Staphylococcus aureus* biofilms to changing micro-chemical conditions. In a schematic, we illustrate how our system differs from existing techniques in terms of the time course of antimicrobial exposure. In the predominant high-throughput assay (Figure 3-1a) suspended bacteria are exposed to constant antimicrobial concentrations. In biofilm flow cell studies (Figure 3-1b) antimicrobial diffuses into the film until the antimicrobial concentration approaches a steady-state value. In our dynamic dosing assay (Figure 3-1c) antimicrobial concentration varies continuously with both position and time throughout the biofilm array. The precisely-controlled geometry of the microfluidic diffusion chamber causes antimicrobial concentration and flux to vary in a predictable fashion across the array. Meanwhile, respiration responses of individual biofilms are determined optically by measuring relative fluorescence of

an O_2-quenched fluorophore dispersed in a thin polystyrene film (Cywinski et al. 2009; Tian et al. 2010).

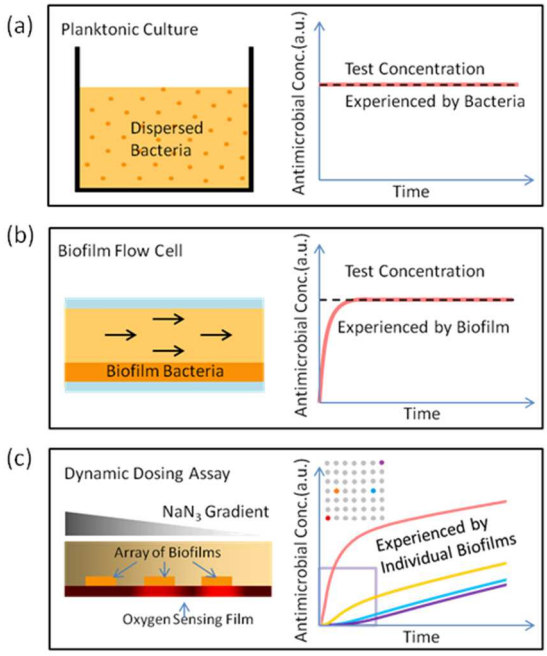

Figure 3-1 Typical experimental approaches used for studying antimicrobial inhibition of bacteria, and the resulting time course of antimicrobial concentration experienced by bacteria. (a) Planktonic bacteria suspended in liquid culture experience a single constant antimicrobial concentration. (b) In a typical biofilm flow cell system, a single concentration flows across a biofilm, and the response of the biofilm is monitored from below. (c) In our dynamic dosing assay, biofilms at different positions experience different and dynamically-changing antimicrobial concentrations. Here, antimicrobial is loaded on the left in the side-view, and nearest the red biofilm in the 7 × 7 array inset. In the side-view, fluorescence intensity under biofilms is quenched with NaN_3-induced changes in biofilm respiration. Colored lines in the graph reflect simulated concentration profiles at the corresponding positions in the array. The lower-left square indicates the time domain of the dynamic experiments described here.

To validate the dynamic dosing assay, we show sequential respiration inhibition of *Staphylococcus aureus* biofilms exposed to NaN_3. This small molecule respiration inhibitor impairs *S. aureus* catalase activity and leads to accumulation of toxic H_2O_2 (Lichstein and Soule 1944; Snyder and Lichstein 1940). Local O_2 depletion under biofilms is measured in real time by measuring relative fluorescence quenching in the film. Finally, microbial responses are related to the local concentration and dosing rate of the antimicrobial.

3.3. Experimental Section

3.3.1 Device Concept

The dynamic dosing assay is comprised of four perimeter source wells and one central sink well. The geometry of the assay and the concentration and diffusivity of the antimicrobial determines the time-dependent diffusive flux throughout a gel-filled diffusion field containing a 7×7 biofilm array (Figure 3-2). A key feature of the dynamic dosing assay design is that antimicrobial can be delivered to different positions at different dosing rates. Also, up to four different solutes can be loaded into the corner wells leading to a dynamically-changing antimicrobial mixture across the diffusion field. Here we introduce an antimicrobial in only one well, so due to symmetry, we achieve 21 duplicated conditions plus the diagonal elements, for a total of 27 distinct and dynamic micro-chemical environments.

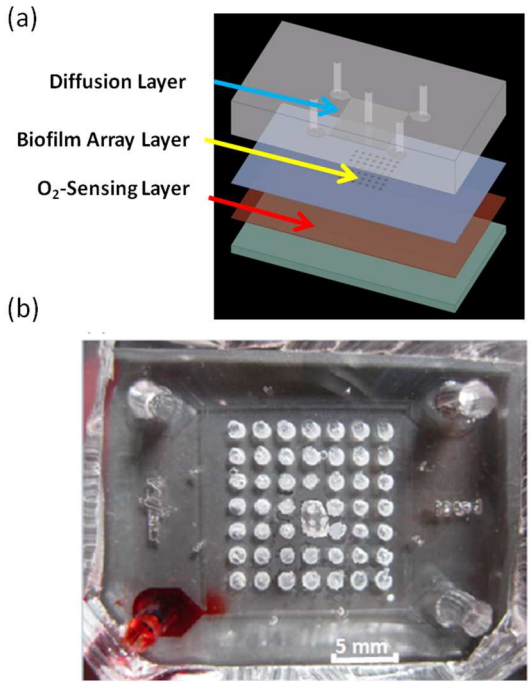

Figure 3-2 Schematic of the dynamic dosing assay.

(a) The dynamic dosing assay consists of an O_2-sensing film on a glass slide, a PDMS layer with a biofilm array patterned on top, all overlain by a PDMS microfluidic diffusion chamber. (b) Photograph of a biofilm array enclosed in a dynamic dosing assay, with red dye loaded in the lower-left perimeter source well.

3.3.2 Device Fabrication

The microfluidic diffusion chamber of the dynamic dosing assay and the stamp for bacteria contact printing were fabricated using standard techniques of photolithography and soft-lithography. Briefly, 210 ± 20 μm (Dektak Model 150, Veeco Instruments, Plainview, NY) SU-8 2100 (Microchem, Newton, MA) was spin-coated onto a 3-inch diameter Si wafer (Nova Electronic Materials, test grade, Flower Mound, TX) and patterned using UV light (45 mW/cm^2, 11 sec, Suss Microtec, Model MA6/BA6, Germany) with a chrome-on-glass photolithography mask (Advanced Reproductions, North Andover, MA).

Microfluidic devices were cast in polydimethylsiloxane (PDMS, Sylgard 184, Dow Corning, Midland, MI) mixed 10:1 with curing agent and degassed in a vacuum desiccator at -75 kPa gage for 15 min. Degassed PDMS poured over the master was cured at 60 ^oC for 2 hr. In all experiments, the height of the PDMS was 8 ± 0.5 mm. Wells were punched with a 3 mm diameter biopsy punch (Miltex, Inc., York, PA).

We also used epoxy masters cast from PDMS devices in some experiments. Epoxy and epoxy curing agent (Environmental Technology, Inc., Fields Landing, CA) were mixed 1:1 then degassed for 20 minutes. A PDMS device was then placed feature-side-down into the epoxy, taking care to allow trapped air to escape, and cured in a level chamber for 2 days at room temperature.

3.3.3 O_2-Sensing Film Fabrication

The available O_2 concentration under individual biofilms was determined from the relative fluorescence intensity of Pt (II) meso tetra-(pentafluorophenyl) porphyrin (Frontier Scientific Inc., Logan, UT) with O_2 quenching. Pt prophyrin has been used in previous studies

for imaging O_2 gradient (Grate et al. 2012) and bacteria respiration (Montagne et al. 2009; Strovas et al. 2006). Fluorescence quenching of Pt (II) meso tetra-(pentafluorophenyl) porphyrin with O_2 is reversible and fast (Cywinski et al. 2009), making it an effective real-time indicator of local O_2 concentration.

Here, polystyrene films of dispersed Pt porphyrin were cast on glass microscope slides (70 mm × 127 mm, 1 mm thick, Ted Pella, Inc., Redding, CA) pre-cleaned with ethanol. Three solutions were spin-coated on each glass slide consecutively. For the first solution, 1 g of polyvinyl-alcohol (Sigma-Aldrich Co., St. Louis, MO) was dissolved in 100 ml of DI water, and 11.5 ml of this solution was spread on the glass slides by spinning at 4000 rpm for 40 sec. For the second solution, 10 g of polystyrene beads (Sigma-Aldrich Co., St. Louis, MO) were dissolved in 150 ml of toluene (Mallinckrodt Baker, Inc., Phillipsburg, NJ; ACS reagent grade) then 0.1 g of Pt (II) meso tetra-(pentafluorophenyl) porphyrin (Frontier Scientific, Inc., Logan, UT) was added and 11.5ml of this solution was spin-coated on the polyvinyl-alcohol layer at 4000 rpm for 40 sec. Finally, PDMS premixed 10:1 with curing agent was thinned with hexane (Certified ACS, Fisher Scientific, Fair Lawn, NJ) at proportions of 2 g PDMS to 1 ml hexane. The mixture was degassed for 5 min, and 16 ml were coated on the slide as follows: ramp to 500 rpm in 5 sec, hold 13 sec, then accelerate to 2700 rpm in 7 sec and hold 1 min. Coated slides were cured at 60 ^{o}C for 2 hr then stored in the dark at room temperature. The thickness of the PDMS layer was 12.1 μm ± 0.6 μm.

3.3.4 Patterning Biofilm Array

Next, we used contact printing to produce a biofilm array of *Staphyloccus aureus*. *S. aureus* is commonly used as a model for biofilm-associated opportunistic human pathogens.

Contact printing methods have been evaluated in previous studies (Rowan et al. 2002; Weibel et al. 2005; Xu et al. 2007). Specifically, Xu et al. have shown that this method does not change the physiological state of the transferred cells (Xu et al. 2007).

Here, *S. aureus* (ATCC 25904) was incubated overnight in Tryptic Soy Broth (TSB) at 37 ºC. Stationary cultures were adjusted to OD_{600} 1.1 with fresh TSB media, and then 400 µl was transferred to a Tryptic Soy Agar (TSA) plate and spread with a sterilized loop. The plate was incubated at 37 ºC for 9 hr in humid air. This procedure results in a continuous homogenous bacteria lawn that was used as the "ink pad" in the subsequent stamping step.

Next, our custom PDMS stamp was pressed gently into the bacteria lawn, then immediately placed on the prepared substrate (Figure 3-3). Our prepared substrate was an O_2-sensing film (coated slide) that had been previously plasma-treated for 45 sec in an evacuated air atmosphere (Harrick PDC-32G, Harrick Plasma, Ithaca, NY). Biofilm heights of six biofilms from six separate stampings of two bacterial lawns were measured using confocal microscopy, and averaged 51 ± 23 µm (mean ± 1stdev).

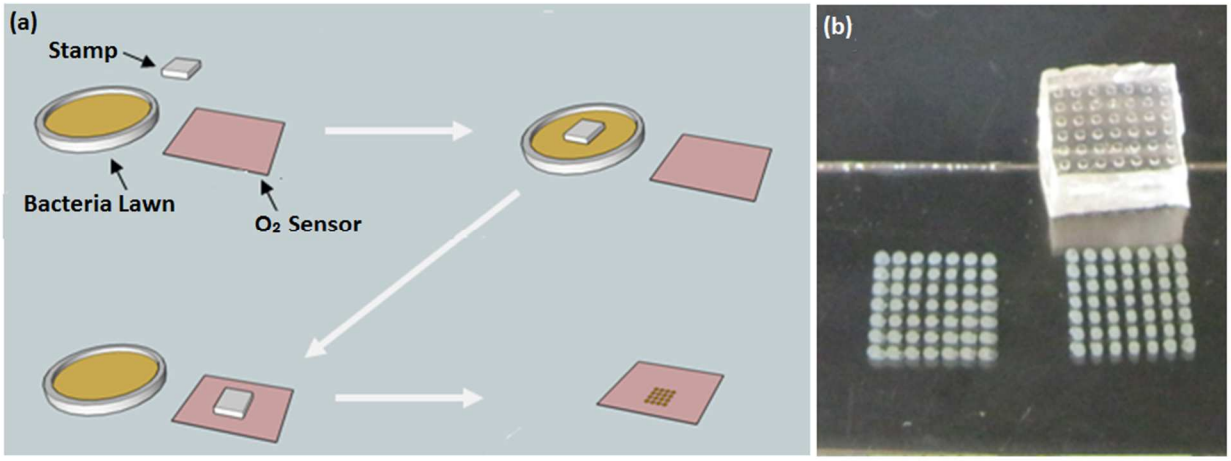

Figure 3-3 Fabrication of contact printed biofilms.

(a) Schematic of the biofilm array stamping procedure. Bacteria are transferred from a bacterial lawn to a glass slide coated with O_2-sensing film via contact printing. (b) Photograph of a PDMS stamp and biofilm array on a coated glass slide. There are 49 1-mm diameter pegs on the PDMS stamp which produces the 7 × 7 biofilm array.

We note the term “biofilm” has been used to describe bacterial colonies grown on an agar plate (Anderl et al. 2000). Although their structure may differ from other biofilm forms, such as flow cell biofilms grown under shear stress, the high cell density, active respiration, and lack of bulk mixing in our array results in O_2 and other gradients and imparts phenotypic differentiation with depth.

After stamping, the featured side of the PDMS diffusion chamber was plasma-treated for 45 sec and bonded to the substrate with the biofilm dots aligned in the observation field. The chamber was filled with 37 ^{o}C 8% gelatin type B (ACROS, Morris Plains, NJ) dissolved in TSB solution delivered near-simultaneously to all four perimeter source reservoirs. Gelatin solution in the reservoirs was removed before gelation, while the observation field remained full due to the high surface tension of water and the small dimensions of the connecting channels. Filling the microfluidic diffusion chamber with hydrogel eliminates pressure-driven flow which, if present, would dominate diffusion. In our experiments, four such microfluidic diffusion chambers were bonded to a single O_2-sensing substrate each time experiments were performed. Three were used for replicate antimicrobial treatments or control experiments and contained bacterial biofilm arrays. The fourth chamber contained no bacteria and served as a background control for relative fluorescence of the O_2-sensing film. All four dynamic dosing assays were surrounded by a water reservoir to prevent drying.

3.3.5 Dynamic Respiration Inhibition Experiments

After gelation in the diffusion field, liquid aqueous NaN_3 (Laboratory Grade, Fisher Scientific, Fair Lawn, NJ) was added to one source well of each microfluidic diffusion chamber while sterilized DI water was loaded in the center sink well. The other three source wells

contained only air. Finally, a layer of clear tape was placed across the top of each microfluidic diffusion chamber to prevent evaporation and to prevent debris from falling into source or sink wells. The concentration gradient between the NaN_3-filled perimeter source well and the central sink well provided the driving force for diffusion. In replicate experiments, we added 3100mM or 6100mM NaN_3 to the source well. The steep gradient between the source well concentration and the changing diffusion field concentration ensured a high antimicrobial flux was sustained. This high flux effectively shortens the time required to reach inhibitory concentrations throughout the biofilm array. These gradients are reproducible, as indicated by images of dye diffusion with time in replicated devices (Figure 3-4).

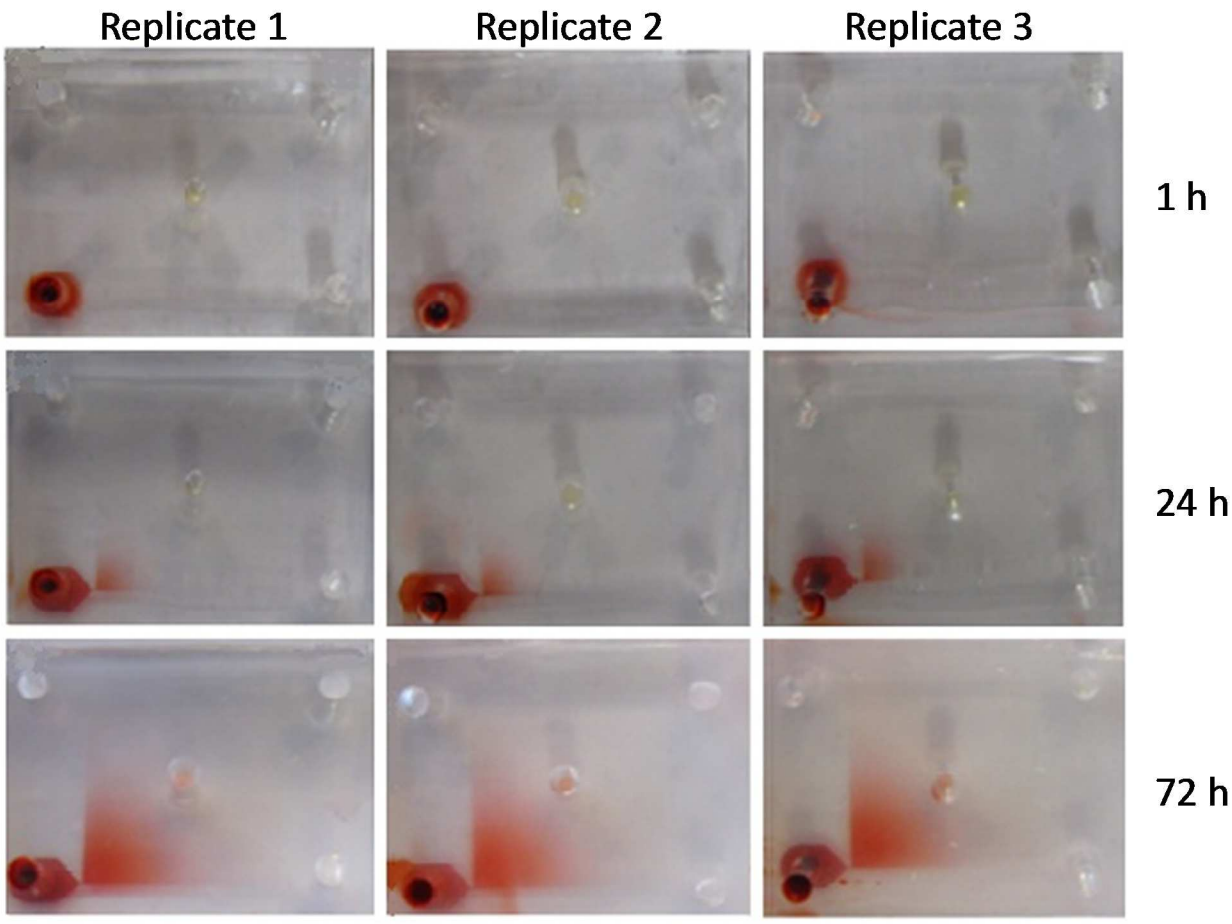

Figure 3-4 Time series showing that diffusion in dynamic dosing assays is reproducible.

Shown above are three different dynamic dosing assays prepared as described here, but with no biofilm. Red dye was loaded into one source well at t=0. Images were taken with a Canon digital camera (PowerShot A3100IS Image Stabilizer; Canon U.S.A., Inc.; Lake Success, NY) every 2 hr.

3.3.6 Constant-concentration Respiration Inhibition Experiments

As an aid to interpreting the dynamic respiration inhibition experiments, constant-concentration respiration inhibition experiments were also performed. Here, biofilm arrays identical to those used in the dynamic experiments were embedded in gelatin hydrogels initially containing 0 mM, 0.03 mM, 0.1 mM and 1 mM NaN_3. Trends among specific fluorescence (area-averaged net fluorescence intensity / area-averaged net opacity) were determined to identify the steady-state concentration of NaN_3 that inhibits respiration of biofilms.

3.3.7 Biofilm Imaging and Analysis

Real-time fluorescence images of the O_2-sensing film under each biofilm in the array were recorded and analyzed to determine local O_2 availability as the respiration inhibitor diffused through the assay.

Fluorescence images were captured using a Carl Zeiss AXIO-observer Z1 automated inverted microscope equipped with an AxioCam MRmRev.3 camera (Carl Zeiss Inc., Germany) using a 5× objective (Zeiss ECPlan-NEOFLUAR; 5×/0,16 ∞/0,17, Carl Zeiss Inc., Germany). A custom-designed dichroic filter set was used to excite the film at 380 nm and measure emission at 650 nm. The set contains an excitation filter (380/14 BrightLine Bandpass Filter, FF01-380/14-25, Carl Zeiss Inc., Germany), a Dichroic Beamsplitter (520 nm BrightLine Dichroic Beamsplitter, FF520-Di02-25×36, Carl Zeiss Inc., Germany) and an emission filter (647/57 BrightLine Bandpass Filter, FF01-647/57-25, Carl Zeiss Inc., Germany). Fluorescence images of all 49 biofilms in the array and at least four positions in a gel-filled control chamber without bacteria were collected every 10 min for 1.5 hr to establish baseline fluorescence intensity of each biofilm prior to antimicrobial exposure. Then, after antimicrobial at the desired

concentration was loaded into the source well, fluorescence images of each biofilm in the array and all control positions were collected every 10 min for 45 hr. Computer-controlled shutters exposed each position for only 800 ms as each image was collected. Use of a narrow-band LED light source (Carl Zeiss Inc., Germany) further limited photobleaching. Bright field images of each biofilm in the array and background control positions were also collected just prior to and 45 hr after adding antimicrobial agent. Real-time area-averaged net fluorescence intensity, $\overline{I_i}$, of each biofilm at each time point was determined using the open-source software package Fiji (based on ImageJ), and is defined by area-averaged intensity with mean intensity of background control positions subtracted, as indicated by

$$\overline{I_i} = \frac{\int_{Area} I(x,y)_i \, dA}{A} - I_{background,i} \ , \qquad \text{(Eq. 3.1)}$$

where $I(x,y)_i$ is the intensity matrix measured for each biofilm at time *i*, *A* is the biofilm area, and $I_{background,i}$ is the mean area-averaged intensity of similarly-sized background control positions at time *i*. The spatial extent of biofilms was defined manually for each biofilm from the corresponding initial bright field image (Figure 3-5).

In this study, all statistical analyses were performed using Stata version 11.2.

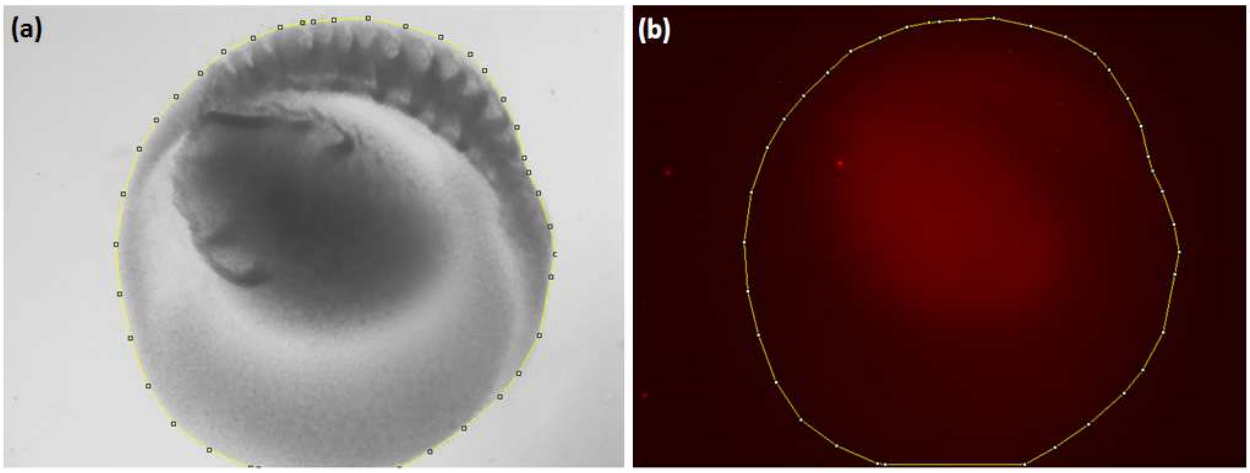

Figure 3-5 Bright field and fluorescent images of a biofilm.

Representative bright field (a) and fluorescent (b) images of the same biofilm to show how the biofilm area was defined and area-averaged opacity or fluorescence intensity was quantified. First, the outer limit of each biofilm was defined manually using the free polygon tool in Fiji and the coordinates were recorded. A motorized stage was used to return precisely to each position over the course of the experiment. For each biofilm, at each observation time, fluorescence intensities inside the defined polygon were averaged, and the average fluorescence intensity of a background area was subtracted. Scale bar shows 300 μm.

3.3.8 Mass Transport Simulations

Antimicrobial concentrations and dosing rates with position and time were simulated using COMSOL Multiphysics 4.1a. The 2-D plan geometry of the dynamic dosing assay was defined in AutoCAD and imported into COMSOL. Microfluidic features were extruded to 210 μm and the source and sink wells were extruded to 8 mm. Wells were modeled using standard water properties and microfluidic regions were modeled using hydrogel properties. The three empty source wells that contained only air were modeled as no-flux boundaries. The assumptions of the model are: mass transport by Fickian diffusion, no convection, with constant isotropic NaN_3 diffusivity; initial concentration C_o = 3100 (0.2 g/ml) or 6100 mM (0.4 g/ml) homogeneously in the source well at t = 0 and C_o = 0 elsewhere in the assay at t = 0; all water or gel interfaces with PDMS or air were modeled as no-flux boundaries. An array of 7 × 7 biofilms was defined as hydrogel cylinders with 1 mm diameter and 50 μm height and a spatial distribution equal to the stamp and centered in the diffusion field. We assume NaN_3 solubility in water equals solubility in hydrogel, and there is no NaN_3 reaction, consumption, or volatilization.

The diffusive permeability of NaN_3 in water at 25 ^oC has been approximated as 8.17×10^{-10} m^2/s as described (McBrady et al. 2006). The effective diffusive permeability of small ions through biofilm is reported to be 58% of the diffusivity in aqueous solution (Stewart 1998), or 4.74×10^{-10} m^2/s. Based on a previous study of diffusion in gelatin hydrogel (Laitinen and Kolthoff 1939), we defined the diffusivity of NaN_3 through 8% gelatin as 6.5×10^{-10} m^2/s. With known initial concentrations and the defined geometry, NaN_3 concentrations and fluxes at each biofilm position at each onset of respiration inhibition time were computed (Figure 3-6**).**

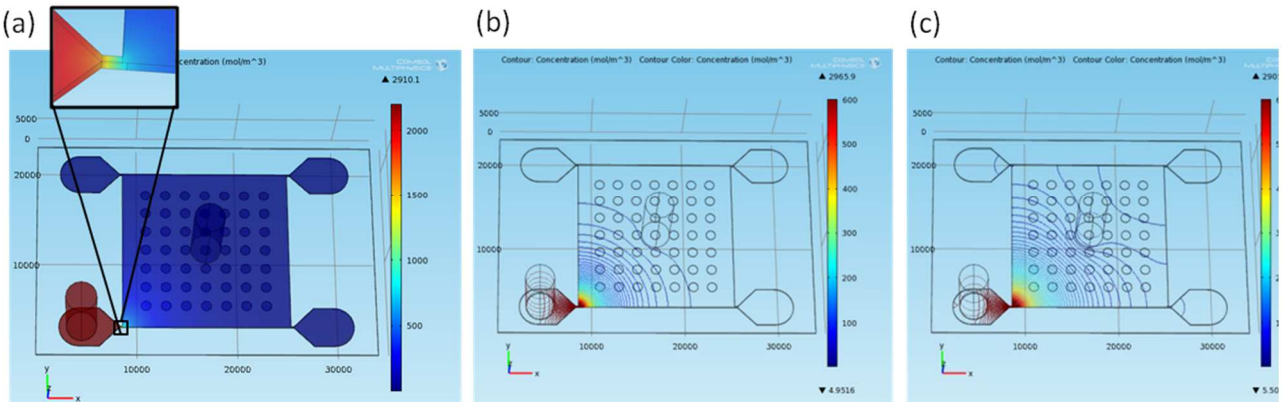

Figure 3-6 Simulation of NaN_3 diffusion in the dynamic dosing assay using COMSOL Multiphysics 4.1a.

(a) Computer model of the microfluidic diffusion layer geometry showing 49 biofilms in the diffusion field. The tall cylinder at the lower left corner is the perimeter source that contains the antimicrobial. The infinite sink is the tall cylinder in the center. Simulated color-coded concentration maps are provided showing lines of constant concentration at (b) t = 8.3 h and (c) t = 27.7 h.

3.4. Results and discussion

3.4.1 Constant-concentration Respiration Inhibition

As an independent check of the dynamic inhibition results, area-averaged net fluorescence and bright field intensities of individual biofilms and control positions were measured after exposure to fixed NaN_3 concentrations. The area-averaged bright field intensity of biofilm *i* is subtracted from average bright field intensities at a background control position. The magnitude of the difference was defined as the area-averaged opacity of each biofilm, as indicated by

$$Opacity_i = \left| I_{bf,i} - I_{bf,background} \right| \quad \text{(Eq. 3.2).}$$

Opacities of biofilms are assumed to be proportional to biofilm biomass, which varied in these experiments. Area-averaged net fluorescence intensities of individual biofilms following NaN_3 exposure were plotted against the corresponding opacities of each biofilm as a measure of biomass-normalized O_2 depletion as a function of NaN_3-induced respiration inhibition (Figure 3-7). For each antimicrobial concentration, biofilms with more biomass had greater opacity and also greater area-averaged net fluorescence intensity. Controlling for biomass, we found no statistically significant difference in specific fluorescence intensity for biofilms exposed to 0 versus 0.03 mM NaN_3. However, specific fluorescence is significantly quenched by higher NaN_3 concentrations of 0.1 mM ($p = 0.0112$) and 1 mM ($p < 0.001$). We conclude that NaN_3 starts to affect biofilm respiration at concentrations between 0.03 mM and 0.1 mM.

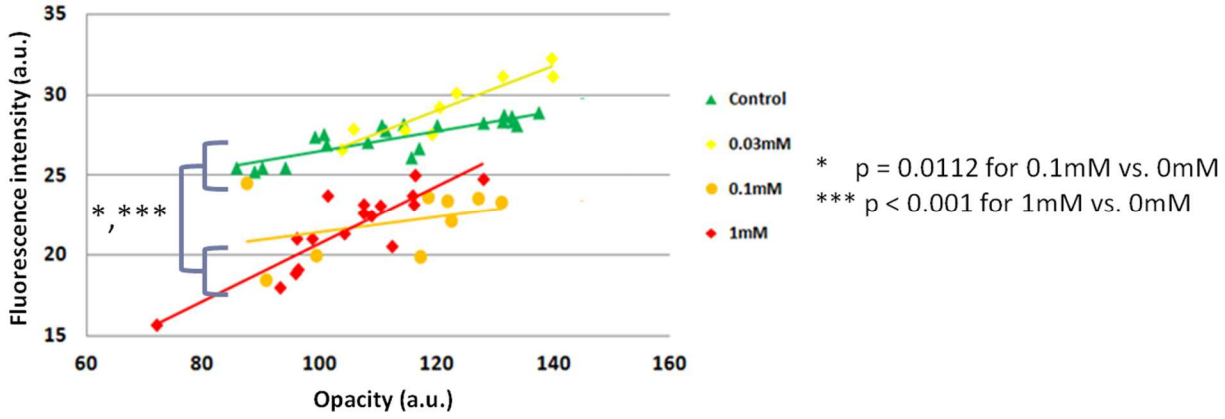

Figure 3-7 Area-averaged fluorescence intensity versus area-averaged opacity of biofilm exposed to different NaN_3 concentrations.

Area-averaged fluorescence intensity (a measure of O_2 depletion in arbitrary units) versus area-averaged opacity (a proxy for biomass in arbitrary units) plotted for individual biofilms gives a measure of baseline O_2 depletion and induced respiration inhibition with NaN_3 exposure for differently-sized biofilms. With exposure to a low NaN_3 concentration (0.03 mM), fluorescence intensity is similar to that of comparably-sized biofilms not exposed to antimicrobial. However, with exposure to NaN_3 concentrations greater than 0.03, biofilms of all sizes show a statistically significant decrease in specific fluorescence intensity. These results suggest respiration inhibition occurs at NaN_3 concentrations between 0.03 mM and 0.1 mM, consistent with time-dependent onset of respiration inhibition results.

3.4.2 Dynamic Respiration Inhibition

In duplicated diffusion experiments, either 6100 mM or 3100 mM NaN_3 solution was loaded in one source well of one of four different microfluidic diffusion chambers. We directly observed changing fluorescence intensities at the base of each biofilm in each array (Figure 3-8a),

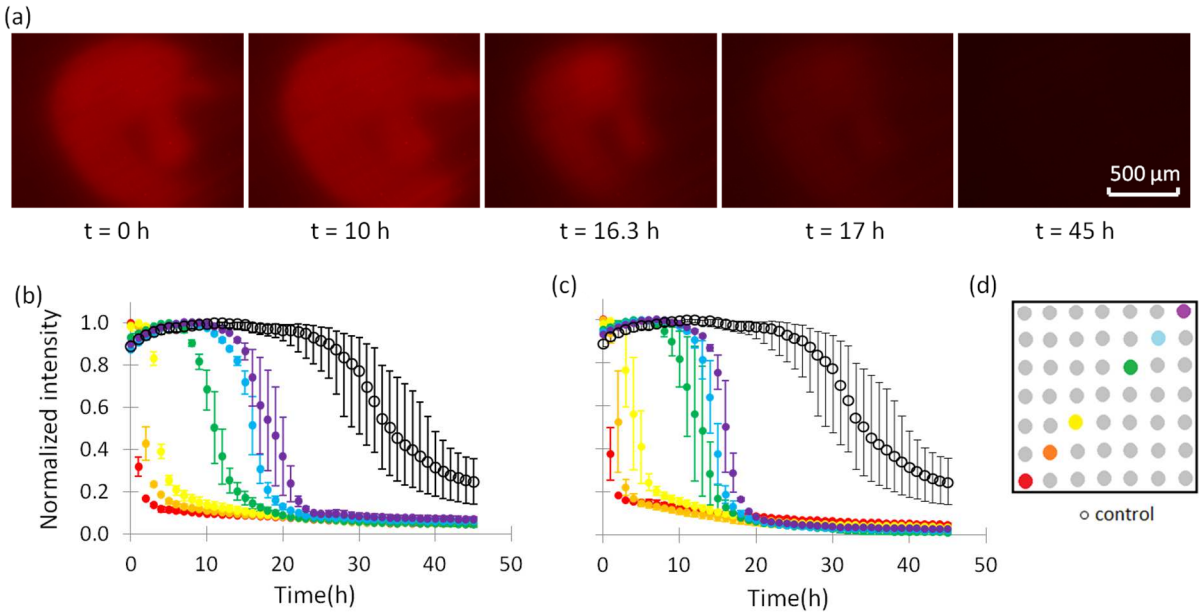

Figure 3-8 Real-time respiratory responses of individual biofilms with exposure of NaN_3.

(a) A representative time series of fluorescence images showing decrease of fluorescence intensity with NaN_3 exposure. Images correspond to blue curve in (b). (b, c) Colored markers: relative fluorescence intensities for six biofilms along a transect. Normalized intensity is area-averaged fluorescence intensity (see Eq. 3.1) normalized to maximum intensity observed for that biofilm. Source well loaded with 3100 mM (panel b) and 6100 mM (panel c) NaN_3 at t = 0. Data show average and range of replicate measurements in separate dynamic dosing assay devices. Open black marks: (control data) average of seven replicate biofilms exposed to 0 mM NaN_3. Error bars show range of replicate measurements. (See Figure 3-9 for data and position of control data). (d) Schematic of biofilm array showing color coding of positions along transect; source well is closest to the red dot in the lower left corner.

and quantified this intensity change as an area-averaged net fluorescence intensity as described above. A plot of normalized area-averaged net fluorescence intensity versus time (Figure 3-8b, c) shows the respiration responses for biofilms located along a diagonal transect. Biofilms located closest to the NaN_3-filled source well exhibit respiration inhibition first and biofilms located further away exhibit sequentially later respiration inhibition. Experiments were performed with two different NaN_3 concentrations loaded into the source wells. As expected, when a higher concentration is loaded into the source well, the driving force for diffusion is higher and the elapsed time before respiration inhibition is observed is correspondingly shorter.

3.4.3 Onset of Respiration Inhibition Time

Changes in fluorescence intensity at the base of each biofilm reflect the change in available O_2 due to changes in biofilm respiration. Healthy and actively respiring biofilms consume O_2 faster than it can be replenished by diffusion from the surroundings. Conversely, locations where biofilm respiration is inhibited by NaN_3 can experience a local increase in O_2 concentration (and therefore a quenching of fluorescence in the film). The normalized time course of fluorescence intensity at the base of the biofilm provides a measure of the changing respiration status of individual biofilms.

Although many applications will be interested in the complete time course of radial O_2 profiles, for simplicity and proof of principle, we focus on area-averaged net fluorescence intensity at one point in time for each biofilm. We define the onset of respiration inhibition (O.R.I.) time as the first of eight consecutive area-averaged net fluorescence intensity observations lower than the moving average of the four prior observations. O.R.I. time is a key moment because prior to the O.R.I. time, antimicrobial exposure is sufficiently low that O_2 is

consumed faster than it can be replenished by diffusion. In other words, respiration is limited by the biofilm's own utilization of O_2. After the O.R.I. time O_2 concentration at the biofilm base begins to increase, indicating O_2 is being replenished faster than it is consumed, and O_2 is no longer limiting. We determined O.R.I. times throughout replicate arrays loaded with different initial antimicrobial concentrations and related O.R.I. time to the corresponding local NaN_3 concentration determined from the 3-D diffusion simulation.

3.4.4 Intrinsic Respiration Inhibition

Eventually, biofilms not exposed to NaN_3 exhibit an intrinsic decrease in fluorescence intensity, presumably due to nutrient depletion. On Figure 3-8b and c, open markers show area-averaged net fluorescence intensity for 7 biofilms in a control experiment not exposed to respiration inhibitor (Figure 3-9). In our experiments, the intrinsic O.R.I. time averaged 14 hrs. Mathematical modeling determined that all positions in the array reach a NaN_3 concentration greater than 0.1 mM within 9.1 hrs (with the lower concentration, 3100 mM, loaded in the source well). Therefore, we interpret respiration inhibition observed in our experiments as resulting from NaN_3 exposure, not from intrinsic respiration inhibition. The time before intrinsic respiration inhibition occurs is the available diagnostic time domain. For slowly-diffusing substances, the available diagnostic time domain can be extended by using smaller biofilm dots and richer media in the gelatin (data not shown). For sparingly-soluble compounds, a modified version of the microfluidic device geometry with shorter, wider inlet dimensions should be considered.

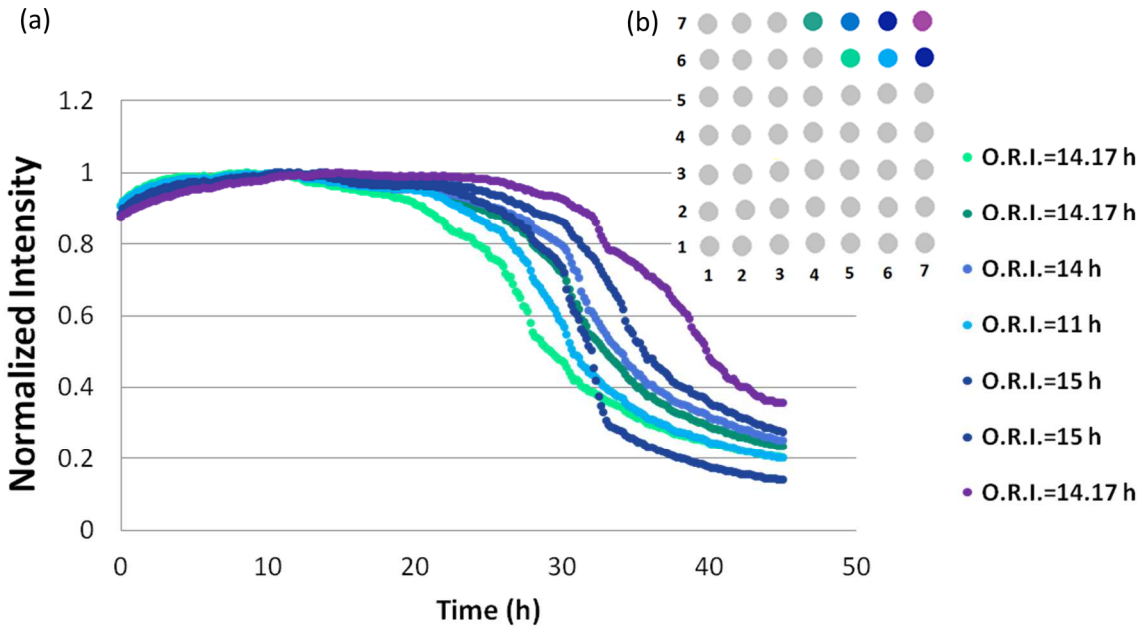

Figure 3-9 Fluorescence intensities of biofilms not exposed to NaN_3, with color coding indicating locations in the array.

Onset of Respiration Inhibition (O.R.I.) determined as described in the text is given for each biofilm. The averages of these data are shown with open black circles in Figure 4 as the background inhibition with 0 mM NaN_3.

3.4.5 Diffusion-based Respiration Inhibition Observed Across the Array

There are 21 biofilms in each array with a duplicate located across the diagonal axis of symmetry (Figure 3-10a). In addition, there are 6 diagonal elements with no replicate (the seventh position, located immediately under the sink well is excluded). Each replicated group ("Left" or "Right") plus the diagonal elements can be ordered from 1 to 27 based on predicted time to reach a threshold antimicrobial concentration (predicted rank from simulation, Figure 3-10b). Based on diffusion modeling, the first position to reach the threshold antimicrobial concentration is defined as position 1, and it is located nearest the source well. The last position to reach the threshold concentration is defined as position 27, and it is located farthest from the source well. Generally, ordering in the array proceeds according to straight-line distance between the source well and the biofilm, but there are exceptions. Positions 10, 16, and 20 are in close proximity to the central sink well, which depresses local concentrations.

For each biofilm position in each group, the time when O.R.I. was observed was ranked from 1 to 27 and defined as the observed rank. Then, this "observed rank" was plotted against the corresponding "predicted rank from simulation." The data show that the observed order in which biofilms exhibited respiration inhibition closely tracked the predicted ordering based on the diffusion simulation for both low (Figure 3-10c) and high (Figure 3-10d) NaN_3 concentrations. Note that predicted rank is not a function of test concentration. While antimicrobial concentration in the source well changes absolute O.R.I. time, it does not change the relative time among positions.

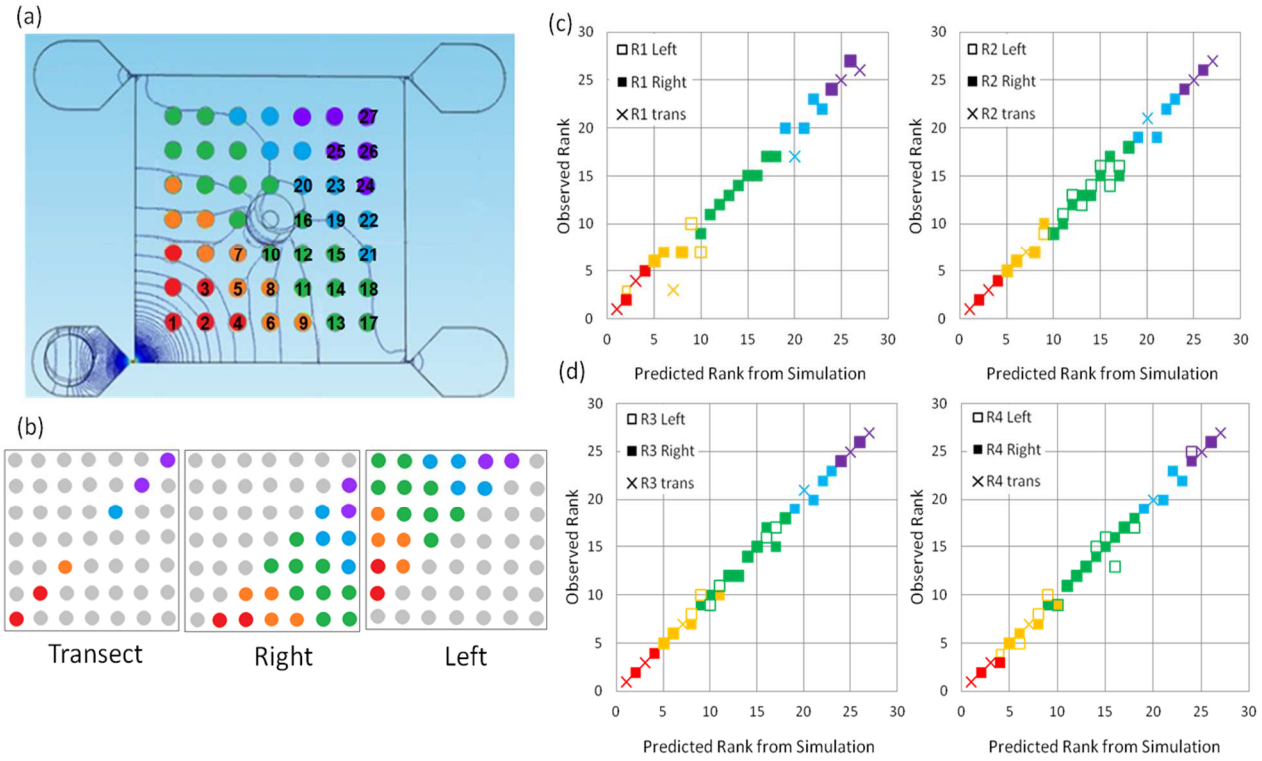

Figure 3-10 Ordering of observed onset of respiration for individual biofilm dots versus the predicted ranking based on the diffusion simulation.

(a) Schematic of biofilm array showing predicted ranking from 1-27 based on diffusion simulation for positions in the array. Inhibitor is placed in the source well nearest position 1. Biofilms are organized into five groups based on proximity to source well: Red group (positions 1-4), Orange group (positions 5-9); Green group (positions 10-18), Blue group (positions 19-23) and Purple group (positions 24-27) are shown. Contours represent constant flux at t = 27.7h. (b) Schematic showing diagonal symmetry of 27 elements, for a total of 48 positions. The biofilm beneath the sink well was excluded. (c) Replicates with 3100 mM in the source well. (d) Replicates with 6100 mM in the source well. Data are plotted using different markers for the left half of the array (open squares), the right half of the array (closed squares), and for diagonal elements (×). Color coding of the data shows locations of the biofilms in the array.

3.4.6 Onset of Respiration Inhibition Concentration

O.R.I. concentrations corresponding with measured O.R.I. times were determined for each position in each replicate dynamic respiration inhibition experiment (n = 192) using the diffusion simulation. The mean O.R.I. concentration for all dynamic experiments was 0.070 mM (see Figure 3-11 for all data), mid-way through the 0.03 to 0.1 mM range determined for the constant-concentration experiments. The inner 90% of O.R.I. values ranged from 0.012 mM to 0.12 mM with a standard deviation of 0.033.

We determined the influence of experimental treatment (3100 or 6100 mM), biofilm area, and antimicrobial dosing rate on the O.R.I. concentrations associated with the observed O.R.I. times. Experiments with 3100 mM in the source well (average O.R.I. concentration 0.073 ± 0.035, mean ± stdev) were not statistically different from experiments with 6100 mM in the source well (average O.R.I. concentration 0.068 ± 0.031, $p = 0.358$, t-test, 2-tailed). This is an important result because the user of the assay will generally not know the effective inhibitory concentration, and our assay allows for consistent respiration inhibition concentration results even when different source concentrations are used in the assay.

Biofilm surface area was measured by manually marking the outer perimeter of each biofilm bright field image as described above. The average area of our 192 test biofilms was 1.5 ± 0.26 mm^2 and ranged from 0.80 to 2.1 mm^2. (This area is slightly larger than the dimensions of the stamp because of spreading.) O.R.I. concentration was not significantly correlated with biofilm area ($\rho = 0.013$, $p = 0.862$). This result may seem counter-intuitive since, as biofilms are larger, the volume for O_2 consumption increases faster than the surface area for mass transport. However, our biofilms have a very small aspect ratio of depth compared with length or width, and a pseudo-1D geometry is suitable for all.

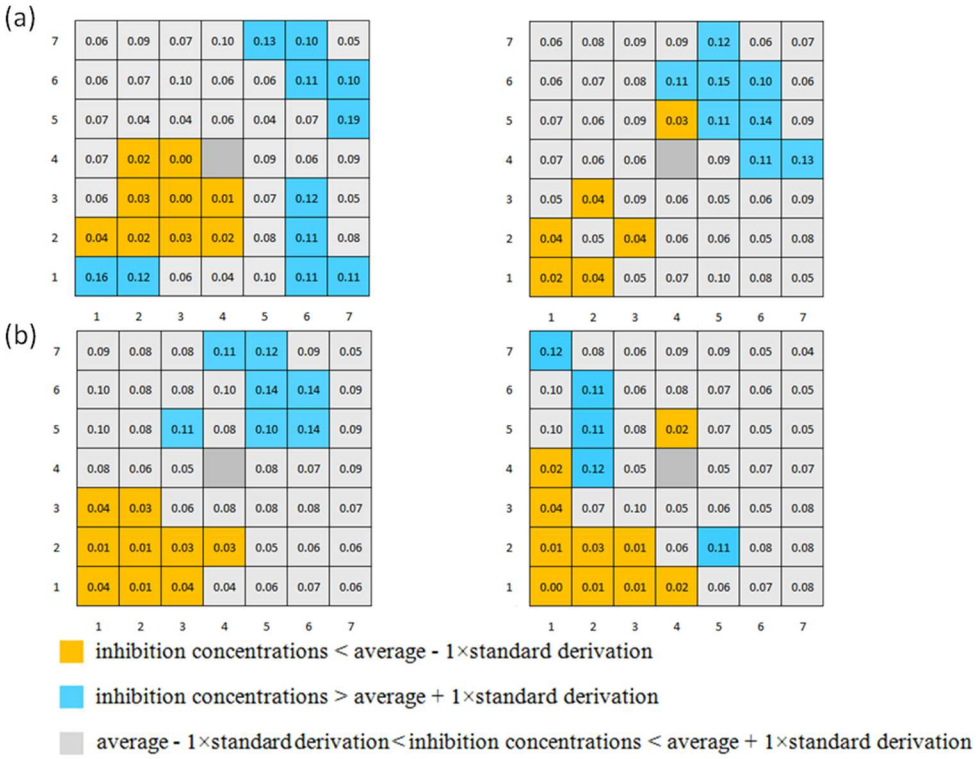

Figure 3-11 Heat maps of onset of respiration inhibition (O.R.I.) concentrations across replicate biofilm arrays.

O.R.I. concentration is defined for each biofilm by finding the simulated NaN_3 concentration corresponding to the coordinates of the biofilm and the time when onset of respiration was first observed (as defined in the text). Biofilm inhibition concentrations are shown for duplicate experiments with (a) 3100 mM or (b) 6100 mM NaN_3 added to source well (lower left corner) at t = 0.

Finally, we evaluated the correlation between O.R.I. concentration and position in the array. Here, position is also linked to the antimicrobial dosing rate. Biofilms were grouped into five zones based on proximity to the source well (Figure 3-10). Zone 1 (red), where the highest antimicrobial dosing rates were observed, includes elements 1-4; zone 2 (orange) includes elements 5-9; zone 3 (green) contains elements 10-18; zone 4 (blue) contains elements 19-23; and zone 5 (purple) contains elements 24-27. O.R.I. concentration increased with increasing distance from the source well (ANOVA, $p < 0.001$); however, the variation in O.R.I. concentration with position was slight. Average O.R.I. concentration (± stdev) by zone was 0.039 ± 0.036 for zone 1; 0.057 ± 0.030 for zone 2; 0.073 ± 0.024 for zone 3; 0.088 ± 0.027 for zone 4; and 0.088 ± 0.036 for zone 5. These results could be evidence of a slight dosing rate-dependence on *S. aureus* susceptibility to NaN_3. However, no mechanism is known for dosing rate-dependent susceptibility of *S. aureus* to NaN_3. The results could also be due to an artifact of the modeling assumptions, such as actual depletion of NaN_3 that is not captured by the model, or slight flaws in the geometry of the microfluidic diffusion chamber.

3.5 Conclusion

Respiratory responses of an array of biofilms to different antimicrobial concentrations and dosing rates can be determined using the dynamic dosing assay described here. Incorporation of an optical O_2 sensor allows local changes in respiration to be observed in real time as a function of a changing micro-chemical environment. Here we validated the assay by measuring respiration inhibition of S. *aureus* biofilms exposed to constant or dynamically-changing NaN_3 concentrations. The results showed that respiration inhibition was observed for NaN_3 exposures above approximately 0.07 mM, regardless of mode of exposure or size of the biofilms. A slight position dependence on the inhibitory concentration was observed. Measurement of actual NaN_3

concentrations throughout the array *in situ* would be needed to independently confirm dosing rate-related differences in biofilm susceptibility.

Unlike most commonly used methods to study biofilm susceptibility, our assay allows biofilm respiration inhibition to be observed in situ, and permits many different antimicrobial concentrations and dosing rates to be studied in parallel. Dosing rate is known to influence bacterial susceptibility to antibiotics through variable expression of antibiotic cleavage enzymes(Walsh 2000) or efflux pumps(Zakeri and Wright 2008) (short-term effect) or lateral gene transfer (longer-term effect). The assay described and validated here could be used to understand the effects of quickly- versus gradually-increasing or oscillating antimicrobial concentrations on evolution of tolerance and resistance in biofilm-associated bacterial populations.

Application of this assay for biofilm inhibition screening using conventional antimicrobials and antimicrobial combinations is the subject of ongoing work. Other extensions of this work include incorporation of additional spatially-resolved sensors of microbial activity, such as optical tracking of short-lifetime fluorescent proteins expressed by the bacteria. The method described here may accelerate the study of biofilm susceptibility to individual or combinatorial therapies, and may contribute mechanistic understanding of emerging biofilm resistance.

3.6 References

Anderl, J. N., M. J. Franklin, et al. (2000). "Role of antibiotic penetration limitation in Klebsiella pneumoniae biofilm resistance to ampicillin and ciprofloxacin." Antimicrobial Agents and Chemotherapy 44(7): 1818-1824.

Anderson, G. G. and G. A. O'Toole (2008). Innate and induced resistance mechanisms of bacterial biofilms. Bacterial Biofilms. 322: 85-105.

Ball, P., F. Baquero, et al. (2002). "Antibiotic therapy of community respiratory tract infections: strategies for optimal outcomes and minimized resistance emergence." Journal of Antimicrobial Chemotherapy. 49(1): 31-40.

Benoit, M. R., C. G. Conant, et al. (2010). "New Device for High-Throughput Viability Screening of Flow Biofilms." Applied and Environmental Microbiology 76(13): 4136-4142.

Brazier, J. S., R. Raybould, et al. (2008). "Distribution and antimicrobial susceptibility patterns of Clostridium difficile PCR ribotypes in English hospitals, 2007-08." Euro Surveill. 13(41).

Ceri, H., M. E. Olson, et al. (1999). "The Calgary Biofilm Device: New technology for rapid determination of antibiotic susceptibilities of bacterial biofilms." Jounal of Clinic Microbiology. 37(6): 1771-1776.

Chung, K., C. A. Rivet, et al. (2011). "Imaging Single-Cell Signaling Dynamics with a Deterministic High-Density Single-Cell Trap Array." Analytical Chemistry. 83(18): 7044-7052.

Crane, M. M., K. Chung, et al. (2010). "Microfluidics-enabled phenotyping, imaging, and screening of multicellular organisms." Lab on a Chip 10(12): 1509-1517.

Curtin, J., M. Cormican, et al. (2003). "Linezolid compared with eperezolid, vancomycin, and gentamicin in an in vitro model of antimicrobial lock therapy for Staphylococcus epidermidis central venous catheter-related biofilm infections." Antimicrobial Agents and Chemotherapy. 47(10): 3145-3148.

Cywinski, P. J., A. J. Moro, et al. (2009). "Ratiometric porphyrin-based layers and nanoparticles for measuring oxygen in biosamples." Sens Actuators, B: Chemical 135(2): 472-477.

Davies, D. (2003). "Understanding biofilm resistance to antibacterial agents." Nature Reviews Drug Discovery 2(2): 114-122.

Grate, J. W., R. T. Kelly, et al. (2012). "Silicon-on-glass pore network micromodels with oxygen-sensing fluorophore films for chemical imaging and defined spatial structure." Lab on a Chip 12(22): 4796-4801.

Hammoudi, T. M., H. Lu, et al. (2010). "Long-Term Spatially Defined Coculture Within Three-Dimensional Photopatterned Hydrogels." Tissue Engineering, Part C: Methods 16(6): 1621-1628.

Herzberg, M. and M. Elimelech (2007). "Biofouling of reverse osmosis membranes: Role of biofilm-enhanced osmotic pressure." Journal of Membrane Science 295(1-2): 11-20.

Houari, A. and P. Di Martino (2007). "Effect of chlorhexidine and benzalkonium chloride on bacterial biofilm formation." Letters in Applied Microbiology. 45(6): 652-656.

Kim, J., M. Hegde, et al. (2012). "A microfluidic device for high throughput bacterial biofilm studies." Lab on a Chip 12(6): 1157-1163.

Kim, K. P., Y.-G. Kim, et al. (2010). "In situ monitoring of antibiotic susceptibility of bacterial biofilms in a microfluidic device." Lab on a Chip 10(23): 3296-3299.

Laitinen, H. A. and I. M. Kolthoff (1939). "A Study of Diffusion Processes by Electrolysis with Microelectrodes." Journal of the American Chemical Society 61(12): 3344–3349.

Lam, R. H. W., M.-C. Kim, et al. (2009). "Culturing Aerobic and Anaerobic Bacteria and Mammalian Cells with a Microfluidic Differential Oxygenator." Analytical Chemistry 81(14): 5918-5924.

Lee, J.-H. L. J. B. K. W. Y. (2008). "Microfluidic devices for studying growth and detachment of Staphylococcus epidermidis biofilms." Biomedical Microdevices 10: 489-498.

Lichstein, H. C. and M. H. Soule (1944). "Studies of the Effect of Sodium Azide on Microbic Growth and Respiration: I. The Action of Sodium Azide on Microbic Growth." Journal of Bacteriology 47(3): 221-230.

Lichstein, M. L. S. A. H. C. (1940). "Sodium azide as an inhibiting substance for gram-negative bacteria." The Journal of Infectious Diseases 67: 113-115.

Macia, M. D., J. L. Perez, et al. (2011). "Dynamics of Mutator and Antibiotic-Resistant Populations in a Pharmacokinetic/Pharmacodynamic Model of Pseudomonas aeruginosa Biofilm Treatment." Antimicrobial Agents and Chemotherapy 55(11): 5230-5237.

Matz, C., D. McDougald, et al. (2005). "Biofilm formation and phenotypic variation enhance predation-driven persistence of Vibrio cholerae." Proceeding of the National Academy of Sciences 102(46): 16819-16824.

McBrady, A. D., R. Chantiwas, et al. (2006). "An absorbance-based micro-fluidic sensor for diffusion coefficient and molar mass determinations." Analytica Chimica Acta 575(2): 151-158.

Merritt, J. H., D. E. Kadouri, et al. (2005). "Growing and analyzing static biofilms." Current Protocols in Microbiology. Chapter 1.

Meyer, M. T., V. Roy, et al. (2011). "Development and validation of a microfluidic reactor for biofilm monitoring via optical methods." Journal of Micromechanics and Microengineering. 21(5).

Montagne, K., K. Komori, et al. (2009). "A micropatterned cell array with an integrated oxygen-sensitive fluorescent membrane." Photochemical & Photobiological Sciences 8(11): 1529-1533.

Morten Hentzer, G. M. T., Grant J. Balzer, Arne Heydorn, and M. G. Soeren Molin, and Matthew R. Parsek (2001). "Alginate Overproduction Affects Pseudomonas aeruginosa Biofilm Structure and Function." Journal of Bacteriology 183(5395-5401).

Muesken, M., S. Di Fiore, et al. (2010). "A 96-well-plate-based optical method for the quantitative and qualitative evaluation of Pseudomonas aeruginosa biofilm formation and its application to susceptibility testing." Nature Protocols 5(8): 1460-1469.

Nelson, L. K., M. M. Stanton, et al. (2010). "Phenotypic diversification in vivo: Pseudomonas aeruginosa gacS(-) strains generate small colony variants in vivo that are distinct from in vitro variants." Microbiology 156: 3699-3709.

Nishimura, S., T. Tsurumoto, et al. (2006). "Antimicrobial susceptibility of Staphylococcus aureus and Staphylococcus epidermidis biofilms isolated from infected total hip arthroplasty cases." Journal of Orthopaedic Science 11(1): 46-50.

Olson, M. E., S. R. Slater, et al. (2010). "Rifampicin enhances activity of daptomycin and vancomycin against both a polysaccharide intercellular adhesin (PIA)-dependent and -independent Staphylococcus epidermidis biofilm." Journal of Antimicrobial Chemotherapy 65(10): 2164-2171.

Or, D., S. Phutane, et al. (2007). "Extracellular polymeric substances affecting pore-scale hydrologic conditions for bacterial activity in unsaturated soils." Vadose Zone Journal 6(2): 298-305.
Pagedar, A., J. Singh, et al. (2012). "Adaptation to benzalkonium chloride and ciprofloxacin affects biofilm formation potential, efflux pump and haemolysin activity of Escherichia coli of dairy origin." Journal of Dairy Research 79(4): 383-389.
Park, A., H.-H. Jeong, et al. (2011). "Effect of shear stress on the formation of bacterial biofilm in a microfluidic channel." BioChip Journal 5(3): 236-241.
Park, E. S., A. C. Brown, et al. (2010). "Continuously perfused, non-cross-contaminating microfluidic chamber array for studying cellular responses to orthogonal combinations of matrix and soluble signals." Lab on a Chip 10(5): 571-580.
Pereira, S. G., J. Paixao, et al. (2011). "Pseudomonas aeruginosa in a hydropathic facility: diversity, susceptibility and imipenem resistance mutation." Letters in Applied Microbiology 53(5): 518-524.
Perez, F., R. Salata, et al. (2008). "Current and novel antibiotics against resistant Gram-positive bacteria." Infection and Drug Resistance: 27-44.
Presterl, E., S. Hajdu, et al. (2009). "Effects of Azithromycin in Combination with Vancomycin, Daptomycin, Fosfomycin, Tigecycline, and Ceftriaxone on Staphylococcus epidermidis Biofilms." Antimicrobial Agents and Chemotherapy 53(8): 3205-3210.
Rao, T. S., A. J. Kora, et al. (2009). "Biofouling and microbial corrosion problem in the thermo-fluid heat exchanger and cooling water system of a nuclear test reactor." Biofouling 25(7): 581-591.
Rowan, B., M. A. Wheeler, et al. (2002). "Patterning bacteria within hyperbranched polymer film templates." Langmuir 18(25): 9914-9917.
Rusconi, R., S. Lecuyer, et al. (2010). "Laminar flow around corners triggers the formation of biofilm streamers." Journal of the Royal Society, Interface 7(50): 1293-1299.
Sauer, K., A. K. Camper, et al. (2002). "Pseudomonas aeruginosa displays multiple phenotypes during development as a biofilm." Journal of Bacteriology. 184(4): 1140-1154.
Shumi, W., J. Lim, et al. (2010). "Environmental factors that affect Streptococcus mutans biofilm formation in a microfluidic device mimicking teeth." BioChip Journal 4(4): 257-263.
Skolimowski, M., M. W. Nielsen, et al. (2010). "Microfluidic dissolved oxygen gradient generator biochip as a useful tool in bacterial biofilm studies." Lab on a Chip 10(16): 2162-2169.
Stewart, P. S. (1998). "A review of experimental measurements of effective diffusive permeabilities and effective diffusion coefficients in biofilms." Biotechnology and Bioengineering 59(3): 261-272.
Stewart, P. S., W. M. Davison, et al. (2009). "Daptomycin Rapidly Penetrates a Staphylococcus epidermidis Biofilm." Antimicrobial Agents and Chemotherapy 53(8): 3505-3507.
Stewart, P. S. and M. J. Franklin (2008). "Physiological heterogeneity in biofilms." Nature Reviews Microbiology 6(3): 199-210.
Strovas, T. J., J. M. Dragavon, et al. (2006). "Measurement of respiration rates of Methylobacterium extorquens AM1 cultures by use of a phosphorescence-based sensor." Applied and Environmental Microbiology 72(2): 1692-1695.

Surdeau, N., D. Laurent-Maquin, et al. (2006). "Sensitivity of bacterial biofilms and planktonic cells to a new antimicrobial agent, Oxsil (R) 320N." Journal of Hospital Infection 62(4): 487-493.

Takenaka, S., H. M. Trivedi, et al. (2008). "Direct visualization of spatial and temporal patterns of antimicrobial action within model oral biofilms." Applied and Environmental Microbiology 74(6): 1869-1875.

Tian, Y. Q., B. R. Shumway, et al. (2010). "A New Cross-Linkable Oxygen Sensor Covalently Bonded into Poly(2-hydroxyethyl methacrylate)-co-Polyacrylamide Thin Film for Dissolved Oxygen Sensing." Chemistry of Matererials 22(6): 2069-2078.

Waharte, F., K. Steenkeste, et al. (2010). "Diffusion Measurements inside Biofilms by Image-Based Fluorescence Recovery after Photobleaching (FRAP) Analysis with a Commercial Confocal Laser Scanning Microscope." Applied and Environmental Microbiology 76(17): 5860-5869.

Walsh, C. (2000). "Molecular mechanisms that confer antibacterial drug resistance." Nature 406(6797): 775-781.

Weibel, D., A. Lee, et al. (2005). "Bacterial printing press that regenerates its ink: Contact printing bacteria using hydrogel stamps." Langmuir 21: 6436-6442.

Weibel, D. B., W. R. DiLuzio, et al. (2007). "Microfabrication meets microbiology." Nature Reviews Microbiology 5(3): 209-218.

Weller, D. M. (1988). "Biological Control of Soilborne Plant Pathogens in the Rhizosphere with Bacteria " Annual Review of Phytopathology 26: 379-407.

Xu, L., L. Robert, et al. (2007). "Microcontact printing of living bacteria arrays with cellular resolution." Nano Letters 7(7): 2068-2072.

Zakeri, B. and G. D. Wright (2008). "Chemical biology of tetracycline antibiotics." Biochemistry and. Cell Biology 86(2): 124-136.

Zhang, W., T. S. Sileika, et al. (2011). "A novel planar flow cell for studies of biofilm heterogeneity and flow-biofilm interactions." Biotechnology and Bioengineering 108(11): 2571-2582.

Chapter 4 Real-time Respiratory Inhibition of *Staphylococcus aureus* Biofilms with Daptomycin Exposure[2]

4.1 Abstract

The structured architecture of a biofilm promotes phenotypic differentiation with position, and biofilm bacteria are much less susceptible to antimicrobials than similar cells suspended in liquid culture. Unfortunately, existing antimicrobial screening techniques either do not maintain the essential biofilm morphology, or do not capture the dynamic nature of biofilm responses. Here, the dynamic respiratory responses of intact *Staphylococcus aureus* biofilms were determined during exposure to Daptomycin. Biofilm arrays were contact-printed on a glass substrate coated with an oxygen-sensing polymer film. The geometry of contact-printed biofilms was characterized using white light interferometry. The changing oxygen concentration was measured optically at the base of each biofilm during 24h exposure to different concentrations of Daptomycin. Then, the changing bulk aerobic respiration rate for biofilms was inferred using a three-dimensional diffusion and reaction model. The results show bulk aerobic respiration rates decrease more rapidly when biofilms are exposed to higher external Daptomycin concentration. Further, bulk aerobic respiration rates stabilize to a lower value when biofilms are exposed to higher external Daptomycin concentrations, and stabilize to a higher value when biofilms are exposed to relatively lower external Daptomycin concentrations. These results may suggest biofilms exposed to higher Daptomycin concentrations may contain lower abundances of slowly-respiring persister cells compared with biofilms exposed to lower Daptomycin concentrations.

[2] In preparation as Deng J, and Shor LM. Real-time Respiratory Inhibition of *Staphylococcus aureus* Biofilms with Daptomycin Exposure.

This research offers insights into the internal function of intact microbial biofilms, and may be useful in determining how antimicrobial type, concentration, and delivery rate act together to promote effectiveness and deter induced resistance in biofilms.

4.2 Introduction

Microbial biofilms are aggregated bacteria, typically on a surface, where individual cells are embedded in a matrix of extracellular polymeric substance (EPS). Bacterial biofilm can tolerate antimicrobial concentrations orders of magnitude higher than dispersed bacteria in liquid culture (Nishimura et al. 2006; Surdeau et al. 2006). Mechanisms for increased antibiotic resistance include: (i) oxygen and nutrient depletion with position leading to phenotypic differentiation (ii) reduced rates of antimicrobial diffusion in the self-secreted extracellular polymeric substance; (iii) increased rates of lateral gene transfer of resistance genes among bacteria.

Minimum Inhibition Concentration (MIC) and Minimum Biofilm Eradicate Concentration (MBEC) are the most widely used criteria to characterize biofilm antimicrobial susceptibility. MIC is usually measured in the planktonic (liquid) state, and MBEC is measured for biofilm. To measure MBEC, biofilm are usually exposed to a series of constant antimicrobial concentrations for 24 to 72h, followed with CFU counting or optical density measurement at the end of antibiotic treatment (LaPlante and Mermel 2007). However, current techniques for antimicrobial susceptibility measurement cannot investigate dynamic responses of bacteria during antimicrobial exposure. Due to various operational issues, reported values of MBEC measured with different protocols vary widely (Brazier et al. 2008) (Salmon and Watts 2000) (Schuurmans et al. 2009).

As described in Chapter 2, Daptomycin is one of the most effective antibiotics for treating biofilms of *Staphylococcus aureus*. However, reports of Daptomycin resistance are increasing. Practical tools are needed to study the response of bacteria in intact biofilm during Daptomycin exposure. Recently, several methods have emerged to measure responses of biofilm in real time during antimicrobial exposure. For example, Buchholz et al. used a chip calorimeter to study changes of heating production rate of biofilm during antimicrobial treatment (Buchholz et al. 2010). They observed increase in the measured heat production of biofilm at the beginning of antimicrobial administration followed by large reduction. Richter et al. employed electrical impedance to measure surface coverage of biofilm on planar electrodes (Richter et al. 2009). However, these techniques rely on indirect measures of biofilm health status upon antibiotic exposure. It is difficult to interpret the significance of a heat production rate or electrical impedance with respect to biofilm inhibition with antibiotic exposure. No prior work has related dynamic changes in biofilm respiratory activity with antimicrobial exposure during treatment.

Here we describe a composite approach including microfabrication, optical sensing, and mathematical modeling to determine the respiratory state of intact biofilms during antimicrobial exposure. This work overcomes the limitations of existing methods, and to offers a more comprehensive and fundamental understanding of biofilm respiratory changes during antibiotic exposure. Here, arrays of biofilms were contact-printed onto an oxygen sensing film, then biofilms were embedded in hydrogel containing different Daptomycin concentrations. The changing intensity of an oxygen-quenched fluorescent reporting molecule immobilized at the base of the biofilms in the array directly reflects the changing oxygen concentration caused by changes in the bulk respiration rate.

During antibiotic exposure, bacteria inside biofilm are inhibited and consume oxygen more slowly than healthy bacteria not exposed to antibiotic. The difference in the bulk oxygen consumption rate with no antibiotic and during antibiotic exposure is scaled and reported as "Respiratory Index", a bulk measure of respiratory status. This technique can provide information about the effectiveness of different antimicrobials, antimicrobial doses, and dosing regimes (i.e., how quickly an antibiotic concentration increases to a steady-state value, or the way concentration may oscillate with time). Relating dose and/or dosing regime with the changing respiratory state of biofilms provides a practical means to optimize antimicrobial treatments and potentially avoid induced resistance of biofilms in the clinical setting.

4.3 Materials and Methods

4.3.1. Bacterial Strains and Biofilm Formation

Staphylococcus aureus (ATCC 25904) was incubated in Tryptic Soy Broth (TSB) at 37 ˚C overnight. Stationary culture was adjusted to OD_{595} 1.1 using fresh TSB. Then, 300 μl of the adjusted liquid culture was transferred onto a Tryptic Soy Agar (TSA) plate and evenly spread by shaking 2 mm sterilized glass across the plate surface. Plates were incubated at 37 C for 9 hrs in humid air, resulting in a homogenous bacterial lawn.

4.3.2. Device Fabrication

The microfluidic device was fabricated using standard methods of photolithography and softlithography, and is described elsewhere (Deng et al. 2013b). Briefly, 200 μm of SU-8 2100 was spin coated on a 3 inch diameter silicon wafer. The coated wafer was then selectively exposed for 11 s to 45 mW/cm^2 UV light using a Mylar photolithography mask. After baking at

95˚C, un-crosslinked SU-8 was removed using SU-8 developer, the mask was rinsed in DI water, and dried under an N_2 stream. Individual microfluidic devices were cast from the master using Polydimethylsiloxane (PDMS, Sylgard 184, Dow Corning, Midland, MI) that had been mixed 10:1 base to curing agent, and degassed in a vacuum dessicator at -75 kPa gage for 20 min. After curing at 60 C for 2 hours, devices were removed from the master, and access ports were created with a 2 mm biopsy punch.

Oxygen sensing films were fabricated as described previously (Deng et al. 2013b). Briefly, 5 ml polyvinyl alcohol (PVA) dissolved in DI water (1:100 w/v) was spin coated on a clean glass slide at 4000 rpm for 30 s. Then 5 ml of Pt (II) meso tetra-(pentafluorophenyl) porphyrin (Frontier Scientific Inc., Logan, UT) dissolved in premade polystyrene-toluene solution (1:15 w/v) was spin coated on top of the PVA layer at 4000 rpm for 30 s. The ratio of Pt (II) reporting molecule to polystyrene was 1:100. Finally, the oxygen sensing film was coated with PDMS using 8 ml of PDMS mixed 10:1 with cross-linking agent then thinned (2:1 w/v) with hexanes. The PDMS layer was spin coated as follows: ramp to 500 rpm in 5 s, hold for 13 s, then ramp to 2700 rpm in 7 s and hold for 1 min. Coated slides were cured at 60 C for 2 h before use.

Bacterial biofilm arrays were patterned over PDMS-coated oxygen sensing films. However, before patterning, the oxygen sensing film was plasma-activated using a plasma cleaner (Harrick PDC-32G, Harrick Plasma, Ithaca, NY) for 45 s to enable subsequent bonding of the PDMS microfluidic device to the PDMS-coated oxygen sensing film substrate. Then the biofilm array was contact-printed onto the activated sensor from the bacterial lawn using a custom-fabricated PDMS stamp. 6 ×6 pegs in the stamp were arranged in an array, and diameter

of individual peg is 500 μm. Then, the PDMS microfluidic device was plasma treated for 45 s and immediately bonded onto the oxygen sensing film, taking care to carefully align the biofilm array with the square-shaped microfluidic chamber.

The concentrations of Daptomycin tested were 0 mM, 0.031 mM, 0.0625 mM, 0.125 mM, 0.25 mM, 0.5 mM and 1 mM. There were 2 replicate devices prepared for each concentration, and at least 10 individual biofilms were imaged across all concentration (the actual number of biofilms imaged for each Daptomycin was 10, 23, 10, 31, 32, 37, and 26, respectively).

In preparing the microfluidic devices, sterile triple-strength TSA containing 0.3% agar, Daptomycin, and 1mM Ca^{2+} was loaded into the microfluidic device. After filling each device with agar, the corner wells were immediately covered with clear tape to prevent drying. In the completed device, each biofilm were embedded in 200 μm agar, and the agar field was contained within an 8 mm-thick PDMS microfluidic device (Figure 4-1).

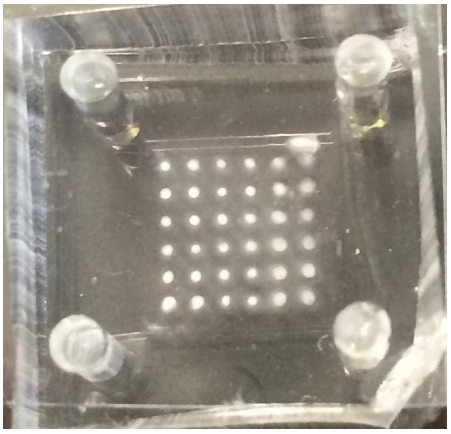

Figure 4-1 Micrograph of of PDMS microfluidic device filled with agar and containing a 6 × 6 array of contact-printed biofilms patterned over an oxygen sensing film.
Scale bar = 2 mm.

4.3.3. Imaging and Image Analysis

The microfluidic device was immediately placed on a Carl Zeiss AXIO-observer Z1 automated fluorescent microscope equipped with an AxioCam MRmREV.3 camera (Carl Zeiss Inc., Germany). A position list was created, corresponding with the coordinates of the oxygen sensing film immediately beneath each biofilm in the array. Fluorescent images were collected using a 5× objective (Zeiss ECPlan-NEOFLUAR; 5×/0,16 ∞/0,17, Carl Zeiss Inc., Germany) at 5 min intervals for a total of 24 h. In all experiments, the first fluorescent image was taken roughly 5 min after loading of the device due to the time required to create the position list of biofilm locations. Bright field images of all biofilms were also collected at the end of 24h antibiotic treatment, to define the footprint of each biofilm.

Fluorescent intensities of each biofilms were analyzed using the open-source software package Fiji, as described elsewhere (Deng et al. 2013b). Briefly, the footprint of each biofilm was determined from the bright field image at the end of experiments. Then, the averaged fluorescence intensity within the footprint of each biofilm was computed at each time point. Fluorescence intensity of the oxygen sensing film below biofilms reflects the bulk respiration state of the biofilm during exposure to different Daptomycin concentrations (see section 4.5.1 Figure 4-6a).

4.3.4 Oxygen Sensing Film Calibration

Fluorescence response of the oxygen sensing film was quantitatively calibrated by determining relative fluorescence intensity of 3 replicate films in contact with known aqueous concentrations. Aqueous oxygen concentrations were measured using a 40 μm diameter needle oxygen microsensor probe (NTH-PSt1-L5-TF-NS40/0.8-OIW, PreSens Precision Sensing GMBH, Germany). First, DI water was de-gassed by sonication under vacuum for 30 min, then by sparging with nitrogen or argon for 20 min. Oxygen-free water was transferred to a 2 cm × 3 cm PDMS chamber plasma bonded onto the oxygen sensing film. The film beneath the fluid was imaged every 15 s for 2 min with 20 min intervals during which time oxygen continued to dissolve into the water from the ambient atmosphere. The average of 8 positions in each of 3 films was determined. Averaged fluorescence intensity of each sets of measurements were plotted against the averaged oxygen concentration measured using the oxygen microsensor probe. The response time for both the film and the probe was determined separately, and is < 10 s (data not shown). In this way, a series of oxygen concentrations could be measured for initially oxygen-free fluid that remains open to the atmosphere. The resulting fluorescence response curve (Figure 4-2) was fit to a logarithmic curve, with the coefficient of determination (R^2) = 0.968. The equation for the log-linear fit was used to convert normalized fluorescence intensity into oxygen concentration.

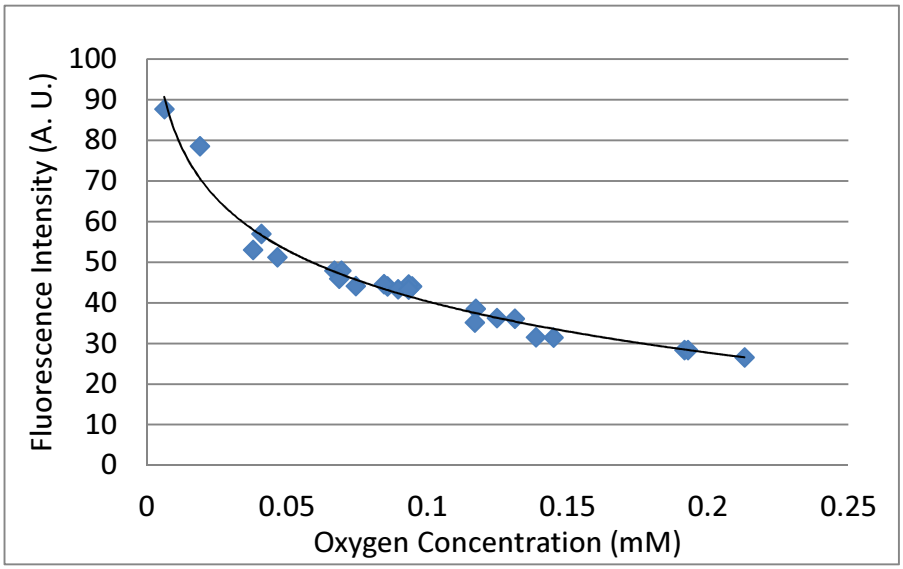

Figure 4-2 Oxygen sensing film calibration.

Fluorescence intensity reversibly indicates the local oxygen concentration. Data fit into curve with R^2=0.968.

4.3.5 Characterization of Typical Geometry of Contact-printed Biofilms

Geometries of contact printed biofilms were measured using White Light Interferometry (New View 5000, Zygo Corporation, CT). Biofilms were contact printed on a glass substrate and then sputtered with gold vapor for 50 s to create a metallic coating with increased light reflection. The following parameters were determined for each of five biofilms: height at edge and center, diameter, and center location (Figure 4-3 and 4-4). These values were then averaged to create a typical contact-printed biofilm geometry used in 3D diffusion reaction modeling (Figure 4-3d).

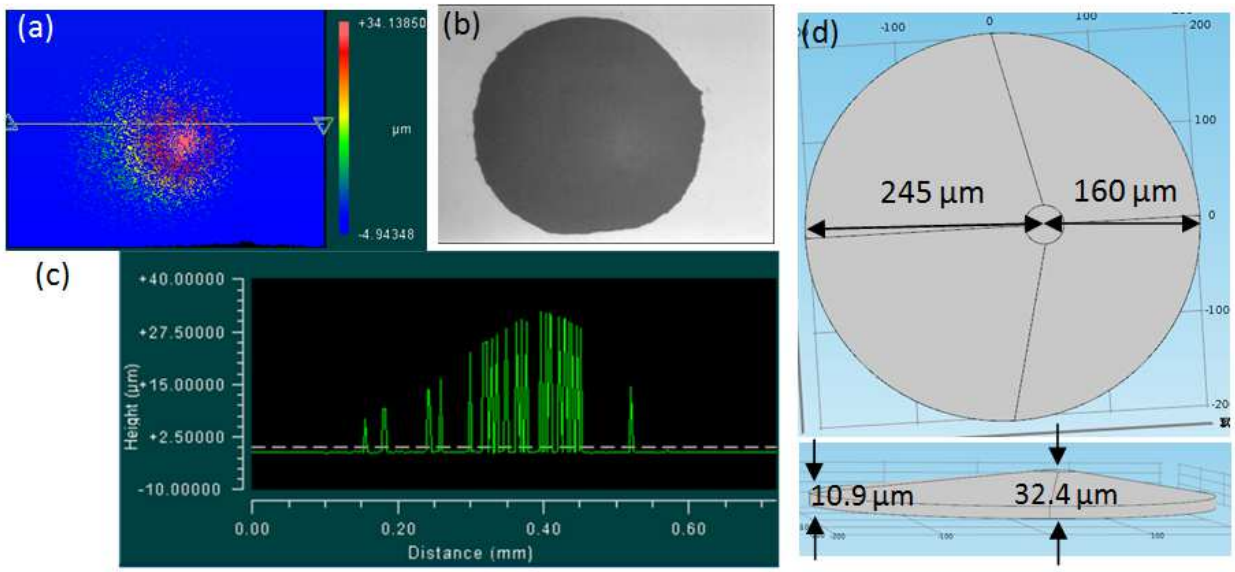

Figure 4-3 White light interferometry measurement of contact printed biofilm geometry.

(a) Surface measurement of relative height of a typical biofilm. Height at biofilm center is higher than the edge. (b) Bright field image of the same biofilm. (c) Height profile of a transect across the biofilm. (d) Typical contact-printed biofilm geometry used in COMSOL modeling. The geometry was averaged from the measurements of five typical contact printed biofilms.

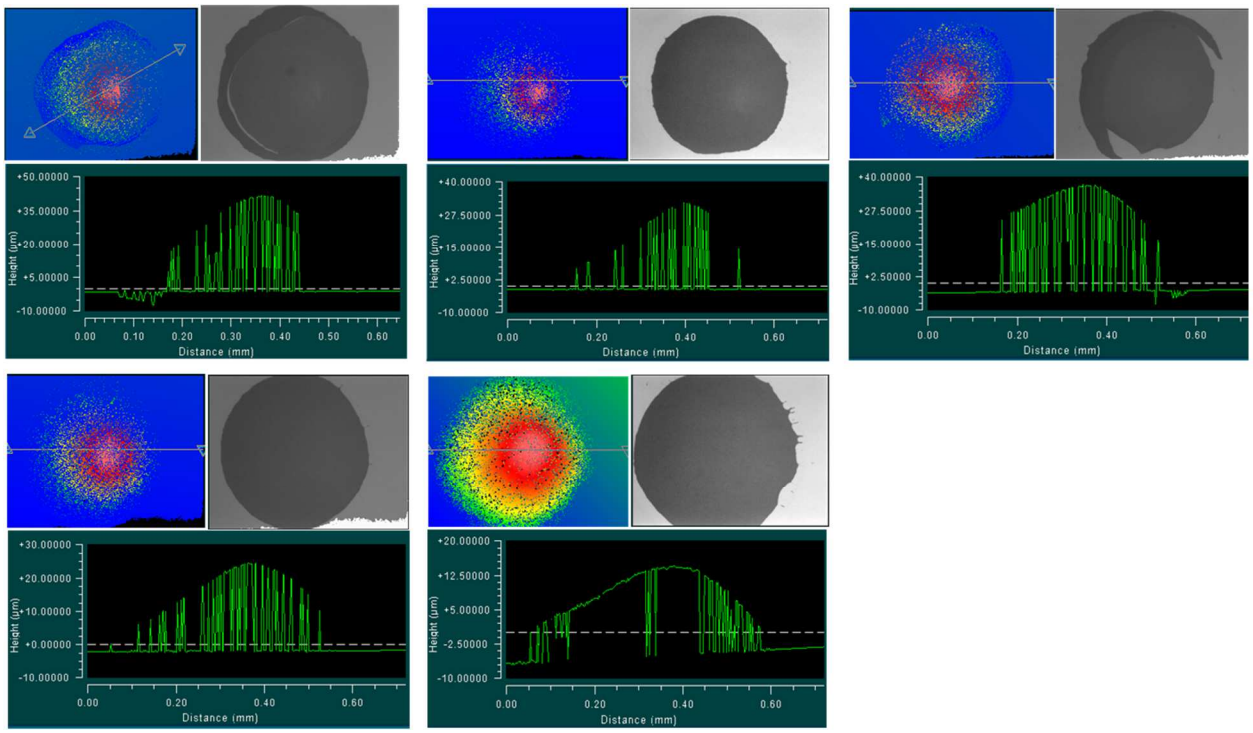

Figure 4-4 Geometry of five biofilms in an array measured using white light interferometry.

4.4 Modeling

In the model, a single simplified unit cell was modeled, using the measured typical biofilm geometry, and embedding that biofilm in an idealized 1.2 mm × 1.2 mm × 200 μm square agar block. This geometry reflects the 1.2 mm spacing of individual biofilms in the array, and the height of the microfluidic device chamber of 200μm.

Oxygen diffusion and consumption in a 3D biofilm embedded was modeled using COMSOL Multiphysics 4.3b as follows (Figure 4-5):

$$\frac{\partial c}{\partial t} = D\left(\frac{\partial^2 c}{\partial x^2} + \frac{\partial^2 c}{\partial y^2} + \frac{\partial^2 c}{\partial z^2}\right) + k; \qquad \text{(Eq. 4.1)}$$

where k is zero order oxygen consumption rate [mol/(m^3 s)], c is oxygen concentration in biofilm [mM]. The initial and boundary conditions in the modeling are listed as below:

$I.C.: t = 0, \quad c = 0.204\ mM \quad \forall x, y, z;$

$B.C.1: x = 0\ \mu m, \quad \frac{\partial c}{\partial x} = 0; \forall y, z;\ \forall t;$

$B.C.2: x = 200\ \mu m, \quad c = 0.204\ mM;\ \forall y, z;\ \forall t;$

$B.C.3: y = -0.6\ mm\ and\ y = +0.6\ mm, \quad \frac{\partial c}{\partial y} = 0\ , \forall x, z;\ \forall t;$

$B.C.4: z = -0.6\ mm\ and\ z = +0.6\ mm, \quad \frac{\partial c}{\partial z} = 0\ , \forall x, y;\ \forall t;$

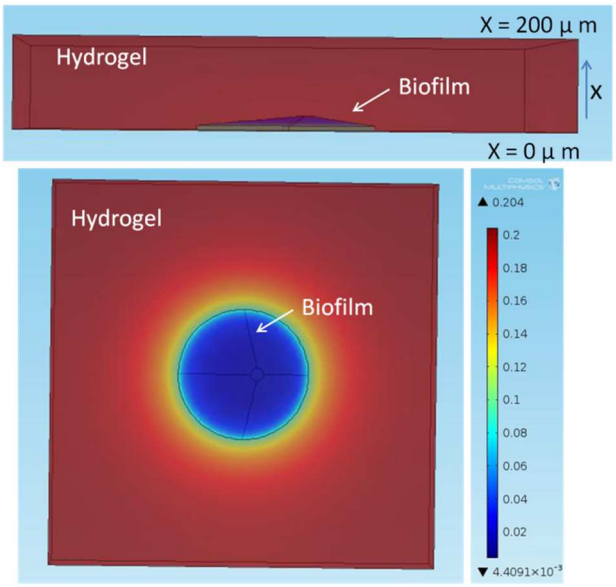

Figure 4-5 COMSOL Multiphysics model used to infer bulk oxygen consumption rate *k* from the measured oxygen concentration at the base of individual biofilms.

Color map indicates steady state oxygen concentration in hydrogel and biofilm for a given *k*.

The initial oxygen concentration in 0.3% agar containing TSB was assumed to be 0.204 mM, as reported at steady state in phosphate buffer in equilibrium with air (Shiku et al. 2006). The initial concentration of oxygen in biofilm was also assumed to be 0.204 mM. The steady state oxygen concentration in PDMS in equilibrium with air is reported to be 2 mM (Shiku et al. 2006). The much higher concentration of oxygen in PDMS, together with the large volume ratio of PDMS to hydrogel (40:1) and to biofilm (>70000:1), make the PDMS a reservoir for oxygen. Therefore we assume a constant concentration boundary condition at all TSB-PDMS interfaces equal to 0.204 mM throughout the experiment.

The diffusivity of oxygen through 0.7% agar was reported to 98.3% of that in water (Van der Meeren et al. 2001). Therefore, we assume the diffusivity through 0.3% agar to be the same as the free aqueous diffusivity of oxygen in water in room temperature, or 2.1×10^{-9} m^2/s (Han and Bartels 1996). The mean effective diffusive permeability of oxygen through biofilm is 48% of the diffusion coefficient in pure water in room temperature , or 1.008×10^{-9} m^2/s (Stewart 1998).

The parameter k reflects the changing respiratory state of the biofilm over the course of daptomycin exposure. When not exposed to Daptomycin, bacteria inside a biofilm are healthy, and they consume oxygen faster than it can diffuse into the biofilm from the surroundings. This result in a relatively low oxygen concentration at the base of the biofilm, reflected by the relatively high fluorescence intensity observed. However, as biofilm respiration is inhibited by Daptomycin, the bulk k is decreased, and oxygen concentration at the base of the biofilm rebounds by diffusion from the surroundings. Hence, the observed changing of oxygen concentration at the base of the biofilms reflects a changing of k with exposure to Daptomycin.

The rate of change in oxygen concentration at the base thus provides a measure of how quickly respiration is being inhibited by Daptomycin.

4.5 Results and Discussion

4.5.1 Conversion of Fluorescence Intensity to Oxygen Concentration at the Base of Biofilms

Here, contact printed *Staphylococcus aureus* biofilm arrays were exposed to various Daptomycin concentrations ranging from 0 mM to 1 mM. Fluorescent images of replicate biofilms (n=10 to 37) were recorded at 5 min intervals over 24 h during exposure to Daptomycin. By applying the logarithm equation to fluorescence intensity curves (Figure 4-6a), intensities were converted to oxygen concentrations at bottom of each biofilm (Figure 4-6b). Within 4 h of treatment, oxygen concentration at the bottom of biofilms in 1 mM Daptomycin raise to 0.15 mM, while oxygen concentrations at the bottom of biofilms exposed to 0.25 mM Daptomycin only increased to 0.1 mM. Exposure to Daptomycin concentrations equal to or less than 0.125mM requires longer exposure time before oxygen concentrations at the base of biofilms were affected. Oxygen concentration at base of biofilms exposed to 0.031mM Daptomycin did not show increase to higher than 0.07mM throughout 24h treatment.

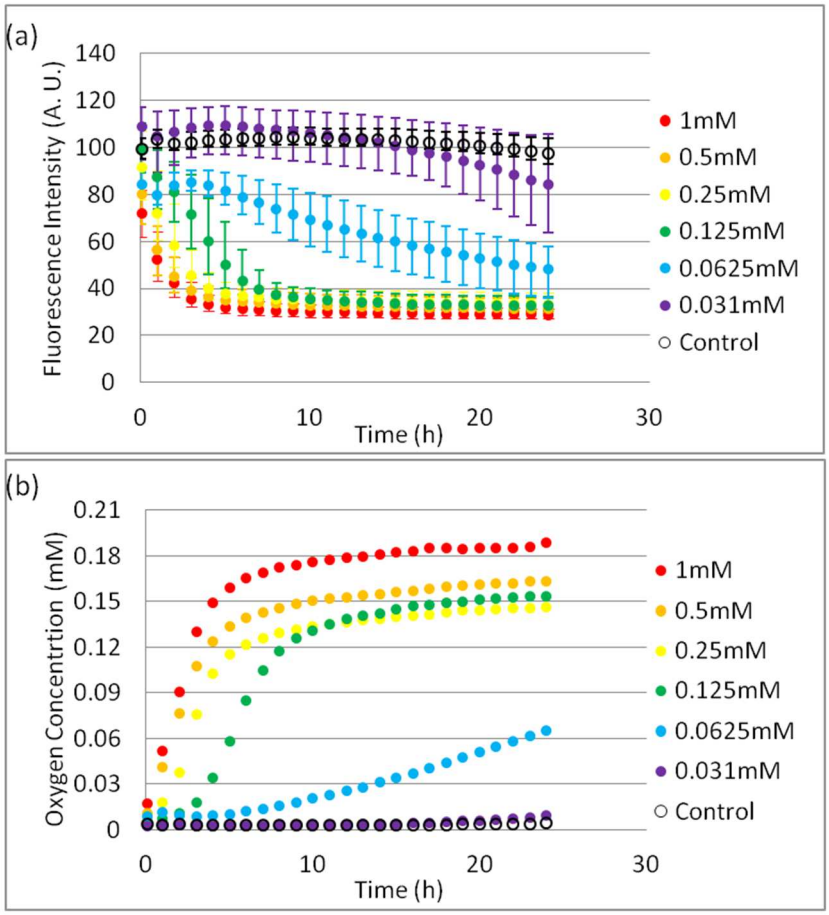

Figure 4-6 Dynamic fluorescence intensity of biofilms exposed to different concentrations of Daptomycin and the corresponding oxygen concentration.

(a) Average measured fluorescence intensity at biofilm base for all biofilms in array (n=10 to >20) with Daptomycin exposure. Error bar reflect full range of measured biofilms. (b) Corresponding oxygen concentration for (a), using oxygen sensing film calibration.

Although higher Daptomycin concentration outside the biofilm will lead to a slightly higher diffusive flux into biofilm, and therefore slightly earlier penetration, compared with lower Daptomycin concentrations, differences in penetration time do not explain the much longer timescale differences in oxygen concentration reported here. Stewart et al. has shown that fluorescently labeled Daptomycin (0.025mM in bulk media) completely penetrate 158 μm *Staphylococcus epidermidis* biofilms within 150 s (Stewart et al. 2009). Hence, in our experiments, penetration of Daptomycin is complete within the first few minutes of the experiment. Subsequent changes in local oxygen conditions reflect changes in respiration rates, not changes in local concentration in the drug.

4.5.2 Oxygen Consumption Rate *k*

Oxygen concentrations at the base of the biofilm quickly adjust to changes in the bulk oxygen consumption rate in the biofilm. As determined by 3D simulation, oxygen concentration at the base of the biofilm reaches steady state less than 30s following a change in k (Figure 4-7a). As a result, we employed a pseudo-steady state assumption, where k was assumed to be constant for each observation. Parameter sweeps were used to find the pseudo-steady state bulk zero-order oxygen utilization rate, k, that best represented the respiration state that would result in the measured oxygen concentrations for each time point, and for each Daptomycin concentration (Figure 4-7b and Table 4.1).

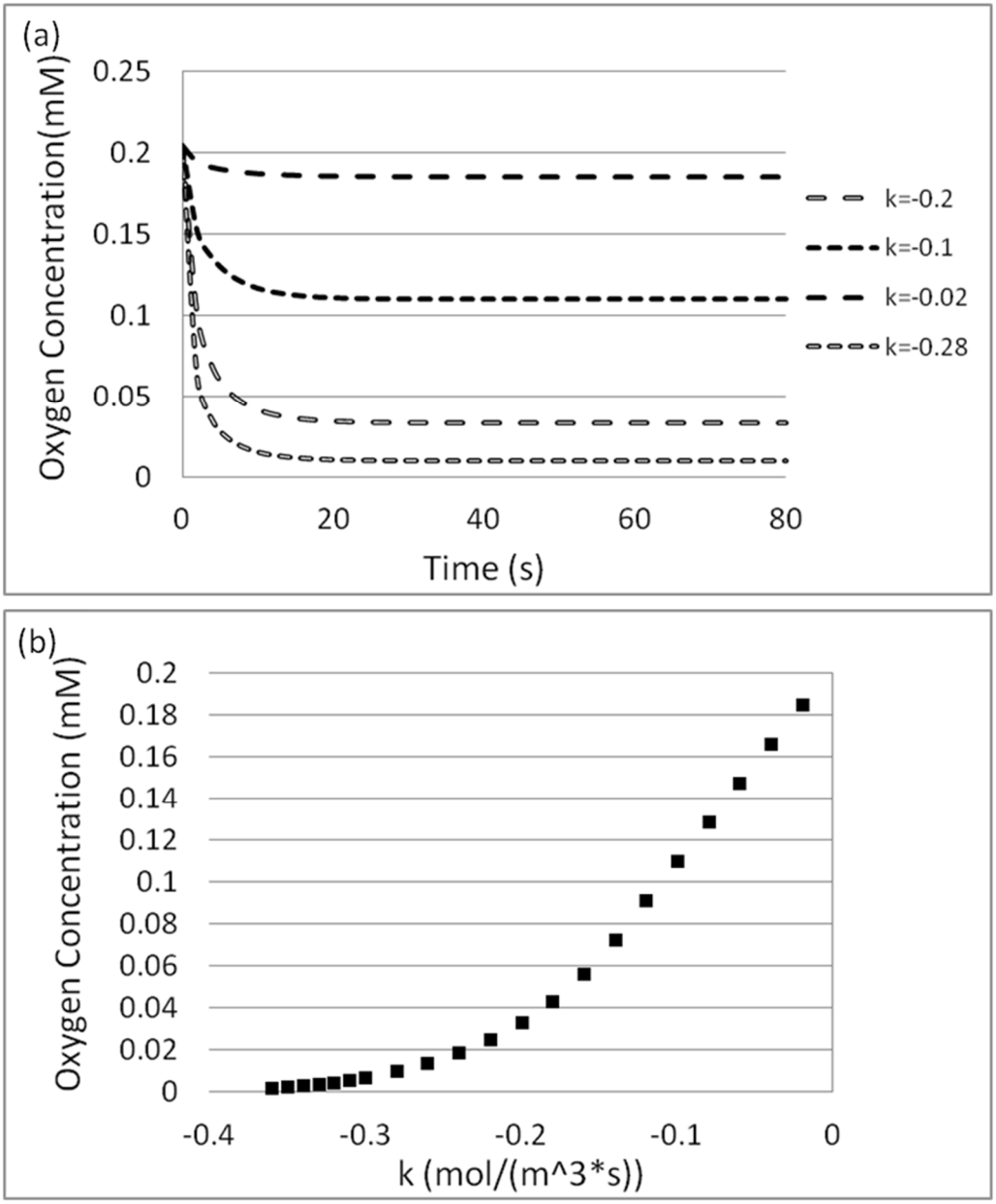

Figure 4-7 With a given k, steady state oxygen concentration can be modeled.

(a) Simulated response time of oxygen concentration at bottom of a biofilm for different modeled *k.* Oxygen concentration becomes stead state within 30s. (b) Simulated Pseudo-steady state oxygen concentration at bottom of biofilm given a series of *k*.

Table 4.1 Inferred bulk oxygen consumption rate k [mol/(m^3s)] versus time with different Daptomycin concentrations

	Daptomycin Concentrations						
	1mM	0.5mM	0.25mM	0.125mM	0.0625mM	0.031mM	0mM
0.08h	-0.25	-0.278	-0.31	-0.33	-0.29	-0.34	-0.34
2h	-0.12	-0.135	-0.19	-0.28	-0.282	-0.34	-0.34
4h	-0.058	-0.077	-0.11	-0.19	-0.281	-0.34	-0.34
6h	-0.04	-0.07	-0.09	-0.13	-0.27	-0.34	-0.34
8h	-0.035	-0.06	-0.08	-0.095	-0.25	-0.34	-0.34
10h	-0.03	-0.055	-0.07	-0.078	-0.23	-0.34	-0.34
12h	-0.026	-0.053	-0.068	-0.07	-0.22	-0.34	-0.34
18h	-0.022	-0.05	-0.062	-0.06	-0.18	-0.322	-0.34
24h	-0.02	-0.043	-0.061	-0.055	-0.15	-0.29	-0.34

4.5.3 Thiele Modulus and Model Validation

To test the concept and accuracy of the modeling, a zero order Thiele modulus describing the relative importance of oxygen consumption by biofilm and oxygen replenishment by diffusion from the surroundings was described by:

$$\phi^2 = \frac{kL_{biofilm}^2}{D_{O_2} S_{O_2}} \quad \text{(Eq. 4. 2)}$$

where k [(mol/(m^3×s)] is the zero-order volumetric oxygen consumption rate, $(L_{biofilm})^2$ [m^2] is the biofilm length scale squared, D_{O2} (m^2/s) is the effective diffusive permeability of oxygen through biofilm, and S_{O2} [mol/m^3] is the concentration of dissolved oxygen at the upper biofilm interface.

When higher fluorescence intensity at the bottom of biofilm is observed, oxygen is depleted at the base and $\phi^2 > 1$ should be obtained. On the contrary, when fluorescence of the reporting molecule on oxygen sensing film is quenched, oxygen diffusion is faster than it is utilized by the bacteria, $\phi^2 < 1$. Since the diameter of a biofilm dot (500 μm) is much larger than its height (about 30 μm), we represent the biofilm as a 1D slab with a thickness of 30 μm. With $k = |k_{max}| = 0.34$, even with oxygen steady state concentration, 0.204mM, ϕ^2 is larger than 1. This is consistent with the observation of high fluorescent intensity at base of biofilms and with our assumption: biofilm is healthy and respiring quickly. With k_{min} =-0.02, ϕ^2 is much smaller than one, indicating oxygen concentration is replenished due to slower oxygen utilization caused by Daptomycin treatment (Figure 4-8).

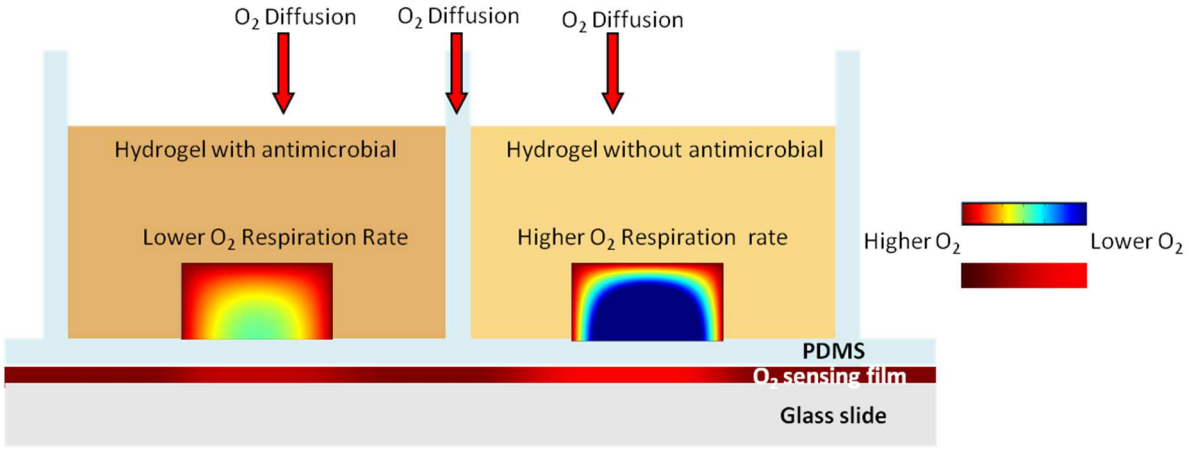

Figure 4-8 Schematic of biofilm embedded in hydrogel with and without antimicrobial (side view).

When biofilm exposed to agar containing high concentration of antimicrobial reagent (left), biofilm respiration was inhibited. With a lower oxygen consumption rate, oxygen diffusing from ambient can replenish oxygen concentration inside the biofilm. Lower fluorescence intensity will be observed at the base of biofilm (Thiele Modulus < 1). When biofilm exposed to no antibiotic, or when k =-0.34 [mol/(m^3×s)], oxygen diffusion speed is smaller than oxygen utilization. Hence oxygen concentration inside biofilm is depleted and a bright fluorescent intensity is observed at bottom of biofilm (Thiele Modulus > 1).

4.5.4 Respiratory Index

Biofilm is a heterogeneous aggregation of bacteria with existing in different respiratory states. Previous studies on biofilm indicate that even penetrated with Tobramycin and Ciprofloxacin, bacteria in biofilm was not completely killed (Walters et al. 2003). Oxygen and nutrient limitation may play a role in changing bacteria respiratory activity and can protecting bacteria in biofilm from antibiotic (Walters et al. 2003). Persister cells in biofilm can show much higher resistance. Hence, even in a "healthy" biofilm, there are some bacteria with very low respiratory activity that consume little or no oxygen. On the contrary, when a biofilm is exposed to high antibiotic stress with most of the bacteria completely inhibited, there might still be some persister cells slowly respiring. As a result, it is difficult to describe the overall respiratory status of a biofilm exposed to antibiotics, and there has been no consolidated term to describe how much a bulk respiration in a biofilm is inhibited with antibiotic exposure.

Here we introduce a new term to describe dynamic respiratory heath status of a biofilm, called the "Respiratory Index". The range Respiratory Index can take on values from 0 to 1, with 1 representing the optimal achievable respiratory status of a healthy biofilm, and corresponding with "optimal respiration" where $k = k_{max} = -0.34$ [mol/(m^3s)]. Conversely, 0 is a datum defining the lowest achievable respiratory status of a biofilm after exposure to a high antibiotic concentration for 24h; in such cases of "fully inhibited" respiration, $k = k_{min} = -0.02$[mol/(m^3s)].

4.5.5 Calculation of Biofilm Respiratory Index from Oxygen Consumption Rate *k*

For any biofilm, the measured oxygen concentration at a given point in time defines the bulk zero-order respiration rate, k. The dynamically-changing k during Daptomycin exposure can be represented in terms of the respiratory index according to:

$$Respiratory\ Index = (k - k_{min})/(k_{max} - k_{min}) \quad \text{(Eq. 4.3)}$$

where *Respiratory Index* ranges from 0 to 1, k_{max} is -0.34 [mol/(m^3×s)] and k_{min} is -0.02[mol/(m^3×s)]. Respiratory index is a function of antibiotic concentration and exposure time.

Respiratory index of biofilm treated with different Daptomycin concentrations during 24 h exposure is shown (Figure 4-9). Control biofilms exposed to no antibiotic and sufficient nutrient show respiratory index 1 throughout 24 h. These results show exposure to 0.031 mM Daptomycin does not inhibit respiration in biofilms until after 10 h of exposure. Biofilms exposed to 0.0625 mM Daptomycin exhibit a more slowly-decreasing respiratory index compared with biofilms exposed to Daptomycin concentrations higher than 0.125 mM. Respiratory index approaches a steady value after different treatment times, depending on the concentration of drug used. It stabilizes after 6 hours for 0.125 mM exposure, after 4 hours for 0.25 mM exposure, and after 2 hours for either 0.5 mM or 1 mM exposure to Daptomycin.

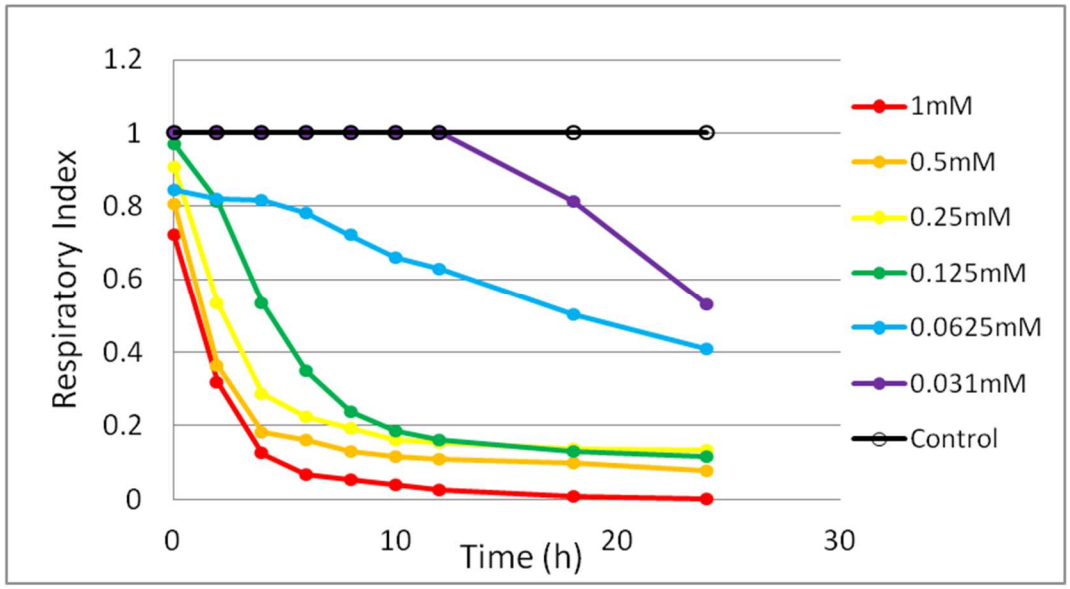

Figure 4-9 Inferred bulk respiratory index for intact biofilms with Daptomycin exposure.

When biofilms were exposed in high Daptomycin concentrations, respiratory index show drastic decreasing and stabilize at a lower value. However, when biofilm exposed to nonsufficient or no Daptomycin, respiratory index of biofilms stabilized at higher value.

Respiratory indexes of all biofilms exposed to Daptomycin concentrations of 0.125mM or higher were able to eventually drop below 0.2. However, the exposure time required for this to occur is different for different concentrations of Daptomycin. These results reflect actual dose-dependent physiological changes to bacteria with exposure to different antimicrobial concentrations, because in all cases, diffusion of Daptomycin was complete within the first few minutes of exposure. For Daptomycin exposures equal or greater than 0.5 mM, only 2 h of treatment is necessary for decreasing respiratory index below 0.2 while longer than 24h of exposure might be required for concentration lower than 0.125mM.

Our results also show biofilm respiratory index stables to different values depending on concentration of Daptomycin used (Figure 4-9). Most concentration effectively reduced the respiratory index to a very low level. However, higher Daptomycin concentrations seems to be able to inhibit an additional proportion of bacteria in the biofilm compared with relatively lower concentration, resulting in lower steady state respiratory index values. While most bacteria inside a biofilm can be effectively inhibited with a fairly high Daptomycin concentration, the last few percentage of bacteria, possibly including so-called "persister cells," may be associated with higher intrinsic resistance, and therefore require and a higher Daptomycin concentration to eradicate. Literature reports show that it is nearly impossible to fully eradicate all bacteria in a biofilm, even with extremely high antibiotic concentrations due to the presence of persister cells (Walters et al. 2003).

4.6 Conclusion

This paper has introduced a novel method to investigate biofilm antimicrobial susceptibility in real time during antimicrobial treatment. A novel term "Respiratory Index" has

been introduced to describe the changing respiratory status of the biofilm during treatment. By coupling experiments and modeling, this work provides a closer look at the Daptomycin inhibition process and its effects on biofilm respiration. This method also has great potential in biofilm antibiotic treatment, with the goal of improving treatment effectiveness and reducing incidence of resistance.

4.7 References

Alborn Jr, W. E., N. E. Allen, et al. (1991). "Daptomycin disrupts membrane potential in growing Staphylococcus aureus." Antimicrobial Agents and Chemotherapy 35(11): 2282-2287.

Brazier, J. S., R. Raybould, et al. (2008). "Distribution and antimicrobial susceptibility patterns of Clostridium difficile PCR ribotypes in English hospitals, 2007-08." Euro Surveill. 13(41): 541-544.

Buchholz, F., A. Wolf, et al. (2010). "Chip Calorimetry for Fast and Reliable Evaluation of Bactericidal and Bacteriostatic Treatments of Biofilms." Antimicrobial Agents and Chemotherapy 54(1): 312-319.

Deng, J., A. Dhummakupt, et al. (2013)b. "Dynamic Dosing Assay Relating Real-Time Respiration Responses of Staphylococcus aureus Biofilms to Changing microchemical Conditions." Analytical Chemistry 85(11): 5411-5419.

Han, P. and D. M. Bartels (1996). "Temperature dependence of oxygen diffusion in H2O and D2O." The Journal of Physical Chemistry 100(13): 5597-5602.

Hayden, M. K., K. Rezai, et al. (2005). "Development of daptomycin resistance in vivo in methicillin-resistant Staphylococcus aureus." Journal of Clinical Microbiology 43(10): 5285-5287.

Jones, T., M. R. Yeaman, et al. (2008). "Failures in clinical treatment of Staphylococcus aureus infection with daptomycin are associated with alterations in surface charge, membrane phospholipid asymmetry, and drug binding." Antimicrobial Agents and Chemotherapy 52(1): 269-278.

LaPlante, K. L. and L. A. Mermel (2007). "In vitro activity of daptomycin and vancomycin lock solutions on staphylococcal biofilms in a central venous catheter model." Nephrology Dialysis Transplantation 22(8): 2239-2246.

LaPlante, K. L. and S. Woodmansee (2009). "Activities of daptomycin and vancomycin alone and in combination with rifampin and gentamicin against biofilm-forming methicillin-resistant Staphylococcus aureus isolates in an experimental model of endocarditis." Antimicrobial Agents and Chemotherapy 53(9): 3880-3886.

Markov, D. A., E. M. Lillie, et al. (2014). "Variation in diffusion of gases through PDMS due to plasma surface treatment and storage conditions." Biomedical Microdevices 16(1): 91-96.

Nishimura, S., T. Tsurumoto, et al. (2006). "Antimicrobial susceptibility of Staphylococcus aureus and Staphylococcus epidermidis biofilms isolated from infected total hip arthroplasty cases." Journal of Orthopaedic Science 11(1): 46-50.

Richter, S. S., K. P. Heilmann, et al. (2009). "Changing Epidemiology of Antimicrobial-Resistant Streptococcus pneumoniae in the United States, 2004-2005." Clinical Infectious Diseases 48(3): E23-E33.

Salmon, S. A. and J. L. Watts (2000). "Minimum inhibitory concentration determinations for various antimicrobial agents against 1570 bacterial isolates from turkey poults." Avian Diseases 44(1): 85-98.

Schuurmans, J. M., A. S. N. Hayali, et al. (2009). "Variations in MIC value caused by differences in experimental protocol." Journal of Microbiological Methods 79(1): 44-47.

Silverman, J. A., N. Oliver, et al. (2001). "Resistance studies with daptomycin." Antimicrobial Agents and Chemotherapy 45(6): 1799-1802.

Steenbergen, J. N., J. Alder, et al. (2005). "Daptomycin: A lipopeptide antibiotic for the treatment of serious Gram-positive infections." Journal of Antimicrobial Chemotherapy 55(3): 283-288.

Stewart, P. S. (1998). "A review of experimental measurements of effective diffusive permeabilities and effective diffusion coefficients in biofilms." Biotechnology and Bioengineering 59(3): 261-272.

Stewart, P. S., W. M. Davison, et al. (2009). "Daptomycin Rapidly Penetrates a Staphylococcus epidermidis Biofilm." Antimicrobial Agents and Chemotherapy 53(8): 3505-3507.

Surdeau, N., D. Laurent-Maquin, et al. (2006). "Sensitivity of bacterial biofilms and planktonic cells to a new antimicrobial agent, Oxsil (R) 320N." Journal of Hospital Infection 62(4): 487-493.

Udekwu, K. I. and B. R. Levin (2012). "Staphylococcus aureus in continuous culture: A tool for the rational design of antibiotic treatment protocols." PLoS ONE 7(7).

Van der Meeren, P., D. De Vleeschauwer, et al. (2001). "Determination of oxygen profiles in agar-based gelled in vitro plant tissue culture media." Plant Cell, Tissue and Organ Culture 65(3): 239-245.

Walters, M. C., F. Roe, et al. (2003). "Contributions of antibiotic penetration, oxygen limitation, and low metabolic activity to tolerance of Pseudomonas aeruginosa biofilms to ciprofloxacin and tobramycin." Antimicrobial Agents and Chemotherapy 47(1): 317-323.

Chapter 5 Synergistic Effects of Soil Microstructure and Bacterial EPS on Drying Rate in Emulated Soil Micromodels[3]

5.1 Abstract

Microbial extracellular polymeric substances (EPS) have been shown to alter soil moisture retention and to improve seedling survival and plant growth at the bulk scale. The mechanisms of EPS-mediated water retention include reversible swelling of the cross-linked polymer matrix and the promotion of an aggregated soil structure. However, the effects of EPS on water retention have never been directly observed at the pore scale. Here, emulated soil micromodels were developed to directly observe the effects of physical, chemical, and biological factors on pore-scale water retention. In this demonstration, a pseudo-2D pore structure was created to represent physical features of a fine silty loam. Replicate micromodels were initially saturated with suspensions of different soil bacteria, and pore-scale air infiltration was directly imaged over time. External evaporativity was held constant through the use of a custom constant-humidity environmental chamber. Micromodels filled with suspensions of highly mucoid *Sinorhizobium meliloti* retained moisture about twice as long as physically identical micromodels filled with suspensions of non-mucoid *S. meliloti*. Relative drying rates in six replicate experiments ranged from 1.1 to 2.5 times slower for mucoid suspensions. Patterns of air infiltration were similar but not identical across replicates. The results suggest that pore fluid

[3] Submitted as Deng J*, Erika P. Orner*, Jessica F. Chau, Emily M. Anderson, Andrea L Kadilak, Rebecca L. Rubinstein, Grant M. Bouchillon, Reed Goodwin, Daniel J. Gage, Shor LM. 2014. Synergistic Effects of Soil Microstructure and Bacterial EPS on Drying Rate in Emulated Soil Micromodels. *Soil Biology & Biochemistry*. Under review. * These authors contribute equally.

EPS and micromodel geometry act together to limit evaporation at pore throats. Advantages of the micromodel approach include direct observation of pore-scale dynamic process, and the ability to systematically replicate complex physical structures. These abilities will enable users to screen benefits from different structures and or from microbial compositions, and build predictive understanding of the overall function of microbe-habitat systems.

5.2. Introduction

Global climate change is predicted to amplify extreme events in the water cycle, leading to widespread reduction in soil moisture (Dai 2011), with important implications for sustainable food, feed, and fiber production. Following a rain event, water is lost from the soil by infiltration and evaporation. The rate of evaporation is dependent on a host of factors including meteorological conditions, land use, and depth of the water table. Other important factors include micro-scale variations in soil characteristics such as soil texture, structure, and organic matter content, and the activities of plants and soil microbes.

As reviewed recently, soil moisture is a key factor influencing microbial respiration (Moyano et al. 2013). In turn, microbial processes modulate water availability in soil through production of extracellular polymeric substance (EPS) (Or et al. 2007b). Roberson & Firestone (1992) showed dramatic shifts in water retention in porous media amended with small amounts of hydrogel, and these authors speculated that bacterial control of the microenvironment could enhance their survival. Since then, the concept of soil as a self-organizing physical-biological system has emerged (Young and Crawford 2004).

In soils, the vast majority of bacteria are found in biofilms, where bacteria embedded in EPS are better protected from changing soil water conditions (Or et al. 2007b) and predation

(Matz and Kjelleberg 2005) and enjoy greater access to water-soluble nutrients (Chenu and Roberson 1996). Microbial biofilms are comprised of one or several species of bacteria embedded in an EPS matrix of proteins, polysaccharides and DNA. EPS has a highly cross-linked structure that enables it to shrink and swell yet remain saturated across a wide range of matric potentials (Or et al. 2007b). The micro-scale structure of biofilms includes several layers of bacteria, each with different phenotypes (Ramos et al. 2001; Sauer et al. 2002a), and pores and networks facilitating the flow of nutrients and oxygen (Li and Yuan 2002).

In a soil system, EPS acts with mineral grains and plants to retain and direct moisture. Mucoid bacteria may contribute to soil structuring (Alami et al. 2000). Production of EPS promotes both the formation (Amellal et al. 1998; Gajic et al. 2010) and the stability (Park et al. 2007) of soil aggregates. Soil aggregates tightly hold moisture in interstitial spaces (Or et al. 2007c) while larger inter-aggregate spaces promote drainage and gas exchange (Morales et al. 2010). Aggregated soils thus tend to sustain the intermediate water contents that are most favorable to plants and soil microbes (Kets et al. 1996). In the rhizosphere, EPS is predicted to act as both a reservoir and a conductor of water to plant roots when bulk soil water is scarce (Carminati et al. 2011).

Prior research has measured the effect of EPS on survival and growth of plants, but only at the bulk scale. For example, Sandhya et al. (2009) showed that inoculation with EPS-producing *Pseudomonas* sp. strain GAP-P45 increased sunflower seedling survival and plant biomass under water-stressed conditions. Similarly, Alami et al. (2000) showed that sunflower seed or soil inoculation with *Sinorhizobium* sp. strain YAS34 caused an increase in root-adhering soil per root dry mass of up to 100%. Root-adhering soil helped to counteract the deleterious effects of water deficit on growth and also promoted fertilizer uptake.

Only occasionally have interacting physical and biological processes been considered at the pore scale. For example, Dechesne et al. (Dechesne et al. 2010) and Wang and Or (Wang and Or 2010) described cell migration and emergence of colony patterns based on spatial distribution of hydrated pore regions. Other researchers have employed agent-based microbial community models to demonstrate emergent functionality in micro-structured habitats (Long and Or 2009; Wang and Or 2013). These studies provide important insights into the interactions of microbes and micro-structured habitats. However, to date, the effect of bacterial EPS on pore-scale evaporation processes has never been determined in a physically micro-structured experimental setting.

Here, soil micromodels were developed to better understand pore-scale effects of bacterial EPS on drying resistance. Micromodels allow faithful replication of micrometer-scale physical and chemical features of microbial habitats, and enable direct observation of microbial responses (Weibel et al. 2007b). Microfluidic devices have been used to study bacterial spatial coordination (Cho et al. 2007b), the stability of microbial communities (Kim et al. 2008), bacterial chemotaxis (Lanning et al. 2008; Long and Ford 2009; Mao et al. 2003), bacteria-enhanced solute dispersion (Singh and Olson 2011), and the mobility of protozoa in narrow channels (Wang et al. 2005b; Wang et al. 2008b). We know of no prior efforts to use microfluidic devices to measure drying resistance at the pore scale, or as a function of bacterial EPS.

The objective of this study was to visualize and measure the effects of bacterial EPS on evaporation of soil water at the pore scale, which is the physical scale most relevant to bacterial colonization and water retention processes. Our hypothesis is that EPS and soil microstructure act together to limit evaporation from soils. Soil micromodels were created to emulate the

physical structure and pore geometry of a sandy loam, but in a pseudo-2D format to allow direct optical visualization of air infiltration into pores. By employing a microfluidic device with emulated soil structure, soil particle size and distribution as well as porosity can be exactly replicated in every experiment.

Here, emulated soil micromodels were colonized with mucoid (EPS+, a strain that produces well-characterized EPS) or non-mucoid (EPS-, a control strain that does not produce any EPS) *Sinorhizobium meliloti*. Air infiltration into the physically-identical micromodels was imaged over time in a constant-humidity chamber placed on an inverted microscope. The effects of EPS on changing water content were imaged directly within the micromodel. In addition, thermal gravimetric analysis (TGA) was used to measure drying of *S. meliloti*-amended soil, and dynamic vapor sorption (DVS) was used to measure drying of bare *S. meliloti* biofilms. By comparing the TGA results with the DVS results, we find additional support for the hypothesis that EPS and soil microstructure act synergistically to limit evaporation from soils. Finally, we propose a mechanism for the increased evaporation resistance observed in EPS+ trials in structured habitats.

5.3. Materials and Methods

5.3.1. Bacterial Strains

Drying experiments in soil micromodels and sterilized air-dried soil samples were performed with mucoid and non-mucoid strains of *Sinorhizobium meliloti*. *S. meliloti* and related bacteria are agriculturally and environmentally important as symbionts of legumes due to their nitrogen fixation abilities (Gage 2004). The commonly used "lab strain" *S. meliloti* Rm1021 has been sequenced, modeled and studied extensively (Galibert et al. 2001; Pellock et al. 2002).

Rm1021 is a quorum sensing mutant with a natural insertion in *expR* that results in relatively low level production of the exopolysaccharidegalactoglucan EPSII (Pellock et al. 2002). Strain Rm8530, which lacks the insertion, is very mucoid due to the over-production of EPSII. In addition, regulation of EPSII by *expR* plays a key role in the ability of *S. meliloti* to form biofilms (Rinaudi and Gonzalez 2009).

Here, we focus on strain Rm8530,designated here as "EPS+", and compare it to *S. meliloti* strain Rm11609 (Rm1021 *exoY*,*expA*) as a "control strain" due to its inability to produce EPSI or EPSII (Mueller and Gonzalez 2011). Strain Rm11609 is designated here as "EPS-" (Table 5.1).

Table 5.1 Characteristics of different strains of *Sinorhizobiummeliloti*.

Strain	**Characteristics**	**EPS characteristics**
Rm8530	Rm1021 *expR*$^{+}$	EPS+
Rm11609	Rm8530*exoY*::OTC^{r}*expA*::Nm^{r}	EPS-

5.3.2. Microfluidic Device Concept

Soil micromodels were comprised of three rectangular channels connected to a single inlet well and a single outlet well (Figure 5-1A). Each 1 mm × 20 mm × 0.034 mm rectangular channel contained a 10 mm-long microstructured region, with pillars of varying sizes and shapes representing a two-dimensional slice of the solid phase of a simulated sandy loam (Figure 5-1B).

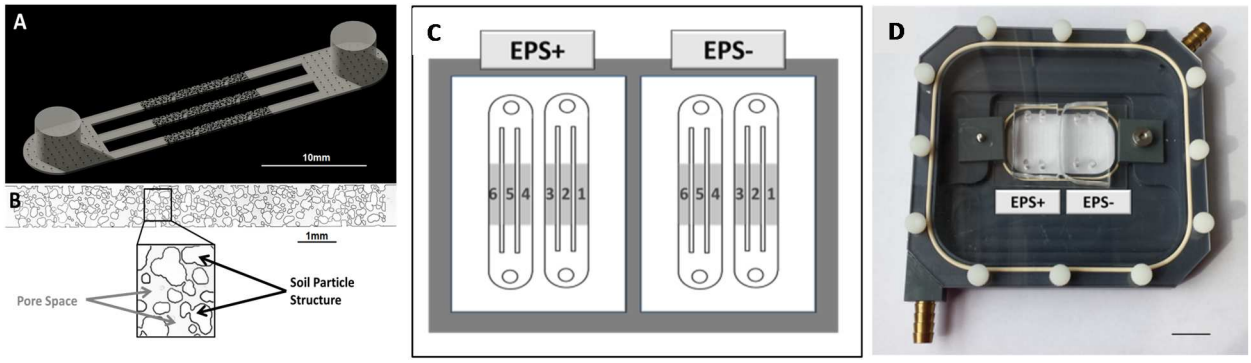

Figure 5-1Schematic of the emulated soil micromodel design.

(A) Scale rendering of the emulated soil micromodel with 3 identical channels, each with a micro-structured region 1 cm long, 1 mm wide, and 34 ± 3 μm-deep. Access ports were 1 cm high and 4 mm in diameter. (B) Tiled micrograph of the 2-D pore structure used in every micromodel (9 tiled micrographs, scale = 1 mm). Features labeled “soil particles” are columns of uniform size in the z-direction. (C) Schematic of drying experiments: replicate soil micromodels each comprised of three identical micro-structured drying channels were loaded with suspensions of mucoid (EPS+) or non-mucoid (EPS-) *S. meliloti* bacteria suspended in artificial groundwater. (D) Photograph of micromodels installed in the custom-built environmental control chamber (scale = 2 cm).

The geometry of the microstructured region was based on a realistic computer-generated three-dimensional packing of ellipsoidal particles into a computational domain of size 100×100×100 voxels. The size distribution of these particles was based on a truncated, experimentally-determined sandy loam particle size distribution (Chau et al. 2011). A scale of one lattice unit to 5 μm (that is, one voxel to $(5\ \mu m)^3=125\ \mu m^3$) was chosen based upon computational and microfluidic device fabrication constraints. Particle sizes were constructed using USDA size ranges (fine sand 125-250 μm, and very fine sand 50-125 μm). A set of particles in the two size fractions was generated randomly, with the particle number tuned to create the appropriate percentage of the total solid volume (56% fine sand, 44% very fine sand). Particles were generated as ellipsoids by drawing radii from a uniform distribution dictated by particle size, then randomly taking sets of three (r_x, r_y, and r_z) and keeping only sets conforming to a sphericity values $0.7 \leq S = r_{min}/r_{max} \leq 0.85$, based on the properties of sand particles (Cho et al. 2006; Friedman and Robinson 2002). Particles were then randomly placed in a three-dimensional computational domain, and a packing algorithm DigiPac (Jia and Williams 2001) was employed to create realistic particle-particle contacts. Finally, a two-dimensional slice of the packed three-dimensional domain was selected with desired porosity and pore geometry.

The selected two-dimensional slice was converted to a two-toned bitmap. AutoCAD Raster Design 2010 was used to manually outline and vectorize the particle contours in the bitmap. The resulting structure was partitioned to completely fill the 1 mm × 10 mm microstructured region in a high-resolution chrome on glass photomask.

Particle diameters ranged from 10-300 μm with an average diameter of 110 μm while pore radii ranged from 16 to 130 μm with an average hydraulic radius of 44 μm (Figure 5-2).

Average particle diameters and pore radii (calculated as the hydraulic radius = 2 × area/perimeter) were obtained using image analysis of the original bitmap version of the micromodel design (Figure 5-1B) MATLAB (MathWorks, Natick, MA). Soil used for TGA was the corresponding 75-250 μm fraction sieved from whole soil. Typical porosities for a sandy loam are in the range of 25-35%. The porosity of our pseudo-2D soil chip was 57%. The higher porosity is expected for a 2-D slice of packed 3-D model that maintains pore connectivity in 2-D (Chau and Or 2006; Chau et al. 2005).

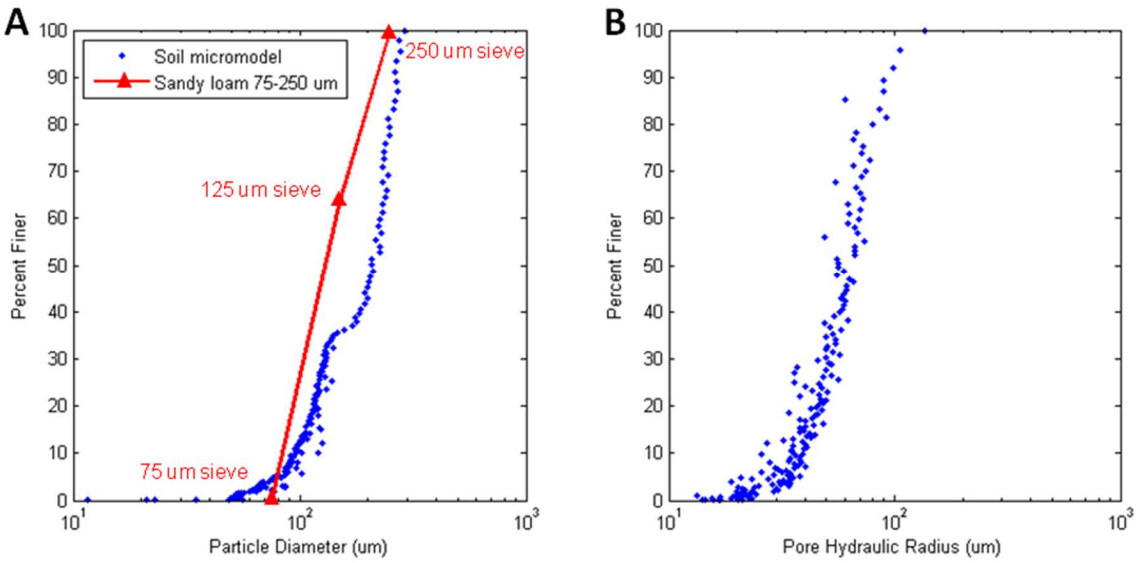

Figure 5-2 Particle size distribution of soil micromodel and sandy loam used in TGA experiments (A) and pore size distribution (B).

5.3.3.Micromodel Fabrication

Physically identical soil micromodels were cast in polydimethylsiloxane (PDMS) from a microfluidic casting master. PDMS($Si(CH_3)_2$-O-)$_n$ is an inexpensive and biocompatible polymer that offers excellent optical clarity and readily conforms to micron-scale physical features (Whitesides et al. 2001). PDMS microfluidic devices have been used extensively for cell culture, especially for applications in the biomedical field. Upon exposure to oxygen plasma, PDMS surface charge is similar to quartz sand (Roman and Culbertson 2006).

Microfluidic casting masters were created using photolithography, a commonly-used technique described in detail elsewhere (Deng et al. 2013a; Markov et al. 2010a). Briefly, a thin layer of SU-8 2025 photoresist (Microchem, Newton, MA) was coated on a 4-inch diameter Si wafer (Nova Electronic Materials, test grade, Flower Mound, TX). The thickness of the photoresist coating was 34 ± 3 μm as determined by profilometry (Dektakmodel 150, VeccoInstruments, Plainview, NY). The photoresist was photo-patterned using a chrome-on-glass photolithography mask (Advanced Reproductions, North Andover, MA) with 26.4 mW cm^{-2} ultraviolet light for 6.1 s (OAI 200 mask aligner, San Jose, CA) followed by cross-linking and developing steps.

Finished masters were silanized to facilitate repeated PMDS casting based on methods described previously (Addae-Mensah et al. 2009; Langelier et al. 2011). Briefly, the master was cleaned with isopropanol (Laboratory Grade, Fisher Chemical, Pittsburgh, PA) and dried with N_2 (Industrial Grade, Airgas, Waterford, CT). To evenly oxidize the surface, the master was treated with O_2 plasma (300 W, 4 min) using a Microwave Plasma System (PS 210, PVA TePla America, Inc., Corona, CA). The plasma-treated master was positioned SU-8-side down on a disposable aluminum weight dish containing 3-5 drops of the silanizing agent (tridecafluoro-1,1,2,2-

tetrahydrooctyl) trichlorosilane (UCT, Inc., Bristol, PA). The dish and master were placed inside a vacuum desiccator, and the silane was evaporated and deposited on the surface of the master under -75 kPa gage vacuum for 1 h. Finally, any remaining silane was volatilized by heating the master uncovered on a hot plate at 150 °C for 10 min.

Emulated soil micromodels were cast 1 cm thick in PDMS (Sylgard 184, Dow Corning, Midland, MI). Briefly, PDMS base and curing agent were fully mixed in a 10:1 ratio then degassed at -75 kPa gage for 30 min, poured over the master, and cured in an oven at 60 ºC for 4 h. Once cured, castings were carefully peeled from the master, trimmed, and access ports were manually punched from the patterned side using a 4 mm biopsy punch (Miltex, Inc., York, PA). Each casting was treated with O_2 plasma for 45 s in an evacuated air atmosphere (Harrick PDC-32G, Harrick Plasma, Ithaca, NY) then aligned and irreversibly bonded to a plasma-treated (45 s) glass microscope slide in the arrangement shown in Figure 5-1C and D.

5.3.4. Micromodel Operation

Once bonded, micromodels were filled with suspensions of bacteria and were considered 100% saturated. Each bacterial strain was cultured for 5 d at 30 ºC and 100 rpm in covered 20 ml Pyrex Vista rimless culture tubes (Corning, Tewksbury, MA) in M9 minimal medium also containing 0.4% glycerol, 500 μg ml^{-1} streptomycin, and 100 μg/ml spectomycin. For *S. meliloti* Rm11609, the medium also contained100 μg ml^{-1} neomycin and 0.75μg ml^{-1} oxytetracycline. Stationary phase cultures were washed three times in artificial groundwater (AGW) (Scholl et al. 1990) containing 0.100 mM KH_2PO_4 then adjusted to OD_{595} 0.012 for *S. meliloti* Rm8530 or OD_{595} 0.010 for *S.meliloti* Rm11609to obtain comparable cell concentrations of 10^7 cells ml^{-1}.

Plasma-treated PDMS has a hydrophilic surface chemistry and can be readily filled with aqueous solutions using capillarity (Bouchillon et al. 2014). Four replicate micromodels were filled with AGW suspensions of bacteria: two with *S. meliloti* Rm8530 (EPS+) and two with *S. meliloiti* Rm11609 (EPS-) (Figure 5-1C). Then, all micromodels were held for a 5 d conditioning period at ambient temperature (approx. 23ºC) and 100% relative humidity. This conditioning period allowed the bacterial community to stabilize biomass, aggregation state, and EPS production rate, and also allowed the PDMS polymer to saturate with water.

5.3.5. Design and Operation of Environmental Control Chamber

A custom-built environmental control chamber was used to hold the external evaporativity constant during prolonged drying experiments, even if the micromodel was temporarily removed from the microscope stage. The design of the chamber was adapted from Steinhaus et al. (Steinhaus et al. 2007). As implemented here, the control chamber fit between the stage and condenser of an AxioObserver Z1 AX10 inverted wide field microscope (Carl Zeiss, Oberkochen, Germany), and was securely installed recessed into a Märzhäuser programmable scanning stage. (Additional technical details of the design are shown in Figures 5-3 and 5-4)

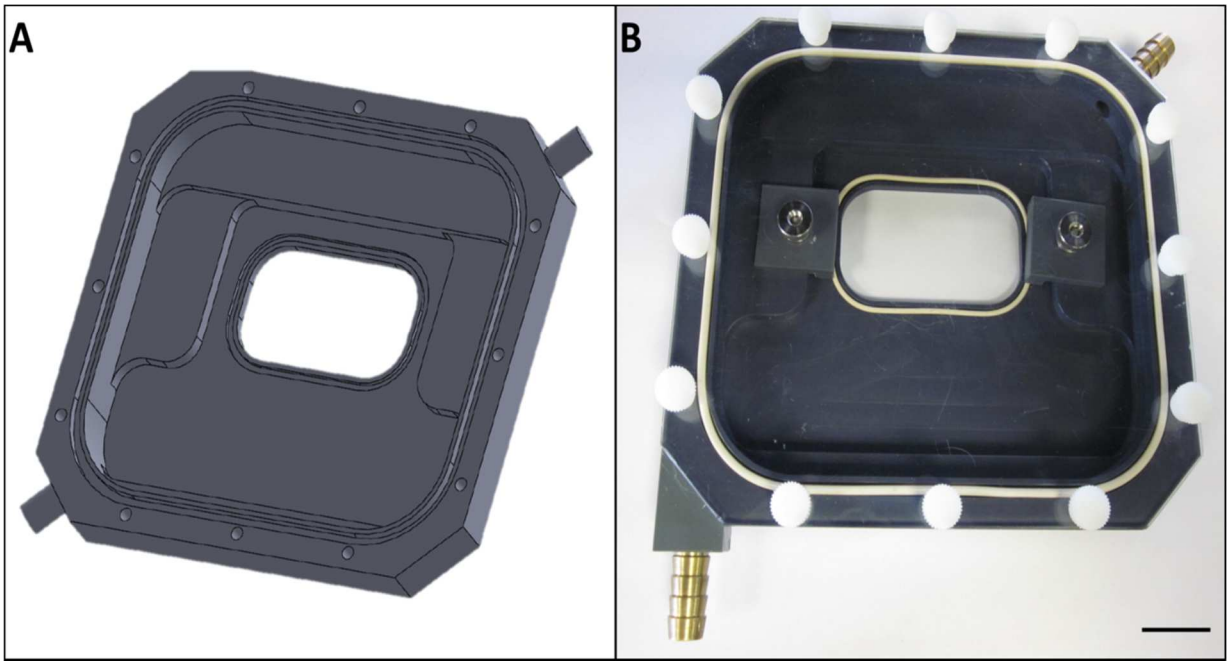

Figure 5-3 3D rendering (A) and photograph (B) of custom-built control chamber.

The emulated soil micromodels bonded on top of a glass slide sit in the small window of the chamber to enable imaging with an inverted microscope. The chamber was machined from PVC and contains O-ring compression seals for glass slide and an acrylic lid. The acrylic lid is fastened using thumbscrews and the microscope slide with the emulated soil micromodels affixed on top is held down using small clamps. Brass nozzles at either end allow circulation of humidified air. The entire assembly fits on top of the stage of an inverted wide field microscope, with the slide held at the normal focusing distance from the objective. Scale bar = 2cm.

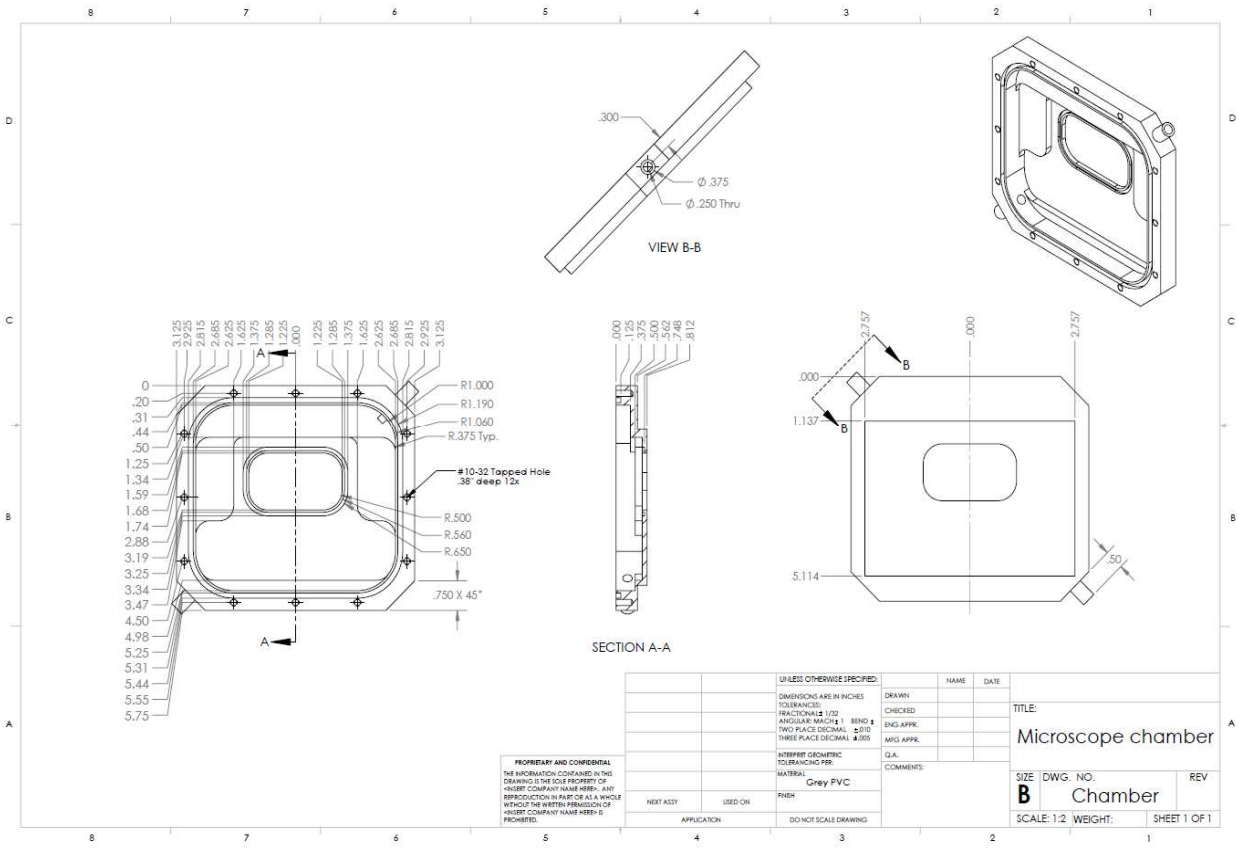

Figure 5-4 Microscope chamber technical drawing outlining dimensions.

After the 5 d conditioning period, micromodels were installed in the environmental control chamber over the open viewing window (Figure 5-1D) and the clear polycarbonate lid was secured. Metal barbed tube fittings at two corners allowed humidity-controlled air to continuously circulate through the environmental chamber. Humidified air was created in a separate 0.5 m^3 mixing chamber containing a Cigar Oasis XL humidifier (Orlando, FL) set to 80% relative humidity, corresponding to 30 MPa (matric potential value). An HT10 USB Humidity Temperature Data Logger (General Tools, New York, NY) placed in the microscope-mounted chamber continuously recorded humidity (78% ± 2%) and temperature (19 ˚C ±0.5 ˚C) during the experiment.

5.3.6. Imaging and Image Analysis

The progression of the air-water interface was determined throughout all 12 microchannels every 30 min from the time when the air interface was at the edge of the microstructured region until air had fully infiltrated. Bright-field composite images were captured using a Carl Zeiss AxioObserver Z1 AX10 automated inverted microscope equipped with an AxioCam MRmRev.3 camera using a 5× objective (Zeiss EC Plan-Neofluar; 5×/0,16 ∞/0,17) using the Multidimensional Acquisition Module. Composite images were constructed by stitching together 9 overlapping frames using the AxioVision 4.8 software (see e.g. Figure 5-1B).

Composite images were analyzed using the open-source Fiji image-processing package (Schindelin et al. 2012). First, each composite image was cropped and then converted to a binary, black and white image. Using a single threshold value, a continuous air interface along hydrated pore space or PDMS pillars could be resolved in all composite images. Next, the continuous air phase was manually filled with black pixels using the position of the air interface as a guide

(Figure 5-5). Total "air" pixels at each time point in each composite image were quantified in Fiji then converted to an air volume (mm^3) using a uniform channel height of 34 μm. Finally, the air volume was subtracted from the known total pore volume to determine the remaining water volume or the relative water saturation.

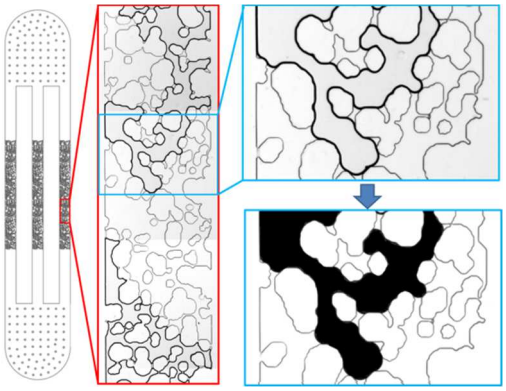

Figure 5-5 Schematic showing image processing scheme.

The position of the air-water interface was identified by applying a binary threshold super-imposed over the tiled image, then the invading air phase was manually converted to black for visual inspection and quantitative image processing.

5.3.7. Thermogravimetric Analysis

As a qualitative support of the results obtained using soil micromodels, evaporation kinetics of a sandy loam soil amended with EPS+ or EPS- bacterial suspensions were measured using thermogravimetric analysis (TGA). TGA involves gravimetric determination of water lost from a sample as a result of a pre-determined temperature cycle. Bacterial-amended soils were first subjected to a period of desiccation and rewetting prior to TGA in order to better simulate the variable environmental conditions to which soil microbes are acclimated.

Paxton and Montauk fine sandy loam was collected from the Horsebarn Hill area of the University of Connecticut Storrs campus. Whole soil was screened in the field, autoclaved, air dried, and sieved to obtain the 75 - 250 μm fraction, corresponding to the particle size distribution of the soil micromodel (Figures 5-1B and 5-2). Stationary-phase AGW suspensions of *S. meliloti* Rm8530 or Rm11609 at 10^7 cells ml^{-1} were prepared as described above. Excess volumes (5 ml) of bacterial AGW suspensions were added to 1 g sterile, air-dry soil in 50 ml centrifuge tube (Corning, Tewksbury, MA), then slurries were covered and allowed to sit at ambient temperature (approx. 23ºC) for 5 d. Slurries were dried at 60 ºC for 2 d, then 100 +/- 1 mg dry bacteria-amended soil was loaded onto a tared hanging weigh pan. Dry bacteria-amended soil was re-hydrated by adding 40μL of AGW, and equilibrated at 23 ºC at 100% relative humidity for 2 h prior to re-drying.

Tared, re-wetted, and equilibrated EPS+ or EPS- *S. meliloti*-amended soil samples were placed on a TGA (Q500, TA Instruments, New Castle, DE), and the change in weight was determined with time as heated dry air flowed past the sample. Samples were dried at 40 ºC for 700 min to estimate labile water under environmental conditions, then dried at 105 ºC for 120 min to

determine total water. Finally, samples were oxidized at 360 ºC for 120 min to determine the total organic carbon content (Schulte 1996).

5.3.8. Dynamic Vapor Sorption

Dynamic Vapor Sorption (Q5000, TA Instruments, New Castle, DE) was used to measure the kinetics of water loss (evaporation) in pure bacterial biofilms collected from confluent bacterial lawns grown on agar plates. Liquid-phase *S. meliloti* Rm8530 (EPS+) and Rm11609 (EPS-) cultures were prepared as described above. Then, 300 µl aliquots of stationary-phase culture were added to M9 agar plates with 0.4%glycerol, spread by shaking with 3mm sterile glass beads, then incubated at 30 ˚C for 3 d. Samples of bacteria biofilm (approx. 10 mg) were carefully scraped from the plates (taking care not to remove any agar) and placed into tared metalized quartz sample pans (TA Instruments, New Castle, DE).

Because initial water content in agar plate scrapings may vary between replicates due to different ambient humidity and temperature on the day of experiments, bacterial biofilm samples were first dried to a consistent, low water content at 40 ˚C and 10% relative humidity in N_2 for 9 h. Then, the humidity was increased to 90% in 10 min, and held steady for 9 h to allow bacterial EPS to rehydrate and swell with water vapor. Finally, the humidity was decreased from 90% to 80%, for comparison with micromodel experiments, as the evaporation rate of water was determined gravimetrically.

5.4. Results

5.4.1. Pore-scale Patterns of Air Infiltration

Composite images of microchannels depict the micro-scale progression of the air interface during drying. A down-selected time series of composite images is provided in Figure 5-6. Across treatments and replicates, microstructural features of the channel geometry constrained the progression of the air interface. For both EPS+ and EPS- treatments, air was observed to initially infiltrate more readily from the left side of each microchannel due to the random arrangement of pore throat sizes at the channel edges. Pore throat geometry also determined the advancement of the air-infiltration front, but the rate of advancement was different for EPS+ and EPS- replicates. In all replicates of both treatments, the air interface at the right remained fixed in either of two positions over several hours. For example, in channel 2 of the EPS- treatment, the air interface in the second composite image (after 2.5 h drying) was located about 8% across the channel, or about 1.6 mm from the right side (Figure 5-6), with similar results for channels 3-5. In the EPS+ treatment, the air interface also stalled at a similar position in channels 1, 3, 4, 5, and 6. However, the interface remained in this position much longer in the EPS+ treatments, up to 16.5 h. A second stall position can be seen in several channels, for example, in the 3^{rd}-5^{th} frames for channel 2 of the EPS+ treatment (Figure 5-6). This second stall position was also observed in the other 5 channels of the EPS+ treatment, but for shorter durations (typically 0.5 h). This second stall position was apparent in all of the channels of the EPS- treatment for durations ranging from 2-5 h.

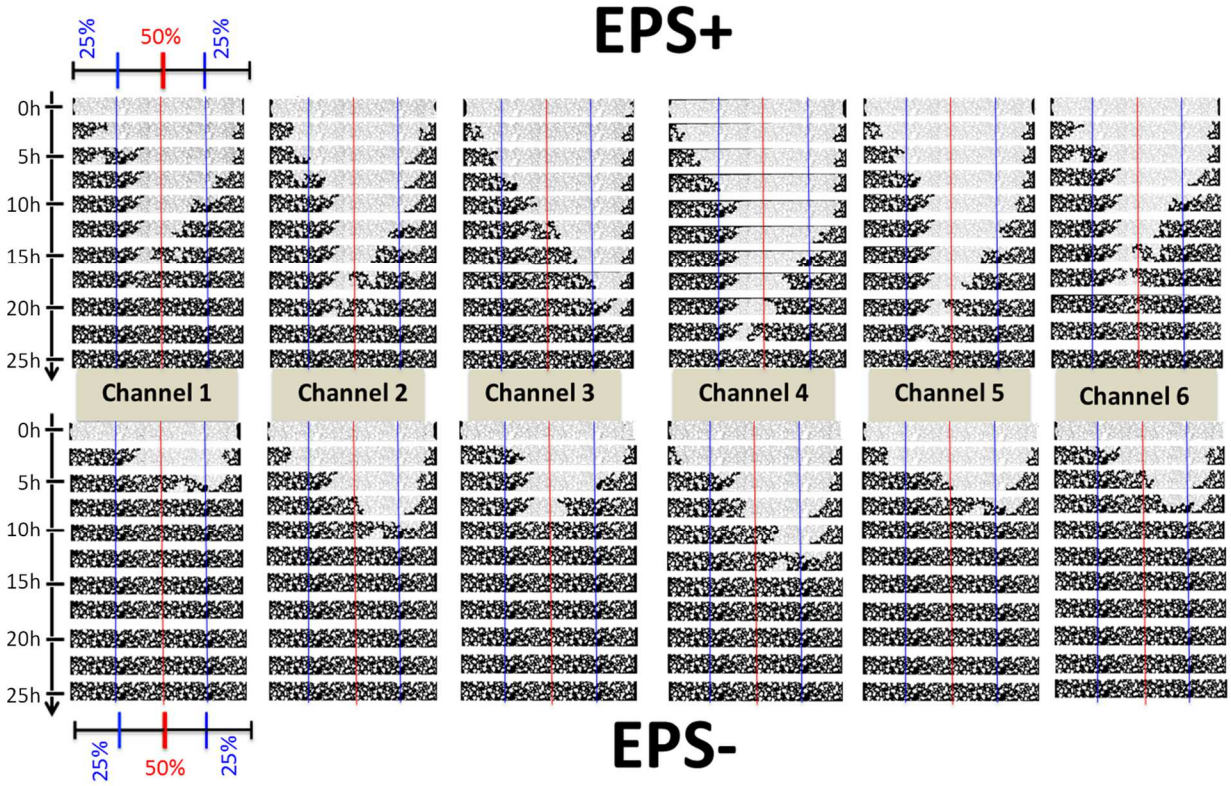

Figure 5-6 Time series of composite images showing air infiltration (in black) in replicate microchannels.

The time between frames is 2.5 h. Physically identical channels filled with EPS+ suspensions are at the top and channels filled with EPS- suspensions are at the bottom. The position of replicate channels in the control chamber is provided in Figure 2A. Vertical lines signify the midline and the quartile distances from each edge of the 20mm-long micro-structured region.

Pore-scale patterns of air infiltration led to the persistence of hydrated pockets in large open pore spaces connected to the rest of the pore network by narrow pore throats similar across several of the channels. One such region that was visible across several of the channels can be visualized in Figure 5-6, channel 1 of the EPS- treatment, frame 3, about 33% along the channel from the right side. This hydrated pocket persists longer in the EPS+ treatment than in the EPS- treatment. For example, it is observed in channel 1 and channel 6 of the EPS+ treatment for 5 frames each (2 h). The pocket is also observed in channels 1, 2, 4, and 5 of the EPS- treatment, but only for an average of 1 h. Small hydrated pockets are also apparent in interstitial spaces between particles. Figure 5-7 employs a chromatic time scale to map persistence of hydration within the microchannel. In the EPS+ treatment, several small spaces measuring just a few microns remain hydrated for up to 5 h (indicated by the dark green color). These same positions remained hydrated for 3 h in the EPS- treatment.

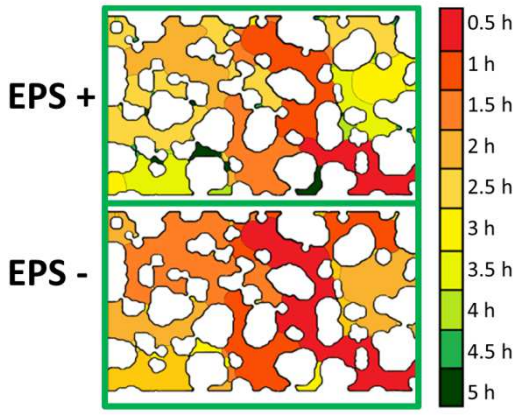

Figure 5-7 Chromatic illustration of air infiltration with time.

Air infiltration that occurs in the first 0.5 h is represented in red, and infiltration at each subsequent 0.5 h period is represented by the chromatic series through green at 5 h. Note the propensity for the air-water interface to exist at pore throats, and the persistence of hydrated pockets in the EPS+ treatment.

5.4.2. Drying Rates in Micromodels Containing EPS+ and EPS- Suspension

Soil micromodels loaded with EPS+ *S. meliloti* suspensions retained moisture longer than micromodels loaded with EPS- *S. meliloti* suspension (Figure 5-8A). On average, *S. meliloti* Rm11609 (EPS-) dried in 12.1 h with a standard deviation of 2.9 h, and Rm 8530 (EPS+) dried in 22.7 h with a standard deviation of 3.1h (Table 5.2).The drying rate for channels filled with the EPS- suspension (Figure 5-8B) decreased continuously, from around 0.3μg min^{-1} at the beginning of the experiment to 0 within 20h. The drying rate for channels in the EPS+ treatment was more consistent over time: generally water was lost at a rate of 0.15 μg min^{-1} for the first several hours and about 0.1 μg min^{-1} from 5-10 h.

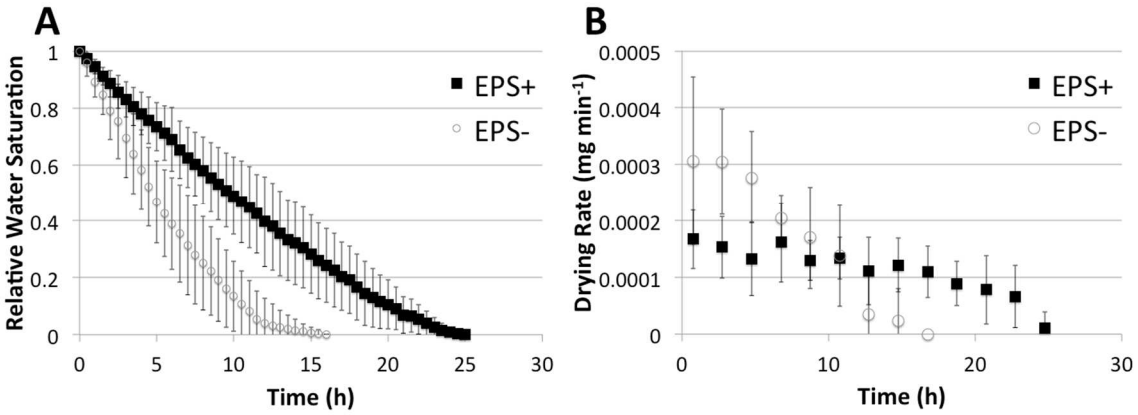

Figure 5-8 Experimental results of relative water saturation and drying rate in microfluidic devices.

(A) Relative water saturation versus time for channels filled with EPS+ or EPS- bacterial suspensions (average and standard deviation of 6 replicates). (B) Instantaneous drying rate using a 2 h moving average (average and standard deviation of 6 replicates).

Table 5.2 Drying times for each microdevice channel

Channel	EPS+ drying time (h)	EPS- drying time (h)	Difference (h)	Ratio (EPS+ drying time/ EPS- drying time)
1	24.0	13.5	10.5	1.8
2	24.5	12.0	12.5	2.0
3	25.5	11.5	14.0	2.2
4	24.5	11.5	13.0	2.1
5	19.0	7.5	11.5	2.5
6	18.5	16.5	2.0	1.1
Average	23	12	11	1.9

At 11 h into the drying process, average drying rates measured for the two treatments were similar (0.16μg min^{-1}). At 11 h, microchannels filled with the EPS- suspension were just 10% saturated, while microchannels filled with the EPS+ suspension were about 45% saturated. Towards the end of the drying process, the drying rate was greater in the EPS+ treatment channels (which still had much more water to lose) than the nearly-desiccated microchannels of the EPS- treatment.

Microchannels filled with EPS+ bacterial suspensions required more time to dry to a given relative saturation compared with microchannels filled with EPS- bacterial suspensions (Figure 5-9). EPS+ treatment microchannels required 4.5 h ±1.4 h (average ±standard deviation) to reach 80% saturation versus 2.8±1.1 h for EPS- treatment microchannels. The EPS- treatment channels dried to 80% saturation 1.6× faster than the EPS+ treatment microchannels. Similarly, the time required to reach other milestones of 60%, 40%, 20%, and 0% relative water saturation were significantly shorter for EPS-treatment channels. The ratio of drying time in EPS- to EPS+ treatments for these milestones was a factor of 2.0, 1.9, 1.9, and 1.9 times faster, respectively.

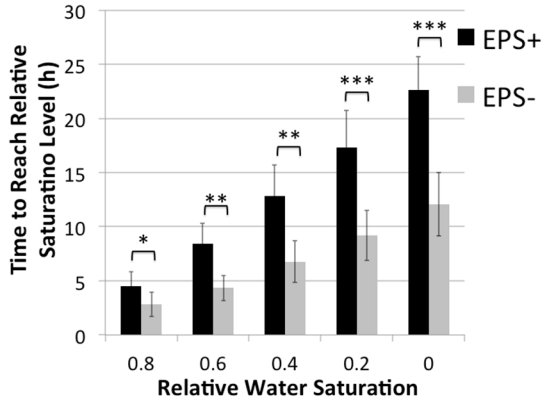

Figure 5-9 Time to reach various water saturation thresholds (average and standard deviation of 6 replicates).

Significance levels: * p<0.05, ** p<0.01,*** p<0.001 (2-tailed t-test, unequal variance).

5.4.3. Thermogravimetric Analysis of Bacteria-Amended Soil

The process of labile water loss from rewetted bacteria-amended soil was determined in duplicate for each bacterial strain treatment. Water evaporation with moderate drying (40 °C) was normalized to the last 3 mg of water added into the 100 mg of soil (Figure 5-10A). No obvious difference in drying rate was observed between EPS- amended soil and EPS+ amended soil samples in the early stages of drying (Figure 5-10A). However, considering the last 3 mg water (7.5%), the normalized water content in EPS- amended soil was lower than the water content of EPS+ amended soil ($p<0.0001$) (Figure 5-10B).

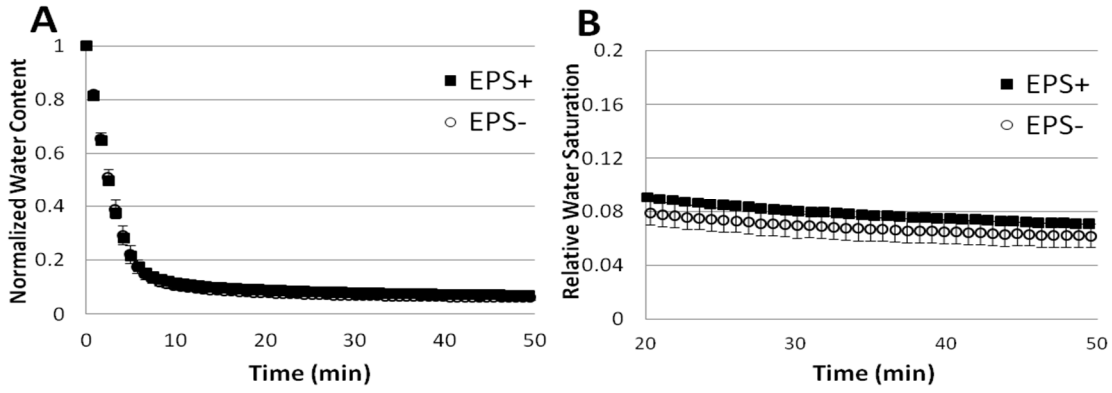

Figure 5-10 Experimental results of bacteria amended soil using thermal gravimetric analysis.

(A) Normalized water content for bacteria-amended whole soil samples (100 mg dry soil) measured using thermal gravimetric analysis (40 ºC, dry air, average and range of duplicates). Water content is normalized to the last 3 mg of water added to 100 mg dry soil. (B) Detail of the 20-50 min time domain.

5.4.4 Dynamic Vapor Sorption Analysis of Unstructured Biofilms

Bacterial EPS can retain moisture in soil two ways: by holding water directly in the cross-linked hydrogel polymer itself, and through soil structuring which alters the physical arrangement of soil grains. Here, to understand the ability of EPS to hold water directly without a physical structure, the swelling and drying behavior of duplicate biofilm samples collected from agar plates for both model strains were analyzed using dynamic vapor sorption.

The weight of each biofilm sample was normalized to its weight at equilibrium in 90% relative humidity. Then, once humidity was reduced to 80%, the loss of weight with evaporation was measured over time (Figure 5-11A and B). Data shows there is no difference in water content in pure bacterial biofilms from the EPS+ and EPS- strains.

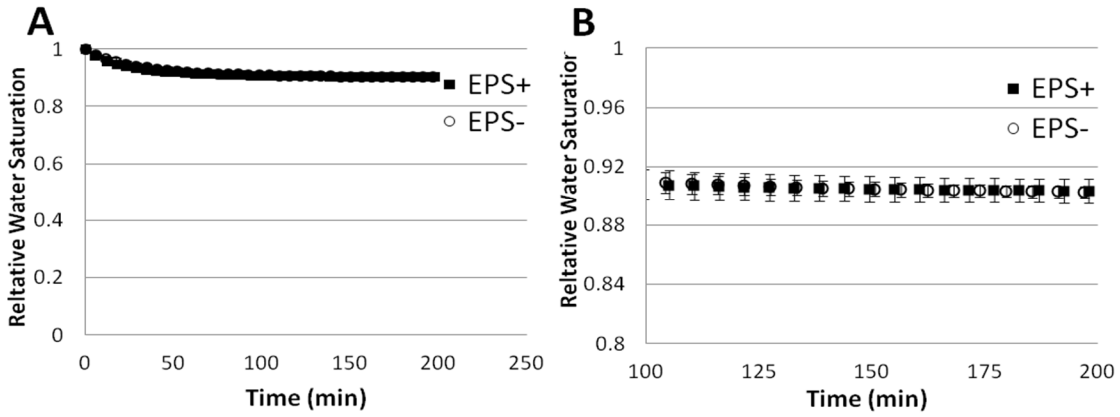

Figure 5-11 Relative water saturation versus time for pure bacterial colony samples measured using dynamic vapor sorption.

(A) Relative water saturation versus time for pure bacteria scraped from a plate measured dynamic vapor sorption (23 ºC, 90% to 80% relative humidity, average and range of duplicates). (B) Detail of the 100-200 min time domain.

5.5. Discussion

5.5.1. Pore-scale Mechanisms of Water Retention and Evaporation.

The rate of air infiltration into replicate emulated soil microdevices depends on the combined effects of micro-scale physical features of the microchannels and the chemical composition of the interstitial fluid. Progression of the air-water interface through the pore spaces in micromodel channels is determined by the evaporative flux of water across the air-water interface and diffusion of water vapor down the air-filled microchannel. The evaporative flux depends on the relative magnitudes of the matric and solute potential of the wetting phase (EPS solution) and the lower potential of water vapor in the air phase.

In our microdevice experiments, all replicates were subject to identical, constant relative humidity and temperature boundary conditions, thus determining the potential of the water vapor according to $R_H=\exp((MW_w\psi_w)/(\rho_w RT))$ (Or and Wraith 2002) where MW_w is the molecular weight of water, ψ_w is water potential, ρ_w is water density, R is the universal gas constant, and T is absolute temperature. The 80% relative humidity applied external to the soil micromodel corresponds to a matric potential of -30 MPa, representing extremely dry conditions under which bacterial respiration would cease in a real soil (Or et al. 2007b; Potts 1994). This condition was chosen to produce reasonable drying times for the micromodels under EPS+ and EPS- conditions.

Because the physical geometry is identical, the diffusivity of water vapor from the air-water interface is also identical between replicate channels. The potential of liquid water is a function of the physical geometry of the microchannel and the chemical composition of the EPS solution. Physical geometry varies with position, and chemical composition may vary with both position and time due to the dynamic activities of live bacteria.

The physical geometry of the micromodels determines the path taken by the invading air phase. Air invasion into a porous medium exhibits invasion-percolation behavior (Sukop and Or 2003) in which the non-wetting fluid (air) first invades the largest pore throat where capillary forces are weakest. Once the throat is breached, the comparatively large pore space behind it fills with air quickly (i.e., the water evaporates), followed by the next-largest pore throat of the new interfacial configuration.

Here, air infiltration behavior is consistent with invasion-percolation behavior. The path taken by the air interface was observed to follow similar patterns across treatments and replicates. Certain regions in the microchannels readily admitted the invading air space, while others regions with narrow pore throats were associated with stall positions of the air interface, or boundaries of persistent hydrated pockets. As in natural porous media, water is held more strongly in narrow hydrophilic spaces between PDMS pillars where capillarity is strongest. As stated earlier, PMDS exhibits a hydrophilic surface chemistry after exposure to oxygen plasma, with a surface charge similar to quartz sand (Roman and Culbertson 2006). Also, the surface chemistry of PMDS remains hydrophilic as long as water is in contact with PDMS (Mukhopadhyay 2007).

Microfabrication conserves the physical geometry across treatments and replicates, resulting in reproducible patterns of air infiltration. However, live bacteria move, grow, and respire within the microchannels. The resulting spatial distribution and population density of microbial communities and the chemical composition of the interstitial fluid after the 5 d conditioning period may vary between replicates, and especially if bacteria have aggregated at critical pore throats. The variable behavior of the bacterial population may have been responsible for the variations observed in patterns with air infiltration across replicates.

The chemical composition of the interstitial fluid also affects the rate of evaporation from microchannels. Here, fluid in the pore spaces contains a mixture of bacterial cells, salts, proteins, small molecules, and especially in the EPS+ treatment, extracellular polymers. Hydrogels are known to retain moisture through the favorable entropy of mixing between H_2O molecules and the polysaccharide, resulting in a lower activity of water in the hydrogel phase relative to pure water phase (Flemming 2011).

Here we show, for both whole soils and soil micromodels, amendment with the EPS+ strain resulted in a marked evaporation resistance. The evaporation time was ranged from 1.1 to 2.5× slower in replicate micromodels, with an average of 1.9× slower for the EPS+ versus EPS- treatment. In the corresponding size fraction of bacteria-amended soil, water content is also higher, but only approaching dryness ($p<0.0001$). In the micromodels, the surface area available for air infiltration are the 1 mm × 34 μm opening at the end of each channel and drying takes place at 20 ˚C and 80 % humidity. In whole soil experiments, there is much more surface area and drying takes place at 40 ˚C and 0% humidity. The smaller air-water interface and the lower external evaporativity lead to greater sensitivity and slower evaporation in the micromodels.

Surprisingly, we observed no difference in water content from pure biofilm collected from agar plates between EPS+ and EPS- strains of *S. meloliti*. The fact that evaporation resistance is only seen in a micro-structured matrix (soil or microdevice), and not in a pure biofilm sample suggests a synergistic effect of physical microstructure and chemical features of the biological sample in evaporation resistance.

We hypothesize that hydrophilic solid surfaces may provide mechanical stability for a dry and denser interface formed at the edges of the collapsing EPS matrix with evaporation

(Roberson et al. 1993). This crust has an intrinsically lower permeability to water, but without mechanical stabilization, cracks may form, thus exposing the EPS interior. Cracking of EPS matrix under desiccation has been observed by microscopy in EPS-amended soils (Chenu 1993). To test this hypothesis, additional experiments are needed to test permeability and mechanical properties of model hydrogel membranes in various physically confined and supported geometries.

5.5.2. Water Evaporation Rate and Implications for Agriculture

We provide direct evidence that microbes can modulate water evaporation at the pore scale. The average wilting point for many crops is between 15 and 27% soil moisture (Powers 1922). Here, micromodels filled with the EPS- bacterial suspension dropped below 15% saturation at about 10 h. Meanwhile, physically identical micromodels filled with the EPS+ bacterial suspension were still 50% saturated at 10 h. Here, the delay in water loss is the key difference between EPS+ and EPS- treatment.

The rate of water loss may have strong implications for agriculture. Global circulation models do not necessarily predict changes in the amount of precipitation in many areas, but the rain that comes will be associated with more extreme events separated by longer rain return intervals (Field et al. 2012). The result of changing precipitation patterns is a robust prediction of reduced soil moisture in many regions. Soil amendment with EPS-producing strains as studied by Sandhya et al. (2009) and Alami et al. (2000), has the potential to slow evaporation. In combination with EPS-mediated soil structuring (Amellal et al. 1998; Emerson and McGarry 2003), the drying resistance effects demonstrated here could translate to an important field-scale effect. These measurable effects are longer timescales than those measured in our study.

5.5.3. Extensions and Limitations

Emulated soil micromodels allow systematic replication or alteration of micro-scale physical geometry. Although physical features can be controlled, variability in bacterial responses may lead to slight variations in overall performance of the bio-physico-chemical system. Fortunately, photolithography and soft lithography approaches are well-adapted to high-throughput analysis with identical physical structures used for multiple replicates across treatments.

The experiments described here employed a single physical geometry. However, our techniques are amenable to systematic alteration of physical pore geometry. Additional experiments are currently underway in which the spatial arrangement of the simulated soil grains are altered to create aggregated and non-aggregated variations. These experiments will help determine the relative importance of physical geometry versus solution chemistry in microbially-mediated pore-scale evaporation resistance.

Our micromodels feature a complex 2-D physical geometry, a uniform solid phase chemistry (a surface-treated polymer, not geological material), and an initially uniform solution chemistry. Clearly, this approach cannot capture all the physical, chemical, or biological features of real soils such as heterogeneous surface chemistry, steep micro-scale gradients in solution composition, and a patchy distribution of microorganisms. In particular, plant exudates in the rhizosphere have been shown to support a microhabitat with drastically different properties than bulk soil. Microfluidic devices have been used to examine responses of bacterial biofilms to chemical gradients (Deng et al. 2013a). Ever more complex micromodels could be developed that also incorporate other important features of the soil system, such as micro-scale gradients of

plant exudates, to probe the effect of localized chemical conditions on microbial EPS production and pore-scale water retention near plant roots.

Finally, the minimum pore throat spacing in the emulated soil micromodels described here is about 5μm. Pore spaces smaller than 5μm are common in soils. Other microfabrication techniques could be used to create physical features down to about 1 μm, provided a commensurate reduction in the depth of the microchannels is also implemented. However, photolithography cannot be used to pattern features smaller than the wavelength of ultraviolet light. Other techniques including electron beam lithography can achieve greater resolution, but with potentially unacceptable costs in terms of materials, time, and a reduction in the device footprint.

5.6. Conclusion

Here we demonstrate the use of emulated soil micromodels to better understand how microbial processes modulate water availability at the pore scale. We provide direct evidence that microbial activities alter water retention at the pore scale. The mechanism proposed for pore-scale moisture retention is a physical stabilization of the polymeric skin at the air-water interface in the EPS+ treatment. Additional work will be needed to test the proposed mechanism and to provide greater predictive capability of microbial-mediated moisture retention in real soils.

Emulated soil micromodels are synthetic, idealized experimental systems. Micromodels are not meant to replace experiments performed with real soils or field-scale investigations. Rather, they provide a systematic approach for building pore-scale understanding of the physical, chemical, and biological factors that interact in real soils at the pore scale. By using emulated soil micromodels, pore scale geometry can be exactly replicated. Geometrically difined air

infiltration openings of the micromodel can greatly increase the sensitivity of water loss measurement compare to standard approaches using real soils. Also, additional features of real soils can be incorporated into micromodels of increasing complexity.

As a starting point, the micromodel approach described here may be useful in developing sustainable agriculture biotechnologies. By holding physical geometry and external evaporativity constant, the technique could be used to screen the ability of different microbial strains to produce EPS under various conditions for the purpose of controlling soil moisture. One day, it may be possible to more sustainably retain soil moisture by stimulating natural microbial processes *in situ.*

5.7 References

Addae-Mensah KA, Retterer S, Opalenik SR, Thomas D, Lavrik NV, Wikswo JP. 2009. Cryogenic Etching of Silicon: An Alternative Method For Fabrication of Vertical Microcantilever Master Molds. J Microelectromech Syst 19(1).

Ahmed T, Shimizu TS, Stocker R. 2010. Bacterial Chemotaxis in Linear and Nonlinear Steady Microfluidic Gradients. Nano Letters 10(9):3379-3385.

Alami Y, Achouak W, Marol C, Heulin T. 2000. Rhizosphere Soil Aggregation and Plant Growth Promotion of Sunflowers by an Exopolysaccharide-Producing Rhizobiumsp. Strain Isolated from Sunflower Roots. Applied and environmental microbiology 66(8):3393-3398.

Alborn Jr WE, Allen NE, Preston DA. 1991. Daptomycin disrupts membrane potential in growing Staphylococcus aureus. Antimicrobial Agents and Chemotherapy 35(11):2282-2287.

Amellal N, Burtin G, Bartoli F, Heulin T. 1998. Colonization of Wheat Roots by an Exopolysaccharide-ProducingPantoea agglomerans Strain and Its Effect on Rhizosphere Soil Aggregation. 64 10(3740-3747).

Anderl JN, Franklin MJ, Stewart PS. 2000. Role of antibiotic penetration limitation in Klebsiella pneumoniae biofilm resistance to ampicillin and ciprofloxacin. Antimicrob. Agents Chemother. 44(7):1818-1824.

Anderson GG, O'Toole GA. 2008. Innate and induced resistance mechanisms of bacterial biofilms. Bacterial Biofilms. p 85-105.

Ball P, Baquero F, Cars O, File T, Garau J, Klugman K, Low DE, Rubinstein E, Wise R, Consensus Grp Resistance P. 2002. Antibiotic therapy of community respiratory tract infections: strategies for optimal outcomes and minimized resistance emergence. J. Antimicrob. Chemother. 49(1):31-40.

Bassetti M, Di Biagio A, Rebesco B, Amalfitano ME, Topal J, Bassetti D. 2001. The effect of formulary restriction in the use of antibiotics in an Italian hospital. European Journal of Clinical Pharmacology 57(6-7):529-534.

Bennett MR, Hasty J. 2009. Microfluidic devices for measuring gene network dynamics in single cells. Nature Reviews Genetics 10(9):628-638.

Benoit MR, Conant CG, Ionescu-Zanetti C, Schwartz M, Matin A. 2010. New Device for High-Throughput Viability Screening of Flow Biofilms. Appl. Environ. Microbiol. 76(13):4136-4142.

Binz M, Lee AP, Edwards C, Nicolau DV. 2010. Motility of bacteria in microfluidic structures. Microelectronic Engineering 87(5-8):810-813.

Bouchillon GM, Chau JF, McManus GB, Shor LM. 2014. Microfluidic passive samplers for in situ collection of live aquatic protists. Analytical Methods 6(20):8350-8357.

Brazier JS, Raybould R, Patel B, Duckworth G, Pearson A, Charlett A, Duerden BI, Network HPARM. 2008. Distribution and antimicrobial susceptibility patterns of Clostridium difficile PCR ribotypes in English hospitals, 2007-08. Euro Surveill. 13(41):541-544.

Buchholz F, Wolf A, Lerchner J, Mertens F, Harms H, Maskow T. 2010. Chip Calorimetry for Fast and Reliable Evaluation of Bactericidal and Bacteriostatic Treatments of Biofilms. Antimicrob. Agents Chemother. 54(1):312-319.

Carminati A, Schneider CL, Moradi AB, Zarebanadkouki M, Vetterlein D, Vogel H-J, Hildebrandt A, Weller U, Schüler L, Oswald SE. 2011. How the rhizosphere may favor water availability to roots. Vadose Zone Journal 10(3):988-998.
Carpenter CF, Chambers HF. 2004. Daptomycin: Another novel agent for treating infections due to drug-resistant gram-positive pathogens. Clinical Infectious Diseases 38(7):994-1000.
Ceri H, Olson ME, Stremick C, Read RR, Morck D, Buret A. 1999. The Calgary Biofilm Device: New technology for rapid determination of antibiotic susceptibilities of bacterial biofilms. J. Clin. Microbiol. 37(6):1771-1776.
Chambers HF. 2001. The changing epidemiology of staphylococcus aureus? Emerging Infectious Diseases 7(2):178-182.
Chau JF, Bagtzoglou AC, Willig MR. 2011. The effect of soil texture on richness and diversity of bacterial communities. Environmental Forensics 12:333-341.
Chau JF, Or D. 2006. Linking drainage front morphology with gaseous diffusion in unsaturated porous media: A lattice Boltzmann study. Physical Review E - Statistical, Nonlinear, and Soft Matter Physics 74(5).
Chau JF, Or D, Sukop MG. 2005. Simulation of gaseous diffusion in partially saturated porous media under variable gravity with lattice Boltzmann methods. Water Resources Research 41(8):1-11.
Cheng S-Y, Heilman S, Wasserman M, Archer S, Shuler ML, Wu M. 2007. A hydrogel-based microfluidic device for the studies of directed cell migration. Lab on a Chip 7(6):763-769.
Chenu C. 1993. Clay- or sand-polysaccharide associations as models for the interface between micro-organisms and soil: water related properties and microstructure. Geoderma 56(1-4):143-156.
Chenu C, Roberson EB. 1996. Diffusion of glucose in microbial extracellular polysaccharide as affected by water potential. Soil Biology & Biochemistry 28(7):877-884.
Cho G-C, Dodds J, Santamaria JC. 2006. Particle shape effects on packing density, stiffness, and strength: natural and crushed sands. Journal of Geotechnical and Geoenvironmental Engineering 132:591-602.
Cho H, Jonsson H, Campbell K, Melke P, Williams JW, Jedynak B, Stevens AM, Groisman A, Levchenko A. 2007a. Self-organization in high-density bacterial colonies: Efficient crowd control. Plos Biology 5(11):2614-2623.
Cho HJ, Jonsson H, Campbell K, Melke P, Williams JW, Jedynak B, Stevens AM, Groisman A, Levchenko A. 2007b. Self-organization in high-density bacterial colonies: Efficient crowd control. Plos Biology 5(11):2614-2623.
Choi WS, Ha D, Park S, Kim T. 2011. Synthetic multicellular cell-to-cell communication in inkjet printed bacterial cell systems. Biomaterials 32(10):2500-2507.
Choi WS, Kim M, Park S, Lee SK, Kim T. 2012. Patterning and transferring hydrogel-encapsulated bacterial cells for quantitative analysis of synthetically engineered genetic circuits. Biomaterials 33(2):624-33.
Chung K, Rivet CA, Kemp ML, Lu H. 2011. Imaging Single-Cell Signaling Dynamics with a Deterministic High-Density Single-Cell Trap Array. Anal. Chem. 83(18):7044-7052.
Crane MM, Chung K, Stirman J, Lu H. 2010. Microfluidics-enabled phenotyping, imaging, and screening of multicellular organisms. Lab Chip 10(12):1509-1517.
Curtin J, Cormican M, Fleming G, Keelehan J, Colleran E. 2003. Linezolid compared with eperezolid, vancomycin, and gentamicin in an in vitro model of antimicrobial lock

therapy for Staphylococcus epidermidis central venous catheter-related biofilm infections. Antimicrob. Agents Chemother. 47(10):3145-3148.
Cywinski PJ, Moro AJ, Stanca SE, Biskup C, Mohr GJ. 2009. Ratiometric porphyrin-based layers and nanoparticles for measuring oxygen in biosamples. Sens Actuators B Chem 135(2):472-477.
Dai A. 2011. Drought under global warming: a review. Wiley Interdisciplinary Reviews: Climate Change 2(1):45-65.
Davies D. 2003. Understanding biofilm resistance to antibacterial agents. Nature Reviews Drug Discovery 2(2):114-122.
Dechesne A, Wang G, Gülez G, Or D, Smets BF, Tiedje JM. 2010. Hydration-controlled bacterial motility and dispersal on surfaces. Proceedings of the National Academy of Sciences of the United States of America 107(32):14369-14372.
Deng J, Dhummakupt A, Samson PC, Wikswo JP, Shor LM. 2013a. Dynamic dosing assay relating real-time respiration responses of *Staphylococcus aureus* biofilms to changing microchemical conditions. Analytical Chemistry 85:5411-5419.
Deng JZ, Dhummakupt A, Samson PC, Wikswo JP, Shor LM. 2013b. Dynamic Dosing Assay Relating Real-Time Respiration Responses of Staphylococcus aureus Biofilms to Changing Microchemical Conditions. Anal. Chem. 85(11):5411-5419.
Dharmasiri U, Witek MA, Adams AA, Osiri JK, Hupert ML, Bianchi TS, Roelke DL, Soper SA. 2010. Enrichment and Detection of Escherichia coli O157:H7 from Water Samples Using an Antibody Modified Microfluidic Chip. Analytical Chemistry 82(7):2844-2849.
Donlan RM. 2001. Biofilm formation: A clinically relevant microbiological process. Clin. Infect. Dis. 33(8):1387-1392.
Donlan RM, Costerton JW. 2002. Biofilms: Survival mechanisms of clinically relevant microorganisms. clin. Microbiol. Rev. 15(2):167-+.
Emerson WW, McGarry D. 2003. Organic carbon and soil porosity. Australian Journal of Soil Research 41(1):107-118.
Field CB, Barros V, Stocker TF, Dahe Q. 2012. Managing the Risks of Extreme Events and Disasters to Advance Climate Change Adaptation: Special Report of the Intergovernmental Panel on Climate Change: Cambridge University Press.
Flemming H-C. 2011. The perfect slime. Colloids and Surfaces B: Biointerfaces 86(2):251-259.
Friedman SP, Robinson DA. 2002. Particle shape characterization using angle of repose measurements for predicting the effective permittivity and electrical conductivity of saturated granular media. Water Resources Research 38:1236.
Gage DJ. 2004. Infection and invasion of roots by symbiotic, nitrogen-fixing rhizobia during nodulation of temperate legumes. Microbiology and Molecular Biology Reviews 68(2):280-300.
Gajic B, Durovic N, Dugalic G. 2010. Composition and stability of soil aggregates in Fluvisols under forest, meadows, and 100 years of conventional tillage. Journal of Plant Nutrition and Soil Science 173:502-509.
Galibert F, Finan TM, Long SR, Puhler A, Abola P, al. e. 2001. The composite genome of the legume symbiont *Sinorhizobium meliloti*. Science 293(5530):668-672.
Gaynes R. 1997. The impact of antimicrobial use on the emergence of antimicrobial-resistant bacteria in hospitals. Infectious Disease Clinics of North America 11(4):757-&.

Grate JW, Kelly RT, Suter J, Anheier NC. 2012. Silicon-on-glass pore network micromodels with oxygen-sensing fluorophore films for chemical imaging and defined spatial structure. Lab Chip 12(22):4796-4801.

Hammoudi TM, Lu H, Temenoff JS. 2010. Long-Term Spatially Defined Coculture Within Three-Dimensional Photopatterned Hydrogels. Tissue Eng., Part C 16(6):1621-1628.

Han P, Bartels DM. 1996. Temperature dependence of oxygen diffusion in H2O and D2O. J. Phys. Chem. 100(13):5597-5602.

Hayden MK, Rezai K, Hayes RA, Lolans K, Quinn JP, Weinstein RA. 2005. Development of daptomycin resistance in vivo in methicillin-resistant Staphylococcus aureus. Journal of Clinical Microbiology 43(10):5285-5287.

Herzberg M, Elimelech M. 2007. Biofouling of reverse osmosis membranes: Role of biofilm-enhanced osmotic pressure. J. Membr. Sci. 295(1-2):11-20.

Houari A, Di Martino P. 2007. Effect of chlorhexidine and benzalkonium chloride on bacterial biofilm formation. Lett. Appl. Microbiol. 45(6):652-656.

Jia X, Williams RA. 2001. A packing algorithm for particles of arbitrary shapes. Powder Technology 120:175-186.

Jones T, Yeaman MR, Sakoulas G, Yang SJ, Proctor RA, Sahl HG, Schrenzel J, Xiong YQ, Bayer AS. 2008. Failures in clinical treatment of Staphylococcus aureus infection with daptomycin are associated with alterations in surface charge, membrane phospholipid asymmetry, and drug binding. Antimicrobial Agents and Chemotherapy 52(1):269-278.

Kaci Y, Heyraud A, Barakat M, Heulin T. 2005. Isolation and identification of an EPS-producing Rhizobium strain from arid soil (Algeria): characterization of its EPS and the effect of inoculation on wheat rhizosphere soil structure. Research in Microbiology 156:522-531.

Karki U, Goodman M. 2011. Short-term soil quality response to forage species and pH. Grass and Forage Science 66:290-299.

Kets EPW, deBont JAM, Heipieper HJ. 1996. Physiological response of Pseudomonas putida S12 subjected to reduced water activity. Fems Microbiology Letters 139(2-3):133-137.

Kim HJ, Boedicker JQ, Choi JW, Ismagilov RF. 2008. Defined spatial structure stabilizes a synthetic multispecies bacterial community. Proceedings of the National Academy of Sciences 105(47):18188-18193.

Kim J, Hegde M, Kim SH, Wood TK, Jayaraman A. 2012. A microfluidic device for high throughput bacterial biofilm studies. Lab Chip 12(6):1157-1163.

Kim KP, Kim Y-G, Choi C-H, Kim H-E, Lee S-H, Chang W-S, Lee C-S. 2010. In situ monitoring of antibiotic susceptibility of bacterial biofilms in a microfluidic device. Lab Chip 10(23):3296-3299.

Kim M, Kim T. 2010. Diffusion-Based and Long-Range Concentration Gradients of Multiple Chemicals for Bacterial Chemotaxis Assays. Analytical Chemistry 82(22):9401-9409.

Kovarik ML, Brown PJB, Kysela DT, Berne C, Kinsella AC, Brun YV, Jacobson SC. 2010. Microchannel-Nanopore Device for Bacterial Chemotaxis Assays. Analytical Chemistry 82(22):9357-9364.

Laitinen HA, Kolthoff IM. 1939. A Study of Diffusion Processes by Electrolysis with Microelectrodes. J. Am. Chem. Soc. 61(12):3344–3349.

Lam RHW, Kim M-C, Thorsen T. 2009. Culturing Aerobic and Anaerobic Bacteria and Mammalian Cells with a Microfluidic Differential Oxygenator. Anal. Chem. 81(14):5918-5924.

Langelier SM, Livak-Dahl E, Manzo AJ, Johnson BN, Walter NG, Burns MA. 2011. Flexible casting of modular self-aligning microfluidic assembly blocks. Lab Chip 11(9):1679-87.

Lanning LM, Ford RM, Long T. 2008. Bacterial chemotaxis transverse to axial flow in a microfluidic channel. Biotechnology and bioengineering 100(4):653-663.

LaPlante KL, Mermel LA. 2007. In vitro activity of daptomycin and vancomycin lock solutions on staphylococcal biofilms in a central venous catheter model. Nephrology Dialysis Transplantation 22(8):2239-2246.

LaPlante KL, Woodmansee S. 2009. Activities of daptomycin and vancomycin alone and in combination with rifampin and gentamicin against biofilm-forming methicillin-resistant Staphylococcus aureus isolates in an experimental model of endocarditis. Antimicrobial Agents and Chemotherapy 53(9):3880-3886.

Lasa I, Del Pozo JL, Penadés JR, Leiva J. 2005. Bacterial biofilms and infection. Anales del Sistema Sanitario de Navarra 28(2):163-175.

Lee J-HLJBKWY. 2008. Microfluidic devices for studying growth and detachment of Staphylococcus epidermidis biofilms. Biomed Microdevices 10:489-498.

Li X, Yuan Y. 2002. Settling velocities and permeabilities of microbial aggregates. Water Research 36:3110-3120.

Lichstein HC, Soule MH. 1944. Studies of the Effect of Sodium Azide on Microbic Growth and Respiration: I. The Action of Sodium Azide on Microbic Growth. Journal of Bacteriology 47(3):221-30.

Long T, Ford RM. 2009. Enhanced transverse migration of bacteria by chemotaxis in a porous T-sensor. Environmental science & technology 43(5):1546-1552.

Long T, Or D. 2009. Dynamics of Microbial Growth and Coexistence on Variably Saturated Rough Surfaces. Microbial Ecology 58(2):262-275.

Mach AJ, Di Carlo D. 2010. Continuous Scalable Blood Filtration Device Using Inertial Microfluidics. Biotechnology and Bioengineering 107(2):302-311.

Macia MD, Perez JL, Molin S, Oliver A. 2011. Dynamics of Mutator and Antibiotic-Resistant Populations in a Pharmacokinetic/Pharmacodynamic Model of Pseudomonas aeruginosa Biofilm Treatment. Antimicrob. Agents Chemother. 55(11):5230-5237.

Mah TF, Pitts B, Pellock B, Walker GC, Stewart PS, O'Toole GA. 2003. A genetic basis for Pseudomonas aeruginosa biofilm antibiotic resistance. Nature 426(6964):306-310.

Mao H, Cremer PS, Manson MD. 2003. A sensitive, versatile microfluidic assay for bacterial chemotaxis. Proceedings of the National Academy of Sciences 100(9): 5449-5454.

Markov DA, Samson PC, Schaffer DK, Dhummakupt A, Wikswo JP, Shor LM. 2010a. Window on a Microworld: Simple Microfluidic Systems for Studying Microbial Transport in Porous Media. Journal of Visualized Experiments 39.

Markov DA, Samson PC, Schaffer DK, Dhummakupt A, Wikswo JP, Shor LM. 2010b. Window on a microworld: simple microfluidic systems for studying microbial transport in porous media. Journal of visualized experiments : JoVE(39).

Matz C, Kjelleberg S. 2005. Off the hook – how bacteria survive protozoan grazing. Trends in Microbiology 13(7):302-307.

Matz C, McDougald D, Moreno AM, Yung PY, Yildiz FH, Kjelleberg S. 2005. Biofilm formation and phenotypic variation enhance predation-driven persistence of Vibrio cholerae. Proc. Natl. Acad. Sci. U. S. A. 102(46):16819-16824.

McBrady AD, Chantiwas R, Torgerson AK, Grudpan K, Synovec RE. 2006. An absorbance-based micro-fluidic sensor for diffusion coefficient and molar mass determinations. Analytica Chimica Acta 575(2):151-158.

Merritt JH, Kadouri DE, O'Toole GA. 2005. Growing and analyzing static biofilms. Curr. Protoc. Microbiol. Chapter 1.

Meyer MT, Roy V, Bentley WE, Ghodssi R. 2011. Development and validation of a microfluidic reactor for biofilm monitoring via optical methods. J. Micromech. Microeng. 21(5).

Montagne K, Komori K, Yang F, Tatsuma T, Fujii T, Sakai Y. 2009. A micropatterned cell array with an integrated oxygen-sensitive fluorescent membrane. Photochem. Photobiol. Sci. 8(11):1529-1533.

Morales VL, Parlange JY, Steenhuis TS. 2010. Are preferential flow paths perpetuated by microbial activity in the soil matrix? A review. Journal of Hydrology 393(1-2):29-36.

Morten Hentzer GMT, Grant J. Balzer, Arne Heydorn,, Soren Molin MG, Matthew R. Parsek. 2001. Alginate Overproduction Affects Pseudomonas aeruginosa Biofilm Structure and Function. Journal of Bacteriology 183(5395-5401).

Moyano FE, Manzoni S, Chenu C. 2013. Responses of soil heterotrophic respiration to moisture availability: an exploration of processes and models. Soil Biology and Biochemistry 59:72-85.

Mueller K, Gonzalez JE. 2011. Complex Regulation of Symbiotic Functions Is Coordinated by MucR and Quorum Sensing in Sinorhizobium meliloti. Journal of Bacteriology 193(2):485-496.

Muesken M, Di Fiore S, Romling U, Haeussler S. 2010. A 96-well-plate-based optical method for the quantitative and qualitative evaluation of Pseudomonas aeruginosa biofilm formation and its application to susceptibility testing. Nat. Protoc. 5(8):1460-1469.

Mukhopadhyay R. 2007. When PDMS isn't the best. Analytical Chemistry 79(9):3248-3253.

Nam S-W, Kim S-T, Lee K-M, Kim SH, Kou S, Lim J, Hwang H, Joo MK, Jeong B, Yoo SH and others. 2009. N-Methyl-D-Aspartate Receptor-Mediated Chemotaxis and Ca(2+) Signaling in Tetrahymena pyriformis. Protist 160(2):331-342.

Nelson LK, Stanton MM, Elphinstone REA, Helwerda J, Turner RJ, Ceri H. 2010. Phenotypic diversification in vivo: Pseudomonas aeruginosa gacS(-) strains generate small colony variants in vivo that are distinct from in vitro variants. Microbiology 156:3699-3709.

Nishimura S, Tsurumoto T, Yonekura A, Adachi K, Shindo H. 2006. Antimicrobial susceptibility of Staphylococcus aureus and Staphylococcus epidermidis biofilms isolated from infected total hip arthroplasty cases. J. Orthop. Sci. 11(1):46-50.

Oki T, Kanae S. 2006. Global Hydrological Cycles and World Water Resources. Science 313(5790):1068 - 1072.

Olson ME, Slater SR, Rupp ME, Fey PD. 2010. Rifampicin enhances activity of daptomycin and vancomycin against both a polysaccharide intercellular adhesin (PIA)-dependent and -independent Staphylococcus epidermidis biofilm. J. Antimicrob. Chemother. 65(10):2164-2171.

Or D, Phutane S, Dechesne A. 2007a. Extracellular polymeric substances affecting pore-scale hydrologic conditions for bacterial activity in unsaturated soils. Vadose Zone J. 6(2):298-305.
Or D, Phutane S, Dechesne A. 2007b. Extracellular polymeric substances affecting pore-scale hydrologic conditions for bacterial activity in unsaturated soils. Vadose Zone Journal 6(2):298-305.
Or D, Smets BF, Wraith JM, Dechesne A, Friedman SP. 2007c. Physical constraints affecting bacterial habitats and activity in unsaturated porous media - a review. Advances in Water Resources 30(6-7):1505-1527.
Or D, Wraith JM. 2002. Soil water content and water potential relationships. In: Warrick A, editor. Soil Physics Companion. Boca Raton: CRC Press. p 49–84.
Pagedar A, Singh J, Batish VK. 2012. Adaptation to benzalkonium chloride and ciprofloxacin affects biofilm formation potential, efflux pump and haemolysin activity of Escherichia coli of dairy origin. J. Dairy Res. 79(4):383-389.
Park A, Jeong H-H, Lee J, Kim KP, Lee C-S. 2011. Effect of shear stress on the formation of bacterial biofilm in a microfluidic channel. Biochip Journal 5(3):236-241.
Park E-J, Sul WJ, Smucker AJ. 2007. Glucose additions to aggregates subjected to drying/wetting cycles promote carbon sequestration and aggregate stability. Soil Biology and Biochemistry 39(11):2758-2768.
Park ES, Brown AC, DiFeo MA, Barker TH, Lu H. 2010. Continuously perfused, non-cross-contaminating microfluidic chamber array for studying cellular responses to orthogonal combinations of matrix and soluble signals. Lab Chip 10(5):571-580.
Pellock BJ, Teplitski M, Boinay RP, Bauer WD, Walker GC. 2002. A LuxR homolog controls production of symbiotically active extracellular polysaccharide II by Sinorhizobium meliloti. Journal of Bacteriology 184(18):5067-5076.
Pereira SG, Paixao J, Leitao R, Cardoso O. 2011. Pseudomonas aeruginosa in a hydropathic facility: diversity, susceptibility and imipenem resistance mutation. Lett. Appl. Microbiol. 53(5):518-524.
Perez F, Salata R, Bonomo R. 2008. Current and novel antibiotics against resistant Gram-positive bacteria. Infect. Drug Resist.:27-44.
Potts M. 1994. Desiccation tolerance of prokaryotes. Microbiological Reviews 58(4):755-805.
Powers WL. 1922. Field Structure Capacity and Wilting Point of Soils. Soil Science 14(2):159-166.
Presterl E, Hajdu S, Lassnigg AM, Hirschl AM, Holinka J, Graninger W. 2009. Effects of Azithromycin in Combination with Vancomycin, Daptomycin, Fosfomycin, Tigecycline, and Ceftriaxone on Staphylococcus epidermidis Biofilms. Antimicrob. Agents Chemother. 53(8):3205-3210.
Raja A, LaBonte J, Lebbos J, Kirkpatrick P. 2003. Daptomycin. Nature Reviews Drug Discovery 2(12):943-944.
Ramos C, Licht TR, Sternberg C, Krogfelt KA, Molin S. 2001. Monitoring bacterial growth activity in biofilms from laboratory flow chambers, plant rhizosphere, and animal intestine. Microbial Growth in Biofilms, Pt B. p 21-42.
Rao TS, Kora AJ, Chandramohan P, Panigrahi BS, Narasimhan SV. 2009. Biofouling and microbial corrosion problem in the thermo-fluid heat exchanger and cooling water system of a nuclear test reactor. Biofouling 25(7):581-591.

Reyes-Romero DF, Behrmann O, Dame G, Urban GA. 2014. Dynamic thermal sensor for biofilm monitoring. Sensors and Actuators, A: Physical 213:43-51.
Richter SS, Heilmann KP, Dohrn CL, Riahi F, Beekmann SE, Doern GV. 2009. Changing Epidemiology of Antimicrobial-Resistant Streptococcus pneumoniae in the United States, 2004-2005. Clinical Infectious Diseases 48(3):E23-E33.
Rinaudi LV, Gonzalez JE. 2009. The Low-Molecular-Weight Fraction of Exopolysaccharide II from Sinorhizobium meliloti Is a Crucial Determinant of Biofilm Formation. Journal of Bacteriology 191(23):7216-7224.
Roberson EB, Chenu C, Firestone MK. 1993. Microstructural changes in bacterial exopolysaccharides during desiccation. Soil Biology and Biochemistry 25(9):1299-1301.
Roberson EB, Firestone MK. 1992. Relationship between desiccation and exopolysaccharide production in a soil Pseudomonas sp. APPLIED AND ENVIRONMENTAL MICROBIOLOGY 58(4):1284-1291.
Robertson EB, Firestone MK. 1992. Relationship between desiccation and exopolysaccharide production in a soil Pseudomonas sp. . Appl Environ Microbiol. 58:1284-1291.
Roman GT, Culbertson CT. 2006. Surface Engineering of Poly(dimethylsiloxane) Microfluidic Devices Using Transition Metal Sol−Gel Chemistry. Langmuir 22:4445-4451.
Rowan B, Wheeler MA, Crooks RM. 2002. Patterning bacteria within hyperbranched polymer film templates. Langmuir 18(25):9914-9917.
Rusconi R, Lecuyer S, Guglielmini L, Stone HA. 2010. Laminar flow around corners triggers the formation of biofilm streamers. J. R. Soc., Interface 7(50):1293-1299.
Salmon SA, Watts JL. 2000. Minimum inhibitory concentration determinations for various antimicrobial agents against 1570 bacterial isolates from turkey poults. Avian Dis. 44(1):85-98.
Sandhya V, Grover M, Reddy G, Venkateswarlu B. 2009. Alleviation of drought stress effects in sunflower seedlings by the exopolysaccharides producing Pseudomonas putida strain GAP-P45. Biology and fertility of soils 46(1):17-26.
Sauer K, Camper AK, Ehrlich GD, Costerton JW, Davies DG. 2002a. Pseudomonas aeruginosa displays multiple phenotypes during development as a biofilm. Journal of Bacteriology 184(4):1140-1154.
Sauer K, Camper AK, Ehrlich GD, Costerton JW, Davies DG. 2002b. Pseudomonas aeruginosa displays multiple phenotypes during development as a biofilm. J. Bacteriol. 184(4):1140-1154.
Schindelin J, Arganda-Carreras I, Frise E, Kaynig V, Longair M, Pietzsch T, Preibisch S, Rueden C, Saalfeld S, Schmid B and others. 2012. Fiji: An open-source platform for biological-image analysis. Nature Methods 9(7):676-682.
Scholl MA, Mills AL, Herman JS, Hornberger GM. 1990. The influence of mineralogy and solution chemistry on the attachment of bacteria to representative aquifer materials. Journal of Contaminant Hydrology 4(4):321-326.
Schulte EE, and Hopkins, B.G. 1996. Estimation of soil organic matter by weight loss-on-ignition. Soil Science Society of America 46:21-31.
Schuurmans JM, Hayali ASN, Koenders BB, ter Kuile BH. 2009. Variations in MIC value caused by differences in experimental protocol. J. Microbiol. Methods 79(1):44-47.

Seymour JR, Ahmed T, Durham WM, Stocker R. 2010. Chemotactic response of marine bacteria to the extracellular products of Synechococcus and Prochlorococcus. Aquatic Microbial Ecology 59(2):161-168.

Shiku H, Saito T, Wu CC, Yasukawa T, Yokoo M, Abe H, Matsue T, Yamada H. 2006. Oxygen permeability of surface-modified poly(dimethylsiloxane) characterized by scanning electrochemical microscopy. Chemistry Letters 35(2):234-235.

Shumi W, Lim J, Nam S-W, Lee K, Kim SH, Kim M-H, Cho K-S, Park S. 2010. Environmental factors that affect Streptococcus mutans biofilm formation in a microfluidic device mimicking teeth. Biochip Journal 4(4):257-263.

Silverman JA, Oliver N, Andrew T, Tongchuan LI. 2001. Resistance studies with daptomycin. Antimicrobial Agents and Chemotherapy 45(6):1799-1802.

Silverman JA, Perlmutter NG, Shapiro HM. 2003. Correlation of daptomycin bactericidal activity and membrane depolarization in Staphylococcus aureus. Antimicrobial Agents and Chemotherapy 47(8):2538-2544.

Singh R, Olson MS. 2011. Transverse mixing enhancement due to bacterial random motility in porous microfluidic devices. Environmental science & technology 45(20):8780-8787.

Skolimowski M, Nielsen MW, Emneus J, Molin S, Taboryski R, Sternberg C, Dufva M, Geschke O. 2010. Microfluidic dissolved oxygen gradient generator biochip as a useful tool in bacterial biofilm studies. Lab on a Chip 10(16):2162-2169.

Smucker AJM, Park E, Dorner J, Horn R. 2007. Soil micropore development and contributions to soluble carbon transport within macroaggregates. Vadose Zone Journal 6(2):282-290.

Snyder ML, Lichstein HC. 1940. Sodium azide as an inhibiting substance for gram-negative bacteria. The Journal of Infectious Diseases 67:113-115.

Steenbergen JN, Alder J, Thorne GM, Tally FP. 2005. Daptomycin: A lipopeptide antibiotic for the treatment of serious Gram-positive infections. Journal of Antimicrobial Chemotherapy 55(3):283-288.

Steinhaus B, Garcia ML, Shen AQ, Angenent LT. 2007. A portable anaerobic microbioreactor reveals optimum growth conditions for the methanogen Methanosaeta concilii. Appl Environ Microbiol 73(5):1653-8.

Stewart PS. 1998. A review of experimental measurements of effective diffusive permeabilities and effective diffusion coefficients in biofilms. Biotechnology and Bioengineering 59(3):261-272.

Stewart PS. 2002. Mechanisms of antibiotic resistance in bacterial biofilms. Int. J. Med. Microbiol. 292(2):107-113.

Stewart PS, Costerton JW. 2001. Antibiotic resistance of bacteria in biofilms. Lancet 358(9276):135-138.

Stewart PS, Davison WM, Steenbergen JN. 2009. Daptomycin Rapidly Penetrates a Staphylococcus epidermidis Biofilm. Antimicrob. Agents Chemother. 53(8):3505-3507.

Stewart PS, Franklin MJ. 2008. Physiological heterogeneity in biofilms. Nat. Rev. Microbiol. 6(3):199-210.

Stocker R, Seymour JR, Samadani A, Hunt DE, Polz MF. 2008. Rapid chemotactic response enables marine bacteria to exploit ephemeral microscale nutrient patches. Proceedings of the National Academy of Sciences of the United States of America 105(11):4209-4214.

Strovas TJ, Dragavon JM, Hankins TJ, Callis JB, Burgess LW, Lidstrom ME. 2006. Measurement of respiration rates of Methylobacterium extorquens AM1 cultures by use of a phosphorescence-based sensor. appl. Environ. Microbiol. 72(2):1692-1695.

Sukop MC, Or D. 2003. Invasion percolation of single component, multiphase fluids with lattice Boltzmann models. Physica B 338:298-303.

Surdeau N, Laurent-Maquin D, Bouthors S, Gelle MP. 2006. Sensitivity of bacterial biofilms and planktonic cells to a new antimicrobial agent, Oxsil (R) 320N. Journal of Hospital Infection 62(4):487-493.

Takenaka S, Trivedi HM, Corbin A, Pitts B, Stewart PS. 2008. Direct visualization of spatial and temporal patterns of antimicrobial action within model oral biofilms. Appl. Environ. Microbiol. 74(6):1869-1875.

Terwee CB, Roorda LD, Dekker J, Bierma-Zeinstra SM, Peat G, Jordan KP, Croft P, de Vet HCW. 2010. Mind the MIC: large variation among populations and methods. J. Clin. Epidemiol. 63(5):524-534.

Tian YQ, Shumway BR, Meldrum DR. 2010. A New Cross-Linkable Oxygen Sensor Covalently Bonded into Poly(2-hydroxyethyl methacrylate)-co-Polyacrylamide Thin Film for Dissolved Oxygen Sensing. Chem. Mater. 22(6):2069-2078.

Udekwu KI, Levin BR. 2012. Staphylococcus aureus in continuous culture: A tool for the rational design of antibiotic treatment protocols. PLoS ONE 7(7).

Van der Meeren P, De Vleeschauwer D, Debergh P. 2001. Determination of oxygen profiles in agar-based gelled in vitro plant tissue culture media. Plant Cell, Tissue and Organ Culture 65(3):239-245.

Waharte F, Steenkeste K, Briandet R, Fontaine-Aupart M-P. 2010. Diffusion Measurements inside Biofilms by Image-Based Fluorescence Recovery after Photobleaching (FRAP) Analysis with a Commercial Confocal Laser Scanning Microscope. Appl. Environ. Microbiol. 76(17):5860-5869.

Walsh C. 2000. Molecular mechanisms that confer antibacterial drug resistance. Nature 406(6797):775-781.

Walters MC, Roe F, Bugnicourt A, Franklin MJ, Stewart PS. 2003. Contributions of antibiotic penetration, oxygen limitation, and low metabolic activity to tolerance of Pseudomonas aeruginosa biofilms to ciprofloxacin and tobramycin. Antimicrob. Agents Chemother. 47(1):317-323.

Wang G, Or D. 2010. Aqueous films limit bacterial cell motility and colony expansion on partially saturated rough surfaces. Environmental Microbiology 12(5):1363-1373.

Wang G, Or D. 2013. Hydration dynamics promote bacterial coexistence on rough surfaces. ISME J 7(2):395-404.

Wang W, Shor LA, LeBoeuf EJ, Wikswo JP, Taghon GL, Kosson DS. 2008a. Protozoan migration in bent microfluidic channels. Applied and Environmental Microbiology 74(6):1945-1949.

Wang W, Shor LM, LeBoeuf EJ, Wikswo JP, Kosson DS. 2005a. Mobility of protozoa through narrow channels. Applied and Environmental Microbiology 71(8):4628-4637.

Wang W, Shor LM, LeBoeuf EJ, Wikswo JP, Kosson DS. 2005b. Mobility of protozoa through narrow channels. Applied and Environmental Microbiology 71(8)(8):4628-4637.

Wang W, Shor LM, LeBoeuF EJ, Wikswo JP, Taghon GL, Kosson DS. 2008b. Protozoa Migration in Bent Microfluidic Channels. Appl. Envir. Microbiol. 74(6):1945-1949.

Weibel D, Lee A, Mayer M, Brady S, Bruzewicz D, Yang J, Diluzio W, Clardy J, Whitesides G. 2005. Bacterial printing press that regenerates its ink: Contact printing bacteria using hydrogel stamps. Langmuir 21:6436-6442.

Weibel DB, DiLuzio WR, Whitesides GM. 2007a. Microfabrication meets microbiology. Nat. Rev. Microbiol. 5(3):209-218.

Weibel DB, DiLuzio WR, Whitesides GM. 2007b. Microfabrication meets microbiology. Nature Reviews Microbiology 5:209-218.

Weller DM. 1988. Biological Control of Soilborne Plant Pathogens in the Rhizosphere with Bacteria Annu. Rev. Phytopathol. 26:379-407.

Whitesides G, Ostuni E, Takayama S, Jiang X, Ingber D. 2001. Soft lithography in biology and biochemistry. Annual Review of Biomedical Engineering 3:335-373.

Willingham TW, Werth CJ, Valocchi AJ. 2008. Evaluation of the effects of porous media structure on mixing-controlled reactions using pore-scale modeling and micromodel experiments. Environmental Science & Technology 42(9):3185-3193.

Xu L, Robert L, Qi O, Taddei F, Chen Y, Lindner AB, Baigl D. 2007. Microcontact printing of living bacteria arrays with cellular resolution. Nano Letters 7(7):2068-2072.

Yamaguchi N, Torii M, Uebayashi Y, Nasu M. 2011. Rapid, Semiautomated Quantification of Bacterial Cells in Freshwater by Using a Microfluidic Device for On-Chip Staining and Counting. Applied and Environmental Microbiology 77(4):1536-1539.

Young IM, Crawford JW. 2004. Interactions and self-organization in the soil-microbe complex. Science 304(5677):1634-1637.

Zakeri B, Wright GD. 2008. Chemical biology of tetracycline antibiotics. Biochemistry and Cell Biology-Biochimie Et Biologie Cellulaire 86(2):124-136.

Zhang W, Sileika TS, Chen C, Liu Y, Lee J, Packman AI. 2011. A novel planar flow cell for studies of biofilm heterogeneity and flow-biofilm interactions. Biotechnology and Bioengineering 108(11):2571-82.

Chapter 6 Conclusion

6.1 Dissertation Overview

In this dissertation, novel systems were developed to investigate biofilm functions important in medicine and agriculture. The system can provide a controlled, micro-structured environment including chemical gradients and physical structures. In the medical context, the devices enable dynamic responses of biofilm bacteria to be screened during exposure to an antibiotic, or during fluctuating exposure to a small molecule respiration inhibitor. A reversible, non-destructive and spatially continuous oxygen sensor was incorporated into the system to facilitate direct measurement of bulk microbial respiration. Microfluidic systems were also created with realistic soil microstructure to systematically investigation the combined effects of microbial EPS secretions and soil microstructure on pore scale water retention. Both systems enable through-put screening and high-content measurement of micro-structured microbe-microbe systems.

Microfluidic devices enable micro-scale chemical gradient and physical structures to be created and replicated. Compared with conventional methods, microfluidics enables extracellular conditions to be controlled more precisely, through the replication small-scale and highly conserved system geometries. With microfluidics, dynamic system properties can be created and replicated, including changing chemical concentrations, variable chemical gradients, and pore-scale changes in humidity. Meanwhile, dynamic biological responses to these micro-scale and dynamic physical and chemical conditions can be observed directly and easily measured many

times over. With microfluidics, modeling fundamental kinetic, thermodynamic, and mass transport phenomena is facilitated through the high degree of control and replication made possible in experiments. The power of microfluidics is fully realized through the combination of experiments and modeling, where interpretations of observed and simulated responses in identical micro-scale phycial and chemical habitats provides novel and unique insights and may offer fundamental explanations of biofilm activity.

6.2 Summary of Major Findings and Contributions

Chapter One motivated the research, and provided the objectives for each portion of this work.

Chapter Two introduced the structure and function of bacterial biofilms in both unstructured and physically structured settings. Also, the mechanism for increased tolerance and resistance of biofilm to antimicrobials was discussed, and the major drawbacks of most existing methods for analyzing biofilms were described. In Chapter two the importance of time-dependent changes in microchemical environment was discussed. Time-dependent factors are important in terms of oxygen availability and respiration state in a biofilm, in dosing regime when measuring antimicrobial effectiveness, and in terms of spatial and temporal changes in pore water content. No existing method can measure such dynamic functions in intact biofilms.

Chapter Three introduced a novel method for investigating antimicrobial concentration and dosing regime on respiration inhibition of intact biofilms. The major contributions and key scientific findings of Chapter Three were:

1) Development of a novel microfluidic device for controlling the dosing rate of one or more antimicrobials delivered to an array of intact biofilms.
2) Development of a novel optical sensor for spatially continuous measurements of available oxygen concentration and dynamics across the biofilm array.
3) Biofilms exposed to a gradually increasing antimicrobial concentration can tolerate higher antimicrobial concentrations before they exhibit respiration inhibition compared with biofimls exposed to more rapidly increasing concentrations.
4) Contact printed *Staphylococcus aureus* biofilms become respiration inhibited above Sodium azide concentrations of 0.003 mM.

Chapter Four provided a deeper understanding of the dynamic nature of biofilm respiration changes during antibiotic exposure. Chapter Four employed similar experimental methods as Chapter Three, but used a clinically important antibiotic, Daptomycin, not a small molecule respiration inhibitor, and investigated dynamic changes in respiration of biofilms in the array during steady state exposures to various antibiotic concentrations. The major findings and contributions of Chapter Four were:

1) The fluorescence response of the oxygen sensing film was quantitatively calibrated to known oxygen concentrations. The reversible, non-destructive, spatially continuous sensor has a quick response time. It opens a window into the inner workings of intact microbial systems.
2) A 3D mathematical model of oxygen diffusion and reaction inside an intact biofilm was built and validated. The model was used to infer the changing respiratory status of intact biofilms during antibiotic exposure. Through constraining the physical

experimental system, systematic experimentation, replication, and first-principles modeling, important aspects of overall system function can be quantitatively and reproducibly determined.

3) The time it takes to reach a given degree of respiration inhibition is dependent on the steady-state antibiotic concentration: however, this is not because of mass transport through the biofilm because the antibiotic itself fully penetrates biofilm within a few minutes.
4) For different Daptomycin concentrations, the optimal exposure time needed to reach a given degree of respiration inhibition can be measured using this method. Proper antibiotic use including dose and time can optimize effectiveness and minimize risk.
5) There are apparently heterogeneous degrees of Daptomycin susceptibility found in contact-printed biofilms from *S. aureus* clones. Buk biofilm respiratory state stabilized to different values depending on the concentration applied. This results suggest a minority component of the bacterial community were never completely inhibited, and this percentage decreased with antibiotic concentration.

Chapter Five introduced a novel system for investigating the synergic effects of biofilm EPS and micro-structured soil geometry on the pore-scale retention of soil water. Water loss was measured in replicate microfluidic devices containing identical realistic soil structures and loaded with different bacterial suspensions. In addition, drying rates were measured for bacteria-amended whole soils and for biofilms alone. The major findings and contributions of Chapter Five were:

1) Development of a novel microfluidic device mimicking soil structure.

2) EPS+ biofilms can hold more water for a longer period of time in both realistic soil and the microfluidic device

3) No significant difference was observed for water loss rate in pure EPS+ or EPS- biofilms.

4) Microbial EPS production and soil micro-structure act synergistically to retain soil moisture.

6.3 Significance and Applications

An integrated systems approach is needed to capture the dynamic nature of biological responses to microscale habitat conditions. In some cases, emergent properties may be observed in synthetic microbe-habitat systems. These emergent properties include the greatly enhanced tolerance of biofilm bacteria to antimicrobials, and the capacity for microbes to modulate water loss in micro-sturctured settings.

In this work, biofilm dynamic responses can be systematically measured and interpreted. There are many applications for the creation of synthetic microbe-habitat systems. In medicine, this approach offers practical methods for high throughput screening of antimicrobials and determination of optimal dosing regimes. In agriculture, this system can be used to better understand the complex interactions among plants, microbes, and soil that control the productivity and resiliency of food crops and terrestrial ecosystems generally. In both contexts, emulation of relevant features of the microenvironment was essential for the emergence of microbe-system properties. Looking forward, this approach can be used to identify better treatments for diseases, and biotechnologies leading to more sustainable food production.

6.4 Future Directions

The concept of antimicrobial dynamic dosing rates affecting biofilm antimicrobial susceptibility has been thoroughly described and testified using the small molecule respiratory inhibitor sodium azide. Sodium azide is an excellent choice for a quantitatively inhibiting respiration under dynamic dosing regime conditions. However, sodium azide is not clinically relevant, and is only commonly used as respiratory inhibitor in culture maintenance. A future direction for this dissertation research is to investigate the time-dependent effects of dosing regime biofilm respiration inhibition.

Preliminary experiments have been performed on biofilm respiratory responses to dynamic delivery of Daptomycin. Here, Daptomycin was introduced not in the agar fill solution, but into one corner of the microfluidic device, as described in Chapter 3. The initial concentration of Daptomycin in source well was 10 mg/ml, or 6.2mM. Daptomycin diffuses through the agar matrix, and creates non-liner gradient across the entire field within 40 h.

Preliminary data show dynamic changes in fluorescence intensity of the oxygen sensing film along a transect of the array shows. The pattern of consecutive decreases in fluorescence intensity is (Figure 6-1), consistent with position- and time-dependent respiration inhibition in biofilms with diffusion of Daptomycin across the array. (The abrupt change in intensity around 25 h most likely reflects some small interruption in the experiment.)

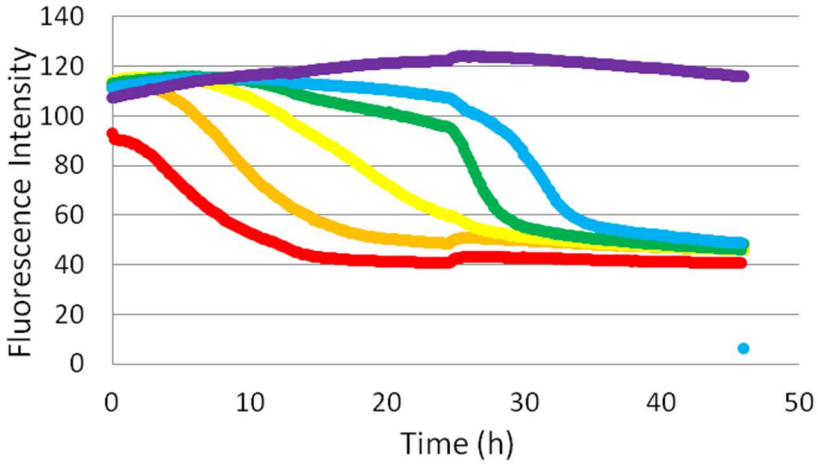

Figure 6-1 Dynamic fluorescence intensity of biofilms on transect line of the array, exposed to different dosing rates in the microfluidic device.

Fluorescence intensities of biofilms were then converted to oxygen concentrations, as described in Chapter 4 (Figure 6-2). Due to the abrupt change around 25h, we ignore neglect unreasonable oxygen concentrations for biofilm 1_1 (red) and 2_2 (orange) after 25 h, and focus on the changes in oxygen availability for biofilms 3_3 (yellow), 4_4 (green), 5_5 (blue) and 6_6 (purple).

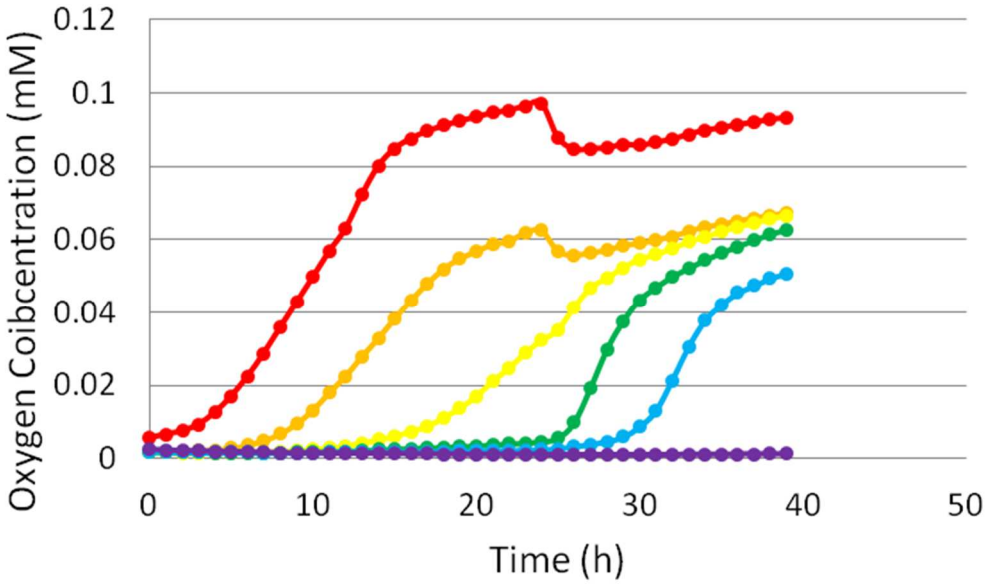

Figure 6-2 Preliminary result on convered oxygen concentration at bottom of biofilms in the array.

System was interupted at around 25h, leading to non-smooth change of fluorescence intensity and convered oxygen concentration.

Preliminary simulations using a 3D mathematical model were used to estimate Daptomycin concentration in 0.3% agar with TSB and in biofilm with approximated Daptomycin diffusivity in agar. In the future, this parameter could be measured using fluorescently-labeled Daptomycin kindly provided by Cubist Pharmaceuticals. Future work would also need to estimate Daptomycin loss; in the preliminary model Daptomycin was treated as a conservative tracer. Biofilms were assumed to be cylinders with 30 μm height and 500 μm diameters for simplicity. With given geometry of the device and biofilm array, Daptomycin concentration at any given position and time during the diffusive exposure could be estimated (Figure 6-3). At the end of 40 h, all biofilms in the array had been exposed to at least 0.3 mM Daptomycin, although actual Daptomycin concentration should be smaller than the modeled value due to Daptomycin consumption, reaction, or loss.

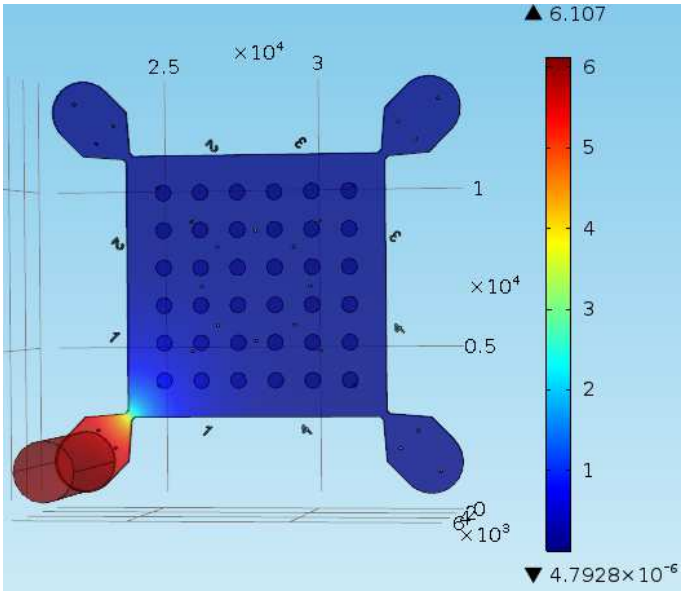

Figure 6-3 Preliminary modeling of Daptomycin diffusion in dynamic dosing assay.

This provides estimated Daptomycin concentrations at any given time and location in the device. The estimated concentration should be higher than actual value due to Daptomycin utilization.

Next, the estimated oxygen consumption rates were converted to the respiratory index (Figure 6-4), indicating the overall "health status" of intact biofilms during the treatment. When Daptomycin concentrations increase gradually, biofilms were able to tolerant Daptomycin exposure throughout the experiment. With the preliminary model, Daptomycin concentration in biofilm 6_6 (purple) increased mildly and eventually reaches to around 0.3mM at the last few hours of experiment. Respiratory Index of biofilm 6_6 was 1 even when the modeled Daptomycin concentration reaches to 0.3mM towards the end of experiment (Figure 6-4). However, when biofilms were exposed to a comparable but constant Daptomycin concentration, 0.25mM, biofilm respiratory index decreased from 1 to 0.2 within 4 h (Figure 4-9 in Chapter 4). This might due to inaccurate modeling of Daptomycin delivery in the device, but they may also reflect emergence of Daptomycin resistance in biofilms exposed to sub-lethal chronic exposures of Daptomycin.

Also noteworthy is the minimum achievable respiratory index is lower for exposures to high, constant bulk concentrations. Conversely, biofilms exposed to fluctuating Daptomycin concentrations maintained a higher respiration status overt time. In the dynamic Daptomyicn dosing experiment, the minimum achievable respiratory index was a function of position in the array: biofilms located nearest the Daptomycin well, that experienced the most quickly-increasing Daptomycin concentrations stabilized to the lower respiratory index values than biofilms from any other position along the diagonal transect (Figure 6-4). However, in the dynamic Daptomycin dosing experiment, all minimum achievable respiratory index values were higher than results from the constant concentration Daptomycin experiments (See Figure 4-9 in Chapter 4), even with modeled dynamic concentration to be at least 0.3mM at all positions at the end of experiments.

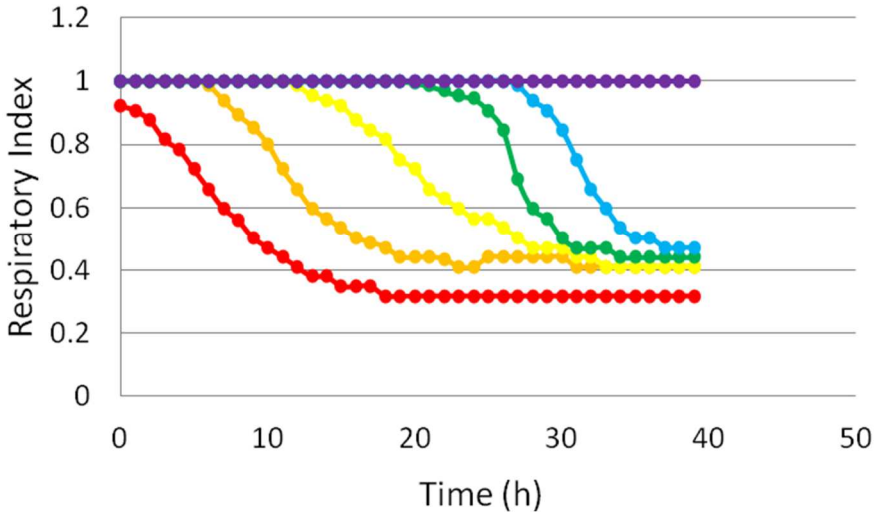

Figure 6-4 Preliminary respiratory index change in response to dynamic Daptomycin delivery.

The lowest respiratory index could be reachied is about 0.3, while in immediate contact with high Daptomycin concentrations, respiratory index could reach around 0.1 (See Figure 4.9 in Chapter 4)

The results highlight the importance of the dosing regime on the antimicrobial effectiveness and the development of tolerance or resistance. Potentially, biofilms experiencing a changing concentration of Daptomycin from low to high are not inhibited effectively by a given dose when compared with exposures to very rapidly increasing concentrations. No other technology is available to generate changing or oscillating antimicrobial exposures and measure the dynamic respiratory responses of arrays of intact biofilms.

More replicates should be done to fully understand how biofilm respiratory activity responds to fluctuations in Daptomycin concentration, or to differences in dose or delivery rate. The devices developed here are also highly amenable to measuring synergistic or antagonistic effects of multiple antimicrobials or other solutes, by loading each corner well with a different solution. The device could also be used to pattern multi-species biofilms, either within individual positions, or in adjacent positions in the array. Fluctuations of sublethal antimicrobial dosage can be maintained for a long time by periodically pipetting antibiotics in and out of the source well. This can capture fluctuation of concentration in clinic in between of two dosage. Ultimately, this tool may one day help clinicians develop better treatments with improved effectiveness and decreased risk.

Some future directions for the research using the emulated soil micromodel include strategies to systematically increase system complexity. For example, different soil structures could be investigated, such as systematic aggregation of the particles (Figure 6-5). Such configurations are characterized by a bimodal distribution of pore diameters. Small pores have strong capillary forces, and are effective in retaining water, while the large open macropores dry readily and offer rapid transport of dissolved constituents including oxygen. Preliminary work

confirms that this geometry leads to rapid clearing of the large spaces, followed by gradual shrinking of the hydrated domain in the aggregated regions.

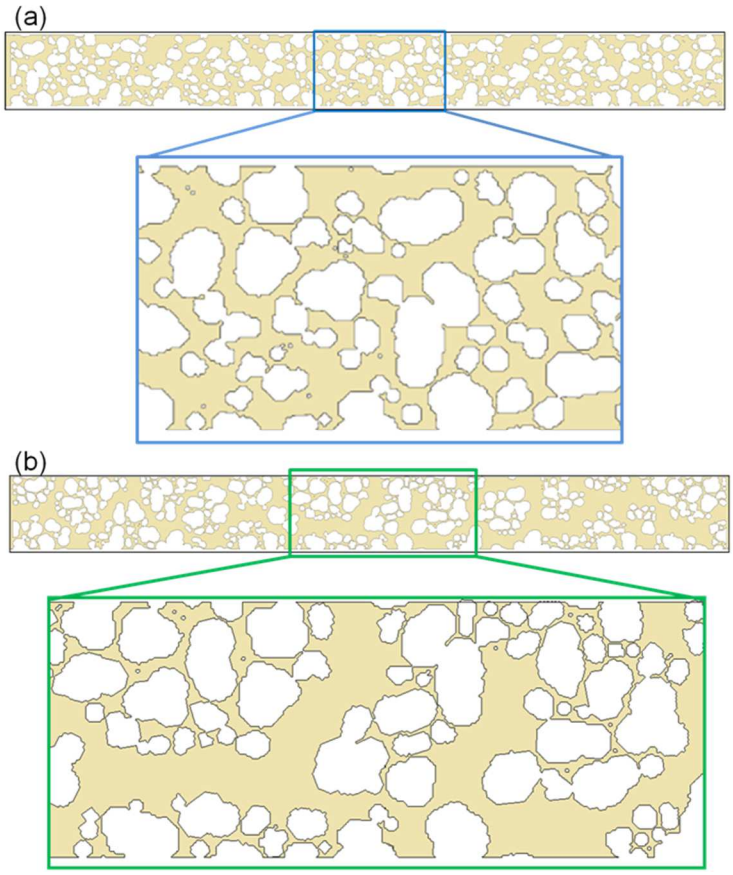

Figure 6-5 Generation of different soil structures by aggregating a soil particle size distribution.

Other micro-scale features important in real rhizosphere systems could be incorporated into future generations of the emulated soil micromodel. For example, devices could be loaded with more complex microbial communities, potentially including protists. Grazing pressure by protists is known to promote EPS production by bacteria, and is therefore expected to also influence water retention. Future iterations of the devices may also include chemical gradients. Real rhizosphere microsystems are under the influence of plant root exudates, which lead to spatially-structured microbial abundances.

As always, the combination of experiments and modeling will provide the greatest benefits: theoretical predictions will enable rational design of experiments and hypothesis testing, and experiments will validate models that predict bulk-scale function of microbe-habitat systems.